Automatic Modulation Classification for MIMO Systems

Dibyajyoti Das

Automatic Modulation Classification for MIMO Systems

A

Thesis Submitted

in Partial Fulfilment of the Requirements

for the Degree of

DOCTOR OF PHILOSOPHY

By

Dibyajyoti Das

Department of Electronics and Electrical Engineering

Indian Institute of Technology Guwahati

Guwahati - 781 039, INDIA.

March, 2020

Dedicated to

My Beloved Parents

Teachers,

Sisters,

and

Friends

Certificate

This is to certify that the thesis entitled "**Automatic Modulation Classification for MIMO Systems**", submitted by **Dibyajyoti Das** (Roll No 126102009), a research scholar in the *Department of Electronics and Electrical Engineering, Indian Institute of Technology Guwahati*, for the award of the degree of **Doctor of Philosophy**, is a record of an original research work carried out by him under our supervision and guidance. The thesis has fulfilled all the requirements as per the regulations of the institute and in our opinion has reached the standard needed for submission. The results embodied in this thesis have not been submitted to any other University or Institute for the award of any degree or diploma.

Date:

Place: Guwahati.

Prof. Prabin Kumar Bora
Professor
Dept. of Electronics and Electrical Engg
Indian Institute of Technology Guwahati
Guwahati - 781 039, Assam, India.

Date:

Place: Guwahati.

Prof. Ratnajit Bhattacharjee
Professor
Dept. of Electronics and Electrical Engg
Indian Institute of Technology Guwahati
Guwahati - 781 039, Assam, India.

Acknowledgements

This thesis could not have been made possible without the precious guidance of my thesis supervisors Prof. Prabin Kumar Bora and Prof. Ratnajit Bhattacharjee. I express my sincere gratitude to them.

I would like to extend my sincere gratitude to the members of my doctoral committee Dr. A Rajesh, Dr. Tony Jacob and Dr. Prithwijit Guha for providing valuable guidance and continuous feedback for improving the work. I would also like to thank all the faculty, staff members and research scholars of the EEE department, IIT Guwahati for providing an interactive and co-operative atmosphere all throughout.

Abstract

The objective of automatic modulation classification (AMC) is to classify the modulation type of an unknown communication signal. AMC is a widely investigated area. The initial works on AMC were primarily devoted to single input single output (SISO) systems. There are two main approaches to AMC, namely the *likelihood based* (LB) and *feature based* (FB) approaches. The former treats AMC as a multiple hypotheses testing problem, where it considers L composite hypotheses H^0,H^1,...,H^{L-1} corresponding to L modulation types. The multiple hypotheses testing procedure maximizes the likelihood function of the received signal with respect to the hypotheses to decide the modulation type of the received signal. The LB approach can provide optimal performance in the Bayesian sense, but it suffers from high computational complexity. The FB methods, on the other hand, are not optimal in the Bayesian sense, but they require less a priori information and a low computational power. Two widely used AMC features are the higher order moments (HOMs) and higher order cumulants (HOCs).

With the rapid development of the multiple input multiple output (MIMO) technology and its remarkable capacity gain over the traditional SISO technology, there are serious efforts to integrate this technology into the current generation wireless systems. Designing AMC algorithms for MIMO systems is a challenging task because the mutual interference generated by MIMO spatial channels alters the statistical properties of the modulated signal. The objective of this research work is to classify the modulation type for MIMO systems. Many studies have addressed this challenging problem. However, there remain several research issues. This thesis addresses some of these issues:

1) The AMC of the QPSK-variant (QPSK, OQPSK and $\frac{\pi}{4}$-QPSK) and 8-PSK signals over spatially correlated MIMO channels is addressed. The HOCs are widely used AMC features

because of their resilience to Gaussian noise. However, the HOCs estimated directly from the equalized signal fail to distinguish the QPSK-variant and 8-PSK signals. This can be attributed to the fact that the HOC values of the QPSK-variant and 8-PSK signals are ambiguous. The QPSK and OQPSK signals exhibit same HOC values. Similarly, the $\frac{\pi}{4}$-QPSK and 8-PSK signals share the same HOC values. To distinguish the above modulation types, a cumulant-based AMC method is proposed by considering the fourth-order cumulants of the signal, the signal down-sampled by a factor of 2 and the backward difference signal. The proposed method produces satisfactory results over the spatially correlated MIMO channel.

2) The emergence of wireless sensor networks (WSN) and coginitve radio (CR) networks makes cooperative classification an attractive strategy to improve the AMC performance. A better statistical estimate can be obtained by combining signals from multiple sensors, thereby enhancing the AMC performance. The cooperative classification has not been explored by the existing works on the AMC for MIMO systems. This thesis proposes a cooperative AMC method for MIMO systems in a multi-antenna sensor network to distinguish the modulation types BPSK, OQPSK, QPSK, $\frac{\pi}{4}$-QPSK, 8-PSK,16-QAM and 64-QAM. The proposed method considers a feature vector comprising of HOCs derived from the signal, the signal down-sampled by a factor of 2 and the backward difference signal and employs a centralized cooperative classification framework with the feature-level fusion. The method performs reasonably well over spatially correlated MIMO channels.

3) The majority of the AMC algorithms for MIMO systems have considered the rich scattering environment that offers a full rank channel matrix. In practice, MIMO systems can also operate in an insufficient scattering environment, leading to a rank deficient channel. A rank deficient channel, such as a keyhole channel can severely degrade the AMC performance. In this thesis, the problem of AMC over spatially correlated MIMO keyhole channels is addressed. A novel algorithm, namely the direct modulation recognition (DMR) algorithm, is proposed to distinguish the lower order PSK constellations, namely BPSK, QPSK and OQPSK. The proposed algorithm employs the ratios of HOCs derived from the received signal and its backward difference as AMC features. These features are chosen so that the contributions of the channel-

coefficients are cancelled. Thus, the DMR algorithm does not require channel state information (CSI) at the receiver. The method produces satisfactory results over a spatially correlated MIMO keyhole channel.

4) The cooperative relaying is an attractive solution to overcome the rank deficiency of MIMO channels. These cooperative relays act as active scatterers, which eventually turns a keyhole channel into a multi-keyhole channel. An AMC method, namely relay assisted (RA)-AMC, is proposed to classify a pool of modulation types, namely BPSK, OQPSK, QPSK, $\frac{\pi}{4}$-QPSK, 8-PSK and 16-QAM, over an AF-relay fading channel. The proposed method involves two steps. In the first step, the method employs a cumulant feature vector derived directly from the received signal to distinguish BPSK, OQPSK and the sub-pool $Q_1 = \{QPSK, \frac{\pi}{4} - QPSK, 8 - PSK, 16 - QAM\}$ as a whole. This cumulant feature provides resistance against noise amplification that occurs in a correlated AF-relay system. In the second step, it employs a cumulant feature vector derived from the equalized signal to distinguish the modulation types in Q_1. The method performs well over the AF-relay fading channel.

Contents

List of Figures

List of Tables

List of Abbreviations

Automatic Modulation Classification	AMC
Single Input Single Output	SISO
Multiple Input Multiple Output	MIMO
Likelihood-Based	LB
Feature-Based	FB
Average Likelihood Ratio Test	ALRT
Hybrid Likelihood Ratio Test	HLRT
Spectrum Monitoring	SM
Link Adaptation	LA
Cognitive Radio	CR
Probability Density Function	PDF
Constant Modulus Algorithm	CMA
Joint Approximation Diagonalization of Eigen-matrices	JADE
Higher Order Moment	HOM
Higher Order Cumulant	HOC
Channel State Information	CSI
Zero Forcing Equalizer	ZFE
Artificial Neural Network	ANN
Independent Component Analysis	ICA
Expectation Maximization	EM
Moment Generating Function	MGF
Cumulant Generating Function	CGF

Wireless Sensor Networks	WSN
Cooperative Automatic Modulation Classification	CAMC
Direct Modulation Recognition	DMR
Signal to Noise Ratio	SNR
Amplify-and-Forward	AF
Relay Assisted-Automatic Modulation classification	RA-AMC

1

Introduction

Contents

1.1 Introduction to Automatic Modulation Classification (AMC)

Automatic modulation classification (AMC) techniques are employed to distinguish the modulation type of an unknown communication signal. AMC is a challenging task as the statistical properties of the transmitted signal are altered by noise and multipath fading.

In the literature, there are two main approaches to AMC, namely the *likelihood-based* (LB) and *feature-based* (FB) approaches. The former treats AMC as a multiple hypotheses testing problem, where it considers L composite hypotheses H^0,H^1,...,H^{L-1} corresponding to L modulation types. The multiple hypotheses testing procedure maximizes the likelihood function of the received signal with respect to the hypotheses to decide the modulation type of the received signal. The LB approach can provide optimal performance in the Bayesian sense, but it suffers from high computational complexity. The FB methods, on the other hand, are not optimal in the Bayesian sense, but they require less a priori information and a low computational power [1].

The early instances of AMC can be found in military intelligence applications like electronic warfare, surveillance and threat analysis. In military application, the knowledge of the modulation type is required for identifying the hostile communication signals, for generating the jamming signal and for reconstructing the intercepted signal.

AMC is also important for many civilian applications such as spectrum monitoring (SM) and cognitive radio (CR). Due to scarcity of the available spectrum, the CR tries to reuse the occupied spectrum when the allotted communication system remains silent. For this, efficient and faster spectrum monitoring and channel estimation techniques are required. The CR selects the best available spectrum slot to transmit the data. The modulation candidate for transmitting the data is selected based on the channel condition. This is known as link adaptation. A link adaptive (LA) system dynamically updates the modulation type from a pool of modulation types depending on the channel condition. This optimizes the transmission reliability and the data rate. For successful detection, the receiver needs the information about the modulation type. One way to inform the receiver about the modulation type is to include this information in each signal frame. Using this information, the receiver demodulates the received signal. The additional information about the modulation type in each frame increases the overhead,

which reduces the data rate. Providing information about the modulation type in each frame is not an efficient approach. This is where the role of AMC comes into play. AMC also plays an important role in SM applications. SM applications are used by a telecommunication regulatory authority (TRA) to ascertain that the allocated spectrum is used by an authorized user.

AMC is a widely investigated area. The initial works on AMC were primarily devoted to single input single output (SISO) systems [2–13]. With the rapid development of the multiple input multiple output (MIMO) technology and its remarkable capacity gain over the traditional SISO technology, there are serious efforts to integrate this technology into the current and future generation wireless systems [14]. Designing AMC algorithms for MIMO systems is a challenging task because the mutual interference generated by MIMO spatial channels alters the statistical properties of the modulated signal.

1.2 AMC for MIMO Systems

Consider a MIMO spatial multiplexing system with N_T transmitting and N_R receiving antennas. The received signal at the receiver can be written as [15]

$$\mathbf{y}(k) = \mathbf{H}\mathbf{x}(k) + \boldsymbol{\eta}(k) \tag{1.1}$$

where $\mathbf{y}(k) = [y_1(k)...y_{N_R}(k)]^T$ is an $N_R \times 1$ received signal vector, $\mathbf{x}(k) = [x_1(k)...x_{N_T}(k)]^T$ is an $N_T \times 1$ transmitted signal vector, $\boldsymbol{\eta}(k) = [\eta_1(k)...\eta_{N_R}(k)]^T$ is an $N_R \times 1$ vector of zero mean white circularly complex Gaussian noise and $\mathbf{H}$ is an $N_R \times N_T$ complex channel matrix.

The goal of AMC now is to determine the modulation type of the transmitted signal from N received samples $\mathbf{y} = [\mathbf{y}(1), \mathbf{y}(2), ..., \mathbf{y}(N)]$. An efficient modulation classifier is expected to have following general characteristics [16]:

1. The modulation classifier should offer robustness against different channel conditions. One way to achieve that is to cancel the channel mixing effect. For that, the receiver needs to estimate the channel state information (CSI). Another way to achieve that is to make the classifier naturally resilient against the channel conditions.

2. In general, the signal of interest is corrupted by noise. In many applications, noise

overrides the signal of interest. The modulation classifier should provide resistance to such noise and high classification accuracy under different noise levels.

3. In some application like CR and software defined radio (SDR), the modulation classifier needs to determine the modulation candidate from a pool of limited number of modulation types. However, in military and spectrum monitoring scenarios, the classifier needs to classify a large pool of modulation schemes.

4. The modulation classifier should be computationally less complex and easily implementable.

A significant amount of research has been devoted to address the AMC problem for MIMO systems [1, 15, 17–28]. In [28], Bahloul et al. provided a comprehensive survey of AMC algorithms designed for MIMO systems. The existing AMC algorithms for MIMO systems can be grouped into two main categories, namely likelihood-based (LB) and feature-based (FB) [28]. A brief outline of these two methods are presented below.

1.3 LB Approach

Suppose a MIMO transmitter selects a modulation type from a pool of modulations A. We denote the hypothesis that the transmitted message is modulated using the modulation type $M(M \in A)$ as H^M. Under this hypothesis, the likelihood function of the received MIMO signal is represented by $f^M(\mathbf{y})$. The likelihood function of the received signal is evaluated for all the possible modulation types of the transmitted signal. The modulation candidate responsible for producing the largest value of the likelihood function is selected as the modulation type for the received MIMO signal. This selection criterion is given by [17]

$$M^* = \underset{M \in A}{argmax}(f^M(\mathbf{y})) \tag{1.2}$$

where M^* represents the detected modulation type. In addition to the modulation type, the likelihood function of the received MIMO signal is dependent on many other communication parameters which are not known to the receiver. One way to solve this issue is to average the likelihood function of the received signal over these unknown parameters. This leads to the

concept of the *average likelihood ratio test* (ALRT) [5]. Another way to tackle this is to find the estimates of these unknown parameters and use these estimates for evaluating the likelihood function. This is known as the *hybrid likelihood ratio test (HLRT)* [5].

1.3.1 ALRT Approach

The ALRT technique treats the unknown data symbols and communication parameters as random variables. It is assumed that the probability density functions (PDFs) of these unknown parameters are known to the receiver. The receiver computes the likelihood function of the received signal by averaging the PDFs over those unknown parameters. Under hypothesis H^M, the likelihood function of the received signal using the ALRT can be written as [28]

$$f^M(\mathbf{y}) = E_{\mathbf{x}^M} E_{\boldsymbol{\phi}}[f(\mathbf{y}|\mathbf{x}^M, \boldsymbol{\phi})] \tag{1.3}$$

where $\mathbf{x}^M$ is an $N_T \times N$ matrix representing the symbols transmitted under the hypothesis H^M; $\boldsymbol{\phi}$ represents the vector of the unknown communication parameters; $E_{\mathbf{x}^M}$ and $E_{\boldsymbol{\phi}}$ are the expectations with respect to the unknowns $\mathbf{x}^M$ and $\boldsymbol{\phi}$, respectively; and $f(\mathbf{y}|\mathbf{x}^M, \boldsymbol{\phi})$ is the conditional likelihood function of the received signal with respect to the hypothesis H^M. The likelihood function is conditioned on the unknowns data symbols and communication parameters. It can be noted that the ALRT requires prior knowledge of the PDFs of the unknown communication parameters. With a perfect knowledge of these PDFs , the ALRT technique achieves the upper bound on the performance of any AMC algorithm [28]. In practical scenarios, such prior knowledge of the PDFs of the unknown communication parameters may not be available at the receiver. The likelihood function of the received signal with respect to H^M can be expressed as [17]

$$f^M(\mathbf{y}) = \frac{1}{|M|^{NN_T}(\pi\sigma_n^2)^{NN_R}} \prod_{k=1}^{N} \sum_{\mathbf{x}(k)\in M^{N_T}} e^{\frac{-\|\mathbf{y}(k) - H\mathbf{x}(k)\|^2}{\sigma_n^2}} \tag{1.4}$$

where σ_n^2 denotes the variance of the additive Gaussian noise; $|M|$ represents the number of possible constellation points for modulation type M; M^{N_T} denotes all the possible combinations of symbols at the transmitter under H^M; and $\|.\|$ denotes the Euclidian norm.

1.3.2 HLRT Approach

The HLRT approach treats the unknown data symbols as random variables, while it considers the unknown communication parameters as unknown constants. This are to be estimated from the received samples. Using the HLRT, the likelihood function of the received signal under H^M can be expressed as [28]

$$f^M(\mathbf{y}) = E_{\mathbf{x}^M}[f(\mathbf{y}, \hat{\boldsymbol{\phi}}^M | \mathbf{x}^M)] \tag{1.5}$$

where $\hat{\boldsymbol{\phi}}^M$ is the estimate of $\boldsymbol{\phi}^M$ under H^M.

1.4 FB Approach

The FB approach comprises three steps, namely channel equalization, signal processing and classification. Prior to AMC, it is imperative to equalize the channel mixing effect as MIMO spatial channels alters the statistical properties of the modulated signal. Two popular blind channel estimation techniques are : 1) the constant Modulus algorithm (CMA) [18, 29, 30] and 2) the Joint Approximation Diagonalization of Eigen-matrices (JADE) method [31, 32]. Reference [33] presented a reduced rank space-Time equalizer. The work use reduced rank channel models to design rank reduced versions of the maximum-likelihood sequence estimator (MLSE) and the decision feedback equalizer (DFE). Reference [34] proposed a new blind source separation (BSS) method based on independent low-rank matrix analysis (ILRMA) with novel sparse regularization. ILRMA simultaneously estimates a demixing matrix and source spectrogram models based on non-negative matrix factorization (NMF).

The signal processing step extracts the features from the equalized signal. The classifier then distinguishes the modulation type of the unknown signal using these features. Two widely used AMC features for MIMO systems are the Higher Order Moments (HOMs) and the Higher Order Cumulants (HOCs) [1, 15, 18, 19, 22]. The HOCs are popular as they offer resistance to Gaussian noise [4]. The HOM and HOC features are outlined below.

1.4.1 Moments

The p^{th} order q-conjugate moment of a zero-mean complex random variable y is defined as [18]

$$\mu_{pq} = E[y^{p-q}(y^*)^q] \tag{1.6}$$

where p denotes the moment order. For example, for $p = 2$ and $q = 0$, Eqn. 1.6 becomes

$$\mu_{20} = E[y^2(y^*)^0] = E[y^2]. \tag{1.7}$$

The theoretical values of selected HOMs of communication signals corresponding to different modulation types are presented in Table 1.1.

1.4.2 Cumulants

The n^{th} order cumulant for the random variables y_1,y_2,...,y_n is given by [18]

$$C(y_1, ..., y_n) = \sum_{\forall v}(-1)^{r-1}(r-1)!E[\prod_{j\epsilon v_1} y_j]...E[\prod_{j\epsilon v_r} y_j] \tag{1.8}$$

where the summation is performed over all partitions $v = (v_1, ..., v_r)$ on the set of indices $1, ..., n$ and r is the number of elements in a given partition. Thus fourth-order cumulants for zero mean random variables y_1, y_2, y_3 and y_4 is given by [4].

$$\begin{aligned} cum(y_1, y_2, y_3, y_4) =& E(y_1y_2y_3y_4) - E(y_1y_2)E(y_3y_4) \\ & - E(y_1y_3)E(y_2y_4) - E(y_1y_4)E(y_2y_3). \end{aligned} \tag{1.9}$$

Now, the n^{th} order m conjugate cumulant of a random variable y is defined as

$$C_{n,m}(y(k)) = Cum[\underbrace{y, ..., y}_{n-m}, \underbrace{y^*, ..., y^*}_{m}]. \tag{1.10}$$

For example, the second-order and fourth-order cumulants of a zero-mean complex random variable y can be defined in the following ways depending upon the placement of the conjugates [4]:

$$C_{20}(y) = E(y^2), \tag{1.11}$$

$$C_{21}(y) = E(|y|^2), \tag{1.12}$$

$$C_{40}(y) = E(y^4) - 3(E(y^2))^2, \tag{1.13}$$

$$C_{42}(y) = E(|y|^4) - |E(y^2)|^2 - 2(E(|y|^2))^2 \tag{1.14}$$

and

$$C_{41}(y) = E(y^3 y^*) - 3(E(y^2))(E(|y^2|)) \tag{1.15}$$

The theoretical values of selected HOCs of signals corresponding to different modulation types are presented in Table 1.2.

1.5 Existing Works on the AMC of MIMO Signals

Choqueuse et al., in [17], proposed two LB-modulation classification (MC) algorithms over time invariant MIMO Rayleigh flat-fading channels, namely the ALRT based algorithm and the HLRT based MC algorithm. The former requires the perfect knowledge of CSI at the receiver. On the other hand, the HLRT based MC algorithm estimates CSI from the received signal using the JADE technique. However, this investigation does not take into account the spatial correlation factor.

In [18], Hassan et al. proposed an FB-AMC approach over spatially correlated MIMO channels. The method involves three steps: 1) equalization of the received signal, 2) feature extraction and 3) classification process. Two equalization techniques, namely the ZF equalizer and the simplified constant modulus algorithm (SCMA), were considered. The method employs the HOMs and HOCs of the received signal as the AMC features and a multilayer feed-forward artificial neural network (ANN) as a classifier. However, ANN requires supervised training.

Muhlhaus et al., in [15], proposed an FB-AMC algorithm over time invariant MIMO Rayleigh flat-fading channels. The method comprises three steps: 1) equalization of the received signal, 2) extraction of the fourth-order zero-conjugate cumulant from the equalized signal and 3) classification process. Three equalization techniques, namely the ZF equalizer, the minimum mean

Table 1.1: The theoretical values of selected HOMs of signals corresponding to different modulation types

HOM	BPSK	QPSK	8-PSK	16-PSK	16-QAM	64-QAM
$m_{2,0}$	1	0	0	0	0	0
$m_{2,1}$	1	1	1	1	1	1
$m_{4,0}$	1	0	1	0	-0.68	-0.619
$m_{4,1}$	1	0	0	0	0	0
$m_{4,2}$	1	0	1	1	1.32	1.38
$m_{6,0}$	1	0	0	0	0	0
$m_{6,1}$	1	1	0	0	-1.32	-1.29
$m_{6,2}$	1	0	0	0	0	0
$m_{6,3}$	1	1	1	1	1.96	2.2
$m_{8,0}$	1	1	1	0	2.2	1.91
$m_{8,1}$	1	0	0	0	0	0
$m_{8,2}$	1	1	0	0	-2.48	-2.75
$m_{8,3}$	1	0	0	0	0	0
$m_{8,4}$	1	0	1	1	3.12	3.96

Table 1.2: The theoretical values of selected HOCs of signals corresponding to different modulation types

HOC	BPSK	QPSK	8-PSK	16-PSK	16-QAM	64-QAM
$C_{2,0}$	1	0	0	0	0	0
$C_{2,1}$	1	1	1	1	1	1
$C_{4,0}$	-2	1	0	0	-0.68	-0.619
$C_{4,1}$	-2	0	0	0	0	0
$C_{4,2}$	-2	-1	-1	-1	-0.68	-0.69
$C_{6,0}$	16	0	0	0	0	0
$C_{6,1}$	16	-4	0	0	2.08	1.797
$C_{6,2}$	16	0	0	0	0	0
$C_{6,3}$	16	4	4	4	2.08	1.797
$C_{8,0}$	-272	-34	1	0	-13.98	-11.5
$C_{8,1}$	-272	0	0	0	0	0
$C_{8,2}$	-272	34	0	0	-13.981	-11.5
$C_{8,3}$	-272	0	0	0	0	0
$C_{8,4}$	-272	-34	-33	-33	-13.981	-11.5

square error (MMSE) equalizer and the JADE equalizer, were considered. The method employs a minimum distance classifier that uses the Euclidean distance as the measure of feature similarity. Four modulation types, namely BPSK, QPSK, 8-PSK and 16-QAM, were considered for classification. The method performs reasonably well over the time invariant Rayleigh flat-fading channel. However, the investigation does not factor in rank deficiency in wireless channels.

In [19], Muhlhaus et al. proposed an FB-AMC algorithm over time invariant MIMO Rayleigh flat-fading channels. Two equalization techniques, namely the ZF equalizer and the JADE equalizer, were considered. The algorithm employs the fourth-order cumulants as the AMC features and the likelihood ratio test (LRT) for decision making. The method produces satisfactory result over the time invariant Rayleigh flat-fading channel. However, it requires the prior knowledge of the noise variance and reference mean and covariance matrix of the feature vector for all the considered modulation types.

Kanterakis et al., in [21], proposed an ALRT based MC algorithm for MIMO systems. The algorithm employs the independent component analysis (ICA) method to blindly separate the transmitted signals. The algorithm assumes that the separated signals are partially independent so as to generate a joint but separable ALRT function. Since the noise vectors from the separated components are not independent, the algorithm is sub-optimum in nature.

In [22], Chikha et al. proposed an MC algorithm over the MIMO relaying broadcast channels with direct link. The algorithm employs the HOMs and HOCs of the received signal as the AMC features and J48 decision tree as a classifier. However, the algorithm assumes that CSI is perfectly available at the receiver.

Kharbech et al., in [24], proposed an AMC method over time-selective MIMO channels. The method comprises three steps: 1) blind source separation (BSS), 2) the extraction of features from the separated components and 3) classification process. A sliding window technique is employed for the BSS of a faded-mixture to cancel the effect of high mobility. The method employs the HOMs and HOCs of the equalized signals as classification features. The ANN classifier is employed to improve the AMC performance.

In [25], Zhu and Nandi proposed an LB-AMC approach over the time invariant MIMO Rayleigh flat-fading channel. The method assumes that the channel matrix and noise variance are unknown to the receiver. The expectation maximization (EM) algorithm is employed to estimate the channel parameters jointly for each modulation candidate. The estimated channel parameters are then fed to an ML classifier to decide the corresponding modulation candidate. BPSK, QPSK, and 16-QAM were the modulation types considered for classification. The approach achieves a good classification accuracy. However, the algorithm suffers from high computational complexity.

The existing AMC algorithms for MIMO systems are summarized in Table 1.3.

1.6 Motivation and Problem Formulation

Based on the above survey, the following observations are made:

1. Tables 1.3 shows that the AMC of the QPSK-variants (QPSK, OQPSK and $\frac{\pi}{4}$-QPSK) and 8-PSK signals has not been addressed for MIMO systems. The HOCs are widely used AMC features as they offer resistance to Gaussian noise. However, the HOCs estimated from the equalized signal fail to distinguish the QPSK-variant and 8-PSK signals. This can be attributed to the fact that the HOC values of the QPSK-variant and 8-PSK signals are ambiguous. The QPSK and OQPSK signals exhibit same HOC values. Similarly, the $\frac{\pi}{4}$-QPSK and 8-PSK signals share the same HOC values.

2. The emergence of wireless sensor networks (WSNs) and CR networks makes cooperative classification as an attractive alternative to improve the AMC performance. For SISO systems, it is reported that a better statistical estimation can be obtained by combining signals from multiple sensors, thereby enhancing the AMC performance [35–44]. However, the multiple receiver situation has not been explored by the existing works on the AMC of MIMO signals.

Table 1.3: Summary of Existing Works on the AMC of MIMO Signals

Authors	Classifier Type	Considered Modulation Types	Channel	Unknown parameters
Choqueuse et al. [17]	LB	BPSK, QPSK, 16-PSK, 32-QAM	Time-invariant frequency-flat Rayleigh-fading	MIMO channel matrix
Hassan et al [18]	FB	BPSK, 8-PSK, 4-ASK, 8-ASK, 16-QAM, 32-QAM, 64-QAM	Time-invariant frequency-flat Rayleigh-fading	MIMO channel matrix
Mhlhaus et al. [15]	FB	BPSK, QPSK, 8-PSK,16-QAM	Time-invariant frequency-flat Rayleigh-fading	MIMO channel matrix
Mhlhaus et al. [1]	FB	BPSK, QPSK, 8-PSK,16-QAM	Time-invariant frequency-flat Rayleigh-fading	MIMO channel matrix
Mhlhaus et al. [19]	FB	BPSK, QPSK, 8-PSK,16-QAM	Time-invariant frequency-flat Rayleigh-fading	MIMO channel matrix
Kanterakis and Su [21]	FB	BPSK, QPSK, 8-PSK,16-QAM	Time-invariant frequency-flat Rayleigh-fading	MIMO channel matrix
Chikha et al. [22]	FB	BPSK, QPSK, 8-PSK, 16-QAM, 64-QAM, 256-QAM	Time-invariant frequency-flat Rayleigh	None
Chikha et al. [23]	FB	BPSK, QPSK, 8-PSK, 16-QAM, 64-QAM, 256-QAM	Nakagami-fading	None

Table 1.3 Continued: Summary of Existing Works on the AMC of MIMO Signals

Authors	Classifier Type	Modulation Types	Channel	Unknown parameters
Kharbech et al. [24]	FB	BPSK, QPSK, 8-PSK, 4-ASK, 8-ASK, 64-QAM	Time-varying frequency-flat Rayleigh-fading	MIMO channel matrix
Zhu and Nandi [25]	LB	BPSK, QPSK, 8-PSK, 16-QAM	Time-invariant frequency-flat Rayleigh-fading	MIMO channel matrix and Noise Variance
Turan et al [26]	LB	BPSK, QPSK, 8-PSK, 16-QAM	Time-invariant frequency-flat Rayleigh-fading	MIMO channel matrix and the number of transmitting antennas
Kharbech et al. [27]	FB	BPSK, QPSK, 8-PSK, 4-ASK, 8-ASK, 64-QAM	Time-invariant frequency-flat Rayleigh-fading	MIMO channel matrix

3. It is noted that the majority of AMC algorithms consider a rich scattering environment which offers a full rank MIMO channel. In practice, MIMO systems can also operate in an insufficient scattering environment, leading to a rank deficient channel. [45–52] . For example, one may consider a scenario where a user device located indoor, transmits signals to a cell tower. In that case, the opaqueness of building walls to the signal transmitted by the user device allows the most of the signal energy to pass through keyholes like windows, doors etc [14] . The presence of a keyhole is also possible in outdoor scenarios, even with a rich scattering environment [50]. It can happen when the ring of scatterers around the transmitter and the receiver is small compared to the distance between the transmitter and the receiver. A rank deficient channel, such as a keyhole channel can severely degrade the AMC performance.

4. The effect of cooperative relays on the performance of the AMC for MIMO signals

has not been well investigated. References [53–61], reported that the cooperative relaying is an attractive solution to overcome the rank deficiency of MIMO channels. These cooperative relays act as active scatterers, which eventually turns a keyhole channel into a multi-keyhole channel.

The aforementioned research gaps motivate us to address the following four problems in this thesis:

1. AMC of QPSK-variant and 8-PSK signals over spatially correlated MIMO channels.
2. Cooperative AMC for MIMO systems in a multi-antenna sensor network.
3. AMC over spatially correlated MIMO Keyhole channels.
4. AMC over correlated MIMO amplify and forward (AF)-relay fading channels.

1.6.1 Thesis Organization

The rest of the thesis is organised as follows:

Chapter 2 provides an introduction to the HOCs. The HOCs for univariate and multivariate random variables are derived. A few important properties of cumulants are also established.

Chapter 3 addresses the AMC of the QPSK-variant and 8 -PSK signals over spatially correlated MIMO channels. To distinguish the above modulation types, a cumulant-based AMC method is proposed by considering the fourth-order cumulants of the signal, the signal down-sampled by a factor of 2 and the backward difference signal.

Chapter 4 presents a cooperative AMC method for MIMO systems in a multi-antenna sensor network. The proposed method employs a centralized cooperative classification framework with the future-level fusion to distinguish the modulation types BPSK, OQPSK, QPSK, $\frac{\pi}{4}$-QPSK, 8-PSK,16-QAM and 64-QAM.

Chapter 5 addresses the problem of AMC over spatially correlated MIMO keyhole channels. A novel algorithm, namely the direct modulation recognition (DMR) algorithm, is proposed to distinguish the lower order PSK constellations, namely BPSK, QPSK and OQPSK. The proposed algorithm employs the ratios of HOCs derived from the received signal and its backward difference as AMC features. These features are chosen so that the contributions of the channel-coefficients are cancelled. Thus, the DMR algorithm does not require the CSI at

the receiver.

Chapter 6 addresses the problem of AMC over correlated MIMO AF-relay fading channels. An AMC method, namely relay assisted (RA)-AMC, is proposed to classify a pool of modulation types, namely BPSK, OQPSK, QPSK, $\frac{\pi}{4}$-QPSK, 8-PSK and 16-QAM. The proposed method involves two steps. In the first step, the method employs a cumulant feature vector derived directly from the received signal to distinguish BPSK, OQPSK and the sub-pool $Q_1 = \{QPSK, \frac{\pi}{4} - QPSK, 8 - PSK, 16 - QAM\}$ as a whole. This cumulant feature provides resistance against noise amplification that occurs in a correlated AF-relay system. In the second step, it employs a cumulant feature vector derived from the equalized signal to distinguish the modulation types in Q_1.

Chapter 7 concludes the thesis with a summary of work done and suggesting a few research directions.

1.7 Summary

This chapter presented a brief introduction to AMC and its potential applications. The chapter also presented a survey of AMC algorithms designed for MIMO systems. The limitations of the existing AMC algorithms were highlighted and four problems were formulated. Finally, the organization of this thesis was presented.

2

Mathematical Preliminaries of Cumulants

Contents

2.1 Introduction

Like moments, cumulants are important parameters of a random variable. The HOCs are widely used AMC features as they are resilient to Gaussian noise. This chapter provides the mathematical preliminaries of cumulants. A few important properties of cumulants are established.

2.2 Cumulants

2.2.1 Moment and Moment Generating Function

Consider a random variable x with probability density function $f_x(u)$, $u \in R_x$. The k^{th} moment of x is defined by

$$E(x^k) = \int_{-\infty}^{\infty} u^k f_x(u) dx \tag{2.1}$$

provided $\int_{-\infty}^{\infty} |u|^k f_x(u) du$ exists.

The moment generating function (MGF) $M_x(s)$ is defined as

$$M_x(s) = E(e^{sx}) = \int_{R_x} f_x(u) e^{su} du. \tag{2.2}$$

Taylor series expansion of $M_x(s)$ about the origin gives

$$M_x(s) = E(e^{sX}) = 1 + sE(x) + \frac{s^2E(x^2)}{2!} + \frac{s^3E(x^3)}{3!} + \frac{s^4E(x^4)}{4!} + ... = \sum_{k=0}^{\infty} \frac{s^kE(x^k)}{k!}. \tag{2.3}$$

2.2.2 Cumulant and Cumulant Generating Function

The cumulant generating function (CGF) $K(s)$ of x is defined as

$$K(s) = lnM_x(s). \tag{2.4}$$

The cumulants are obtained from the Taylor series expansion of $K(s)$ about the origin. Thus

$$K(s) = \sum_{k=1}^{\infty} \frac{s^kC_k(x)}{k!} \tag{2.5}$$

where $C_k(x)$ is the k^{th}-order cumulant of x and can be derived as

$$C_k(x) = \frac{d^k ln M_x(s)}{ds^k}|_{s=0}. \tag{2.6}$$

2.2.2.1 Relationship between Moments and Cumulants

From Eqn. 24

$$M_x(s) = e^{K(s)}. \tag{2.7}$$

In terms of the power series expansion of both the sides, we get

$$1 + sE(x) + \frac{s^2E(x^2)}{2!} + \frac{s^3E(x^3)}{3!} + ... = 1 + (sC_1(x) + \frac{s^2C_2(x)}{2!} + ...) + \frac{(sC_1(x) + \frac{s^2C_2(x)}{2!} + ...)^2}{2!} + ... \tag{2.8}$$

Comparing the coefficients of $s^k, k = 1, ..., 4$ in both the sides, the relations between moments and cumulants can be obtained. For example, the first four moments can be expressed in terms of the cumulants as

$$E(x) = C_1(x), \tag{2.9}$$

$$E(x^2) = C_2(x) + (C_1(x))^2, \tag{2.10}$$

$$E(x^3) = C_3(x) + 3C_2(x)C_1(x) + (C_1(x))^3 \tag{2.11}$$

and

$$E(x^4) = C_4(x) + 4C_3(x)C_1(x) + 3(C_2(x))^2 + 6C_2(x)(C_1(x))^2 + (C_1(x))^4. \tag{2.12}$$

Similarly, the first four cumulants can be expressed in terms of the moments as

$$C_1(x) = E(x), \tag{2.13}$$

$$C_2(x) = E(x^2) - (E(x))^2, \tag{2.14}$$

$$C_3(x) = E(x^3) - 3E(x^2)E(x) + 2(E(x))^3 \tag{2.15}$$

and

$$C_4(x) = E(x^4) - 4E(x^3)E(x) - 3(E(x^2))^2 + 12E(x^2)(E(x))^2 - 6(E(x))^4. \tag{2.16}$$

2.2.3 Properties of Cumulants

2.2.3.1 Additive Property

The additive property of cumulants states that the cumulant of sum of two independent random variables is equal to the sum of the cumulants of the individual random variables. Consider two independent random variables x and y. According to the additive property,

$$C_k(x+y) = C_k(x) + C_k(y). \tag{2.17}$$

Proof: We have

$$K_{x+y}(s) = lnE(e^{s(x+y)}) \tag{2.18}$$

$$= lnE[e^{sx}e^{sy}] \tag{2.19}$$

$$= ln(E[e^{sx}]E[e^{sy}]) \tag{2.20}$$

$$= ln(E[e^{sx}] + lnE[e^{sy}]) \tag{2.21}$$

$$= K_x(s) + K_y(s). \tag{2.22}$$

Therefore,

$$C_k(x+y) = C_k(x) + C_k(y). \tag{2.23}$$

2.2.3.2 Scaling Property

Let $x = ay$, a is constant. The k^{th} order cumulnat of x is given as

$$C_k(x) = a^k C_k(y). \tag{2.24}$$

2.2.4 Cumulants of Normal Random Variables

The PDF of a normal random variable x is given by

$$f_x(u) = \frac{1}{\sqrt{2\pi\sigma^2}} e^{-\frac{(u-\mu)^2}{2\sigma^2}} \tag{2.25}$$

where μ is the mean and σ^2 is the variance of the distribution. The corresponding MGF $M_x(s)$ is given as

$$M_x(s) = e^{\mu s + \frac{\sigma^2 s^2}{2}}. \tag{2.26}$$

The CGF of x is then given as

$$K(s) = \mu s + \frac{\sigma^2 s^2}{2}. \tag{2.27}$$

Therefore,

$$C_1(x) = \frac{d}{ds}(\mu s + \frac{\sigma^2 s^2}{2})|_{s=0} = \mu, \tag{2.28}$$

$$C_2(x) = \frac{d^2}{ds^2}(\mu s + \frac{\sigma^2 S^2}{2})|_{s=0} = \sigma^2 \tag{2.29}$$

and

$$C_3(x) = \frac{d^3}{ds^3}(\mu s + \frac{\sigma^2 s^2}{2})|_{s=0} = 0 \tag{2.30}$$

Therefore, $C_k(x) = 0,\ for\ k \geq 3$. Thus, the HOCs are resistant to the Gaussian noise. This property is exploited when cumulants are used as classification features.

2.2.5 Multivariate Cumulants

Consider a random vector $\mathbf{x} = (x_1, x_2, ..., x_n)$. Adopting Einsteins summation [62] convention for notational simplicity, we denote $s_i x_i = s_1 x_1 + s_2 x_2 + ... + s_n x_n$, $s_i s_j x_i x_j = (s_1 x_1 + s_2 x_2 + ... + s_n x_n)^2 = (s_i x_i)^2$, $s_i s_j s_k x_i x_j x_k = (s_1 x_1 + s_2 x_2 + ... + s_n x_n)^3 = (s_i x_i)^3$,and so on.

Now, $M_{\mathbf{x}}(s)$ can be expanded as

$$M_{\mathbf{x}}(s) = E(e^{s_1 x_1 + s_2 x_2 + ... + s_n x_n}). \tag{2.31}$$

The Taylor series expansion of $M_{\mathbf{x}}(s)$ about the origin gives

$$M_{\mathbf{x}}(s) = 1 + s_i E(x_i) + \frac{1}{2!} s_i s_j E(x_i x_j) + \frac{1}{3!} s_i s_j s_k E(x_i x_j x_k) + ... \tag{2.32}$$

Now, the CGF of $\mathbf{x}$ is given as

$$K_{\mathbf{x}}(s) = lnM_{\mathbf{x}}(s). \tag{2.33}$$

The cumulants $C(x_i, x_j), C(x_i, x_j, x_k), ...$ are obtained as coefficients in the Taylor series expansion of $K_{\mathbf{x}}(s)$ about the origin

$$K_{\mathbf{x}}(s) = s_i C(x_i) + \frac{1}{2!} s_i s_j C(x_i, x_j) + \frac{1}{3!} s_i s_j s_k C(x_i, x_j, x_k) + ... \tag{2.34}$$

Now, MGF can be written as

$$M_{\mathbf{x}}(s) = e^{s_i C(x_i)+\frac{1}{2!}s_i s_j C(x_i,x_j)+\frac{1}{3!}s_i s_j s_k C(x_i,x_j,x_k)+\ldots} \tag{2.35}$$
$$= 1 + s_i C(x_i) + \frac{1}{2!}s_i s_j C(x_i, x_j) + \frac{1}{3!}s_i s_j s_k C(x_i, x_j, x_k) + \ldots +$$
$$\frac{1}{2!}(s_i C(x_i) + \frac{1}{2!}s_i s_j C(x_i, x_j) + \frac{1}{3!}s_i s_j s_k C(x_i, x_j, x_k) + \ldots)^2 + \ldots$$

Comparing the coefficients in both the sides in Eqn. 2.35, the moments can be expressed in terms of the cumulants as follows:

$$E(x_i x_j) = C(x_i, x_j) + C(x_i)C(x_j), \tag{2.36}$$

$$E(x_i x_j x_k) = C(x_i, x_j, x_k) + C(x_i, x_j)C(x_k) + C(x_i, x_k)C(x_j) + C(x_j, x_k)C(x_i) + C(x_i)C(x_j)C(x_k) \tag{2.37}$$
$$= C(x_i, x_j, x_k) + C(x_i, x_j)C(x_k)[3] + C(x_i)C(x_j)C(x_k),$$

$$E(x_i x_j x_k x_l) = C(x_i, x_j, x_k, x_l) + C(x_i, x_j, x_k)C(x_l)[4] + C(x_i, x_j)C(x_k, x_l)[3] + C(x_i x_j)C(x_k)C(x_l)[6] \tag{2.38}$$
$$+ C(x_i)C(x_j)C(x_k)C(x_l),$$

$$E(x_i x_j x_k x_l x_p x_q) = C(x_i, x_j, x_k, x_l, x_p, x_q) + C(x_i)C(x_j, x_k, x_l, x_p, x_q)[6] + C(x_i, x_j)C(x_k, x_l, x_p, x_q)[15]$$
$$+ C(x_i, x_j, x_k)C(x_l, x_p, x_q)[10] + C(x_i)C(x_j)C(x_k, x_l, x_p, x_q)[15]$$
$$+ C(x_i)C(x_j, x_k)C(x_l, x_p, x_q)[60] + C(x_i, x_j)C(x_k, x_l)C(x_p, x_q)[15] \tag{2.39}$$
$$+ C(x_i)C(x_j)C(x_k)C(x_l, x_p, x_q)[60] + C(x_i)C(x_i)C(x_k, x_l)C(x_p, x_q)[60]$$
$$+ C(x_i)C(x_j)C(x_k)C(x_l)C(x_p, x_q)[15] + C(x_i)C(x_j)C(x_k)C(x_l)C(x_p)C(x_q)$$

and so on. Each parenthetical number indicates a sum over distinct partitions having the same

block sizes. Now, the cumulants can be expressed in terms of the moments as

$$C(x_i, x_j) = E(x_i x_j) - E(x_i)E(x_j), \tag{2.40}$$

$$C(x_i, x_j, x_k) = E(x_i x_j x_k) - E(x_i x_k)E(x_j)[3] + 2E(x_i)E(x_j)E(x_k), \tag{2.41}$$

$$C(x_i, x_j, x_k, x_l) = E(x_i x_j x_k x_l) - E(x_i x_j x_k)E(x_l)[4] - E(x_i x_j)E(x_k x_l)[3] \tag{2.42}$$

$$- 2E(x_i x_j)E(x_k)E(x_l[6] - 6E(x_i)E(x_j)E(x_k)E(x_l), \tag{2.43}$$

$$\begin{aligned} C(x_i, x_j, x_k, x_l, x_p, x_q) = {} & E(x_i x_j x_k x_l x_p x_q) - E(x_i)E(x_j x_k x_l x_p x_q)[6] - E(x_i x_j)E(x_k x_l x_p x_q)[15] \\ & - E(x_i x_j x_K)E(x_l x_p x_q)[10] + 2E(x_i)E(x_j)E(x_k x_l x_p x_q)[15] \\ & + 2E(x_i)E(x_j x_k)E(x_l x_p x_q)[60] + 2E(x_i x_j)E(x_k x_l)E(x_p x_q)[15] \\ & - 6E(x_i)E(x_j)E(x_k)E(x_l x_p x_q)[60] - 6E(x_i)E(x_i)E(x_k x_l)E(x_p x_q)[60] \\ & + 24E(x_i)E(x_j)E(x_k)E(x_l)E(x_p x_q)[15] + E(x_i)E(x_j)E(x_k)E(x_l)E(x_p)E(x_q) \end{aligned} \tag{2.44}$$

and so on. Now, the n^{th} order cumulant for the random variables x_1,x_2,...,x_n is given by [18]

$$C(x_1, ..., x_n) = \sum_{\forall v} (-1)^{r-1}(r-1)!E[\prod_{j \epsilon v_1} y_j]...E[\prod_{j \epsilon v_r} x_j] \tag{2.45}$$

where the summation is performed over all partitions $v = (v_1, ..., v_r)$ on the set of indices $1, ..., n$ and r is the number of elements in a given partition. For example, the fourth-order cumulants for zero mean random variables x_1, x_2, x_3 and x_4 is given by

$$\begin{aligned} C(x_1, x_2, x_3, x_4) = {} & E(x_1 x_2 x_3 x_4) - E(x_1 x_2)E(x_3 x_4) \\ & - E(x_1 x_3)E(x_2 x_4) - E(x_1 x_4)E(x_2 x_3). \end{aligned} \tag{2.46}$$

Now, the n^{th} order m conjugate cumulant of a random variable x is defined as

$$C_{n,m}(x) = C(\underbrace{x, ..., x}_{n-m}, \underbrace{x^*, ..., x^*}_{m}). \tag{2.47}$$

For instance, the fourth order cumulants of random variable x can be written in three ways depending upon the placement of conjugates. They are given as:

$$\begin{aligned} C_{40}(x) &= E(xxxx) - E(xx)E(xx) - E(xx)E(xx) - E(xx)E(xx) \\ &= E(x^4) - 3(E(x^2))^2, \end{aligned} \tag{2.48}$$

$$\begin{aligned} C_{41}(x) &= E(xxxx^*) - E(xx)E(xx^*) - E(xx)E(xx^*) - E(xx^*)E(xx) \\ &= E(x^3x^*) - 3(E(x^2))(E(|x^2|)) \end{aligned} \tag{2.49}$$

and

$$\begin{aligned} C_{42}(x) &= E(xxx^*x^*) - E(xx)E(x^*x^*) - E(xx^*)E(xx^*) - E(xx^*)E(xx^*) \\ &= E(|x|^4) - |E(x^2)|^2 - 2(E(|x|^2))^2 \end{aligned} \tag{2.50}$$

2.3 Summary

This chapter provided an introduction to cumulants. The HOCs for univariate and multivariate random variables were derived here. A few important properties of cumulants were also established.

3

Automatic Modulation Classification of QPSK-Variant and 8-PSK Signals over Spatially Correlated MIMO Channels

Contents

3.1 Introduction

In the current generation wireless system, the MIMO technology is preferred to the SISO technology as it provides a remarkable capacity gain [14]. Recently, the AMC of MIMO signals has drawn significant attention. In the earlier chapters, we discussed the utility of AMC in MIMO systems. For instance, an LA-MIMO system dynamically updates the modulation type depending on the channel condition. The receiver requires the modulation type information to demodulate the received signal. For that, the transmitter needs to send the modulation type information in each signal frame. It involves an overhead which can be avoided by using AMC.

A number of algorithms have been proposed to address the AMC problem for MIMO systems [1, 15, 17–28]. These works were summarized in Table 1.3. of Chapter 1. The majority of these works have employed the FB approach as they are easily implementable and computationally less complex. The HOMs and HOCs are employed as AMC features by these FB approaches. The HOCs are more widely used for their resistance to Gaussian noise. Different algorithms considered different modulation types for classification. However, the discrimination among the modulation types QPSK, OQPSK, $\frac{\pi}{4}$-QPSK and 8-PSK has not been addressed.

Swami et al., in [4], showed that different digitally modulated signals exhibit distinct 4^{th}-order cumulant values. The robustness of 4^{th}-order cumulants against Gaussian noise makes them attractive AMC features. In [15], Muhlhaus et al. proposed an AMC algorithm based on the 4^{th}-order cumulants over an uncorrelated MIMO channel. However, the 4^{th}-order cumulants fail to distinguish the QPSK-variant and 8-PSK signals. This can be attributed to the fact that the HOC values of the QPSK-variant and 8-PSK signals are ambiguous. The QPSK and OQPSK signals exhibit same HOC values. Similarly, the $\frac{\pi}{4}$-QPSK and 8-PSK signals share the same HOC values.

This chapter addresses the AMC of QPSK variants and 8-PSK over spatially correlated MIMO channels. We adopt a feature-based strategy with the 4^{th}-order cumulants as the AMC features. The rest of the chapter is organized as follows: Section 3.2 presents the system model. Section 3.3 presents the channel equalization techniques. 4^{th}-order cumulants of the QPSK variants and the 8-PSK signals are discussed in Section 3.4. Section 3.5 describes the proposed

cumulant features. The proposed AMC method is presented in Section 3.6. The simulation results and the evaluation of the proposed method are presented in Section 3.7. Finally, a summary is presented in Section 3.8.

3.2 MIMO System Model

Consider the spatial multiplexing MIMO system with N_T transmitting and N_R receiving antennas as discussed in Section 1.2. The received signal at the k^{th} instant can be written as

$$\mathbf{y}(k) = \mathbf{H}\mathbf{x}(k) + \boldsymbol{\eta}(k), \tag{3.1}$$

where $\mathbf{y}(k) = [y_1(k)...y_{N_R}(k)]^T$ is an $N_R \times 1$ received signal symbol vector, $\mathbf{x}(k) = [x_1(k)...x_{N_T}(k)]^T$ is an $N_T \times 1$ transmitted signal symbol vector, $\boldsymbol{\eta}(k) = [\eta_1(k)...\eta_{N_R}(k)]^T$ is an $N_R \times 1$ vector of zero mean white circularly complex Gaussian noise and $\mathbf{H}$ is an $N_R \times N_T$ spatially correlated complex channel matrix and can be represented as

$$\mathbf{H} = \begin{pmatrix} h_{11} & h_{12} & \cdots & h_{1N_T} \\ h_{21} & h_{22} & \cdots & h_{2N_T} \\ \vdots & \vdots & \ddots & \vdots \\ h_{N_R1} & h_{N_R2} & \cdots & h_{N_RN_T} \end{pmatrix}, \tag{3.2}$$

where $h_{i,j}$ is the channel response between i^{th} receiving antenna and j^{th} transmitting antenna. Here, it is assumed that the channel is frequency flat and time invariant MIMO channel. In this work, we consider two kinds of fading, namely Rayleigh fading and Rician fading.

3.2.1 Rayleigh Fading

Rayleigh fading is exhibited by the multipath environment with no direct path between the transmitter and the receiver [14]. The channel response $h_{i,j}$ can be represented by a sum of a number of random complex phasors having random amplitudes and random phase angles. It is reasonable to assume that the phase is uniformly distributed as the phase angles have no preferential values. Therefore , $h_{i,j}$ is a sum of IID circularly symmetric complex random variables. Using central limit theorem, one can show that $h_{i,j} = X + iY$ is a complex Gaussian random variable i.e., X and Y represent the IID zero-mean Gaussian random variables with equal

variances σ^2. The magnitude response of the channel entries (i.e., $|h_{i,j}|$) is Rayleigh distributed. The magnitude of $|h_{i,j}|$ can be written as

$$|h_{i,j}| = \sqrt{(X^2 + Y^2)}. \tag{3.3}$$

The probability density function (PDF) of $|h_{i,j}|$ is given by [14]

$$f_{|h_{i,j}|}(z) = \frac{z}{\sigma^2} e^{-\frac{z^2}{2\sigma^2}}, z \geq 0. \tag{3.4}$$

3.2.2 Rician Fading

Rician fading occurs in a multipath environments with a direct path between the transmitter and the receiver [14]. It captures the effect of both Rayeigh fading and line of sight propagation. The channel matrix can be modelled as

$$\mathbf{H} = \sqrt{\frac{K}{K+1}}\mathbf{H}_{LOS} + \sqrt{\frac{1}{K+1}}\mathbf{H}_S \tag{3.5}$$

where $\mathbf{H}_S$ is the component of the channel matrix contributed by scattering, $\mathbf{H}_{LOS}$ is the component of the channel matrix contributed by the line of sight propagation and K is known as the Rician factor, which is defined as $K \triangleq \frac{Power\ in\ direct\ component}{Power\ in\ scattered\ component}$ [14].

In addition to the spatial fading, the spatial correlation plays a crucial role in practical MIMO systems [14]. The spatially correlated MIMO system is discussed next.

3.2.3 Spatial Correlation

The antennas become correlated when they are closely spaced. The close spacing of antennas increases the electromagnetic coupling that decreases the differences in the channel gains of the separated antennas. This in turn increases the correlation between the neighbouring antennas. In addition to this, the channel correlation also depends on: 1) the range of angles over which signals depart the transmitter, known as angle-of-departure (AoD) and 2) the range of angles over which multipath signals arrive at the receiver, known as angle-of-arrival (AoA). The channel correlation tends to increase with a decrease in AOD and AOA.

The Kronecker model is widely used in the MIMO literature for its simplicity [14, 18, 63,

64]. It assumes that the spatial receiver and transmitter correlations are separable. Here, for the investigation, we also employ the Kronecker model. Now, the spatially-correlated MIMO channel model can be written as as [18]

$$\boldsymbol{H} = \boldsymbol{\theta}_R^{1/2} \boldsymbol{H}_1 \boldsymbol{\theta}_T^{1/2} \tag{3.6}$$

where $\boldsymbol{H}_1$ is an $N_R \times N_T$ full rank channel gain matrix, $\boldsymbol{\theta}_R$ and $\boldsymbol{\theta}_T$ are the receiver and the transmitter correlation matrices respectively and $(.)^{1/2}$ stands for the Hermitian square root of a matrix.

For this investigation, we consider the exponential correlation model. For an L- antenna array, the exponential correlation matrix is more preferred over the uniform correlation matrix as it is a more realistic model [65–68] . This is contributed by the fact that the correlation of the adjacent antennas is higher than that of the distant antennas. The exponential correlation matrix $\boldsymbol{\theta}$ of size $L \times L$ can be written as [69]

$$\boldsymbol{\theta} = \begin{pmatrix} 1 & \rho & \cdots & \rho^{L-1} \\ \rho^* & 1 & \cdots & \rho^{L-2} \\ \vdots & \vdots & \ddots & \vdots \\ (\rho^*)^{L-1} & (\rho^*)^{L-2} & \cdots & 1 \end{pmatrix}, \tag{3.7}$$

where ρ is the correlation coefficient of adjacent antennas.

Let ρ_T and ρ_R denote the correlation coefficient of two adjacent antennas of the transmitter and the receiver, respectively. Putting $\rho = \rho_T$ and $L = N_T$ in Eqn. 3.7, we get $\boldsymbol{\theta}_T$ matrix . Similarly substituting $\rho = \rho_R$ and $L = N_R$ gives $\boldsymbol{\theta}_R$ matrix.

3.3 Channel Equalization

The mutual interference generated by the spatial channel **H** alters the statistical properties of the modulated signal. This makes AMC a challenging task. Therefore, it is imperative to cancel the channel mixing effect prior to AMC. In this work, we consider two channel equalization techniques, namely the zero forcing (ZF) equalizer [14] and the joint approximate diagonalization of eigen matrices (JADE) algorithm [31, 70]. The first requires channel state information

(CSI) at the receiver while the second estimates CSI blindly from the observed signal. These two techniques are outlined below.

3.3.1 ZF Equalization

The ZF equalizer pre-multiplies the received signal by the Moore-Penrose pseudo inverse $\mathbf{H}^+$ of $\mathbf{H}$. $\mathbf{H}^+$ is given by [14]

$$\mathbf{H}^+ = (\mathbf{H}^H\mathbf{H})^{-1}\mathbf{H}^H. \tag{3.8}$$

The equalized signal can be written as

$$\begin{aligned}\mathbf{z}(k) &= \mathbf{H}^+\mathbf{y}(k) \\ &= (\mathbf{H}^H\mathbf{H})^{-1}\mathbf{H}^H\mathbf{H}\mathbf{x}(k) + (\mathbf{H}^H\mathbf{H})^{-1}\mathbf{H}^H\boldsymbol{\eta}(k) \\ &= \mathbf{x}(k) + \mathbf{w}(k)\end{aligned} \tag{3.9}$$

where $\mathbf{w}(k) = (\mathbf{H}^H\mathbf{H})^{-1}\mathbf{H}^H\boldsymbol{\eta}(k)$, is a noise term enhanced by the least squares.

The elimination of interference in zero-forcing detection comes at the expense of the noise amplification. Also, it is assumed that the receiver has CSI.

3.3.2 JADE Equalization

JADE is a popular independent component analysis (ICA) technique [31, 70]. The ICA methods are used to separate the independent components (ICs) from a linear mixture of random processes. The general idea to determine the ICs is to calculate a demixing matrix which approximates the inverse of the mixing matrix. The identifiability of the ICs requires: 1) the sources to be separated are statistically independent and 2) the number of observations is equal or greater than the number of sources (i.e. mixing matrix is full rank). If there are N_T sources and N_R mixtures, the ICA model (without noise) can be represented as

$$\begin{pmatrix} y_1(k) \\ \vdots \\ y_{N_R}(k) \end{pmatrix} = \begin{pmatrix} h_{11} & h_{12} & \cdots & h_{1N_T} \\ h_{21} & h_{22} & \cdots & h_{2N_T} \\ \vdots & \vdots & \ddots & \vdots \\ h_{N_R1} & h_{N_R2} & \cdots & h_{N_RN_T} \end{pmatrix} \begin{pmatrix} x_1(k) \\ \vdots \\ x_{N_T}(k) \end{pmatrix} \tag{3.10}$$

The above expression can also be written as

$$\mathbf{y} = \mathbf{Hx} \tag{3.11}$$

The goal of ICA is to extract the independent sources **x** and mixing matrix **H** from **y**. This can be done by calculating a demixing matrix, **W**, which approximates the inverse of **H**.

The JADE algorithm separates the ICs by using the cumulant tensor. The details of the JADE method can be found in [31, 70] and is outlined below.

The cumulant tensor can be considered as a four dimensional array whose entries are given by the fourth-order cross-cumulants of the data $C(y_i, y_j, y_k, y_l)$, where the indices i,j,k,l are from 1 to n, . We can derive all fourth-order cumulants of linear combinations of y_i as linear combination of the cumulants of y_i. One can observe this using the additive properties of the cumulants. Now, for a linear combination of y_i, the kurtosis is given by

$$\begin{aligned} Kurt \sum_i w_i y_i &= C(\sum_i w_i y_i, \sum_j w_j y_j, \sum_k w_k y_k, \sum_l w_l y_l) \\ &= \sum_{i,j,k,l} w_i^4 w_j^4 w_k^4 w_l^4 C(y_i, y_j, y_k, y_l). \end{aligned}$$

where *Kurt* denotes the kurtosis.

One can note that all the cumulants with at least two different indices vanish if the y_i are independent.

The cumulant tensor is a linear operator. For such a tensor, there exists a linear transformation on the space of $n \times n$ matrices. The i, jth entry of the matrix given by the transformation, say $F_{i,j}$, can be defined as

$$\mathbf{F}_{ij}(\mathbf{M}) = \sum_{k,l=1,n} m_{kl} C(y_i, y_j, y_k, y_l), 1 \leq i, j \leq n \tag{3.12}$$

where m_{kl} denotes the entries of **M** and $C(y_i, y_j, y_k, y_l)$ denotes the 4^{th}-order cross-cumulant of the data.

As any symmetric linear operator, the cumulant tensor has an eigenvalue decomposition (EVD). An eigen matrix of the tensor is, by definition, a matrix M such that

$$F(\mathbf{M}) = \lambda \mathbf{M} \tag{3.13}$$

i.e., $F_{ij}(M) = \lambda M_{ij}$, where λ is a scalar eigenvalue.

Consider the ICA model, with whitened data:

$$\mathbf{z} = \mathbf{W}^T \mathbf{x} \tag{3.14}$$

There exists a special structure of the cumulant tensor of z which can be observed in the eigenvalue decomposition. In fact, eigen matrix is of the form

$$\mathbf{M} = \mathbf{w}_m \mathbf{w}_m^T, m = 1, ..., n \tag{3.15}$$

The vector $\mathbf{w}_m$ represents one of the rows of the matrix $\mathbf{W}$. This can be validated by calculating the linearity properties of cumulants.

$$\begin{aligned} F_{ij}(\mathbf{w}_m \mathbf{w}_m^T) &= \sum_{kl} w_{mk} w_{ml} C(z_i, z_j, z_k, z_l) \\ &= \sum_{kl} w_{mk} w_{ml} C(\sum_q w_{qi} x_q, \sum_{q'} w_{q'j} x_{q'}, \sum_r w_{rk} x_r, \sum_{r'} w_{r'l} x_{r'}) \\ &= \sum_{klqq'rr'} w_{mk} w_{ml} w_{qi} w_{q'j} w_{rk} w_{r'l} C(x_q x_{q'} x_r x_{r'}) \end{aligned}$$

Now, as x_i are independent, only those cumulants where $q = q^{'} = r = r^{'}$ are non-zero, which leads to

$$F_{ij}(\mathbf{w}_m \mathbf{w}_m^T) = \sum_{klq} w_{mk} w_{ml} w_{qi} w_{qj} w_{qk} w_{ql}\ kurt(x_q) \tag{3.16}$$

As the rows of W are orthognal, we have $\sum_k w_{mk} w_{qk} = \delta_{mq}$, and likewise for index l. Taking the sum first with respect to k and then with respect to l results in

$$\begin{aligned} F_{ij}(\mathbf{w}_m \mathbf{w}_m^T) &= \sum_{lq} w_{ml} w_{qi} w_{qj} \delta_{mq} w_{ql}\ kurt(x_q) \\ &= \sum_q w_{qi} w_{qj} \delta_{mq} \delta_{mq}\ kurt(x_q) = w_{mi} w_{mj}\ kurt(x_m) \end{aligned}$$

This validates that matrices are of the form in (3.15) are eigen matrices of the tensor. The kurtosis of the independent components gives the corresponding eigen values. Furthermore, it can be shown that all other eigen values of the tensor are zero.

The JADE algorithm solves the problem of equal eigenvalues of the cumulant tensor. The algorithm considers the the tensor EVD as a preprocessing step. We can view the Eigenvalue decomposition as diagonalization. In the present case, the above developments can be stated as follows: The matrix $\mathbf{W}$ diagonalizes $\mathbf{F}(\mathbf{M})$ for any $\mathbf{M}$. To put it another way, $\mathbf{WF}(\mathbf{M})\mathbf{W}^T$ is diagonal. This is contributed by the fact that the matrix $\mathbf{F}$ is of a linear combination of terms of the form $w_i w_i^T$ under the assumption that the ICA model holds.

Therefore, it is possible to take a set of different matrices$\mathbf{M}_i, i = 1, .., k$, and try to make the matrices $\mathbf{WF}(\mathbf{M}_i)\mathbf{W}^T$ as diagonal as possible. In reality, making exact diagonal is not possible because of model mismatch and sampling errors.

We can measure the diagonality of a matrix $Q = \mathbf{WF}(\mathbf{M}_i)\mathbf{W}^T$; for instance, one can calculate the sum of the squares of off-diagonal elements: $\sum_{k \neq l} q_{kl}^2$. In other words, as an orthogonal matrix $\mathbf{W}$ does not alter the total sum of squares of a matrix, minimization of the sum of squares of off-diagonal elements is equivalent to the maximization of the sum of squares of diagonal elements. Thus, the following measure is adopted:

$$\mathcal{J}_{JADE}(\mathbf{W}) = \sum_i ||diag\mathbf{W}F(\mathbf{M}_i)\mathbf{W}^T||^2 \tag{3.17}$$

where $||diag(.)||^2$ denotes the sum of squares of the diagonal elements. Maximization of $\mathcal{J}_{JADE}$ is then one method of joint approximate diagonalization of the $\mathbf{F}(\mathbf{M}_i)$.

3.3.3 4^{th}-Order Cumulants of a QPSK Signal

In a QPSK signalling scheme, the bit transitions of the even and odd bit streams occur at the same time instants. This allows the phase of a QPSK signal to change as high as 180^o at an instant. The normalised constellation of a QPSK signal is given by

$$\mathbf{C}_1 = \{1, -1, +i, -i\}. \tag{3.18}$$

Consider a QPSK signal $x_1(k)$ at an instant k . The probability mass function (PMF) of the RV x_1 representing the QPSK constellation is given by

$$P_{x_1}(x) = \left\{ \frac{1}{4}, x \in \mathbf{C}_1 \right. . \tag{3.19}$$

Using Eqns. 2.48-2.50, Chapter 2, the 4^{th}-order cumulants of x_1 are obtained as

$$C_{40}(x_1) = \frac{1}{4}(1^4 + (-1)^4 + i^4 + (-i)^4) - 3(\frac{1}{4}(1^2 + (-1)^2 + i^2 + (-i)^2)^2 = 1, \tag{3.20}$$

$$\begin{aligned} C_{42}(x_1) = \frac{1}{4}(1^4 + |-1|^4 + |i|^4 + |-i|^4) - \frac{1}{16}(|(1^2 + (-1)^2 + (i)^2 + (-i)^2|^2) \\ - \frac{1}{8}(|1|^2 + |-1|^2 + |i|^2 + |-i|^2)^2 = -1 \end{aligned} \tag{3.21}$$

and

$$\begin{aligned} C_{41}(x_1) = \frac{1}{4}(1^4 + (-1)^4 + (i)^3(i)^* + (-i)^3(-i)^*) - \frac{3}{16}(1^2 + (-1)^2 + i^2 + (-i)^2) \\ (|1|^2 + |-1|^2 + |i|^2 + |-i|^2) = 0. \end{aligned} \tag{3.22}$$

3.3.4 4^{th}-Order Cumulants of an OQPSK Signal

An OQPSK signal has the same constellation as that of a QPSK signal. The only difference is that in an OQPSK signal, there is an offset of one bit period in the relative alignment of the even and odd bit streams. This does not allow the phase of an OQPSK signal to change by greater than 90^o. Suppose, $x_2(k)$ is an OQPSK signal. The PMF of the RV x_2 representing the OQPSK constellation is given by

$$P_{x_2}(x) = \left\{ \frac{1}{4}, x \in \mathbf{C}_1 \right. . \tag{3.23}$$

Using Eqns. 2.48-2.50, Chapter 2, the 4^{th}-order cumulants of x_2 are obtained as

$$C_{40}(x_2) = \frac{1}{4}(1^4 + (-1)^4 + i^4 + (-i)^4) - 3(\frac{1}{4}(1^2 + (-1)^2 + i^2 + (-i)^2)^2 = 1, \tag{3.24}$$

$$C_{42}(x_2) = \frac{1}{4}(1^4 + |-1|^4 + |i|^4 + |-i|^4) - \frac{1}{16}(|(1^2 + (-1)^2 + (i)^2 + (-i)^2|^2) - \frac{1}{8}(|1|^2 + |-1|^2 + |i|^2 + |-i|^2)^2 = -1 \tag{3.25}$$

and

$$C_{41}(x_2) = \frac{1}{4}(1^4 + (-1)^4 + (i)^3(i)^* + (-i)^3(-i)^*) - \frac{3}{16}(1^2 + (-1)^2 + i^2 + (-i)^2) (|1|^2 + |-1|^2 + |i|^2 + |-i|^2) = 0. \tag{3.26}$$

3.3.5 4^{th}-Order Cumulants of a $\frac{\pi}{4}$-QPSK Signal

A $\frac{\pi}{4}$-QPSK modulator selects its symbols from the QPSK and $\frac{\pi}{4}$-shifted QPSK constellations. If the modulator selects the odd symbols from the QPSK constellation, the even symbols will be selected from the $\frac{\pi}{4}$ shifted QPSK constellation or vice versa. The normalized constellation points of $\frac{\pi}{4}$-QPSK modulator is given by

$$\mathbf{C}_2 = \{1, -1, +i, -i, (\frac{1}{\sqrt{(2)}})(1+i), (\frac{1}{\sqrt{(2)}})(1-i), (\frac{1}{\sqrt{(2)}})(-1+i), (\frac{1}{\sqrt{(2)}})(-1-i)\}. \tag{3.27}$$

Consider a $\pi/4$-QPSK modulated signal $x_3(k)$. The PMF of the RV x_3 representing the $\pi/4$-QPSK constellation is then given by

$$P_{x_3}(x) = \left\{ \frac{1}{8}, x \in \mathbf{C}_2 \right. . \tag{3.28}$$

Using Eqns. 2.48-2.50, Chapter 2, the 4^{th}-order cumulants of $\frac{\pi}{4}$-QPSK signal are given as

$$C_{40}(x_3) = \frac{1}{8}(1^4 + (-1)^4 + (i)^4 + (-i)^4 + ((\frac{1}{\sqrt{(2)}})(1+i))^4 + ((\frac{1}{\sqrt{(2)}})(1-i))^4 + ((\frac{1}{\sqrt{(2)}})(-1+i))^4 + ((\frac{1}{\sqrt{(2)}})(-1-i))^4) - 3(\frac{1}{8}(1^2 + (-1)^2 + i^2 + (-i)^2 + ((\frac{1}{\sqrt{(2)}})(1+i))^2 + ((\frac{1}{\sqrt{(2)}})(1-i))^2 + ((\frac{1}{\sqrt{(2)}})(-1+i))^2 + ((\frac{1}{\sqrt{(2)}})(-1-i))^2))^2 = 0, \tag{3.29}$$

$$
\begin{aligned}
C_{42}(x_3) = \frac{1}{8}(1^4 + |-1|^4 + |i|^4 + |-i|^4 + |(\frac{1}{\sqrt{(2)}})(1+i)|^4 + |(\frac{1}{\sqrt{(2)}})(1-i)|^4 \\
+ |(\frac{1}{\sqrt{(2)}})(-1+i)|^4 + |(\frac{1}{\sqrt{(2)}})(-1-i)|^4) - \frac{1}{64}|(1)^2 + (-1)^2 + (i)^2 + (-i)^2 \\
+ ((\frac{1}{\sqrt{(2)}})(1+i))^2 + ((\frac{1}{\sqrt{(2)}})(1-i))^2 + ((\frac{1}{\sqrt{(2)}})(-1+i))^2 \\
+ ((\frac{1}{\sqrt{(2)}})(-1-i))^2|^2 - \frac{1}{32}(|1|^2 + |-1|^2 + |i|^2 + |-i|^2 + |(\frac{1}{\sqrt{(2)}})(1+i)|^2 \\
+ |(\frac{1}{\sqrt{(2)}})(1-i)|^2 + |(\frac{1}{\sqrt{(2)}})(-1+i)|^2 + |(\frac{1}{\sqrt{(2)}})(-1-i)|^2)^2 = -1
\end{aligned}
\tag{3.30}
$$

and

$$
\begin{aligned}
C_{41}(x_3) = \frac{1}{8}(1^4 + (-1)^4 + (i)^3(i)^* + (-i)^3(-i)^* + ((\frac{1}{\sqrt{(2)}})(1+i))^3((\frac{1}{\sqrt{(2)}})(1+i))^* \\
+ ((\frac{1}{\sqrt{(2)}})(1-i))^3((\frac{1}{\sqrt{(2)}})(1-i))^* + ((\frac{1}{\sqrt{(2)}})(-1+i))^3((\frac{1}{\sqrt{(2)}})(-1+i))^* \\
+ ((\frac{1}{\sqrt{(2)}})(-1-i))^3((\frac{1}{\sqrt{(2)}})(-1-i))^*) - \frac{3}{64}(1^2 + (-1)^2 + i^2 + (-i)^2 \\
+ ((\frac{1}{\sqrt{(2)}})(1+i))^2 + ((\frac{1}{\sqrt{(2)}})(1-i))^2 + ((\frac{1}{\sqrt{(2)}})(-1+i))^2 \\
+ ((\frac{1}{\sqrt{(2)}})(-1-i))^2)(|1|^2 + |-1|^2 + |i|^2 + |-i|^2 + |(\frac{1}{\sqrt{(2)}})(1+i)|^2 \\
+ |(\frac{1}{\sqrt{(2)}})(1-i)|^2 + |(\frac{1}{\sqrt{(2)}})(-1+i)|^2 + |(\frac{1}{\sqrt{(2)}})(-1-i)|^2) = 0.
\end{aligned}
\tag{3.31}
$$

3.3.6 4^{th}-Order Cumulants of an 8-PSK Signal

An 8-PSK signal has the same constellation as that of a $\frac{\pi}{4}$-QPSK signal. Consider an 8-PSK signal $x_4(k)$. The PMF of the RV x_4 representing the 8-PSK constellation is given by

$$
P_{x_4}(x) = \left\{ \frac{1}{8}, x \in \mathbf{C}_2 \right. . \tag{3.32}
$$

Using Eqns. 2.48-2.50, Chapter 2, the fourth-order cumulants of $x_4(n)$ are given as

$$\begin{aligned} C_{40}(x_4) = \frac{1}{8}(1^4 + (-1)^4 + (i)^4 + (-i)^4 + ((\frac{1}{\sqrt{(2)}})(1+i))^4 + ((\frac{1}{\sqrt{(2)}})(1-i))^4 \\ + ((\frac{1}{\sqrt{(2)}})(-1+i))^4 + ((\frac{1}{\sqrt{(2)}})(-1-i))^4) - 3(\frac{1}{8}(1^2 + (-1)^2 \\ + i^2 + (-i)^2 + ((\frac{1}{\sqrt{(2)}})(1+i))^2 + ((\frac{1}{\sqrt{(2)}})(1-i))^2 + ((\frac{1}{\sqrt{(2)}})(-1+i))^2 \\ + ((\frac{1}{\sqrt{(2)}})(-1-i))^2))^2 = 0, \end{aligned} \tag{3.33}$$

$$\begin{aligned} C_{42}(x_4) = \frac{1}{8}(1^4 + |-1|^4 + |i|^4 + |-i|^4 + |(\frac{1}{\sqrt{(2)}})(1+i)|^4 + |(\frac{1}{\sqrt{(2)}})(1-i)|^4 \\ + |(\frac{1}{\sqrt{(2)}})(-1+i)|^4 + |(\frac{1}{\sqrt{(2)}})(-1-i)|^4) - \frac{1}{64}|(1)^2 + (-1)^2 + (i)^2 + (-i)^2 \\ + ((\frac{1}{\sqrt{(2)}})(1+i))^2 + ((\frac{1}{\sqrt{(2)}})(1-i))^2 + ((\frac{1}{\sqrt{(2)}})(-1+i))^2 \\ + ((\frac{1}{\sqrt{(2)}})(-1-i))^2|^2 - \frac{1}{32}(|1|^2 + |-1|^2 + |i|^2 + |-i|^2 + |(\frac{1}{\sqrt{(2)}})(1+i)|^2 \\ + |(\frac{1}{\sqrt{(2)}})(1-i)|^2 + |(\frac{1}{\sqrt{(2)}})(-1+i)|^2 + |(\frac{1}{\sqrt{(2)}})(-1-i)|^2)^2 = -1 \end{aligned} \tag{3.34}$$

and

$$\begin{aligned} C_{41}(x_4) = \frac{1}{8}(1^4 + (-1)^4 + (i)^3(i)^* + (-i)^3(-i)^* + ((\frac{1}{\sqrt{(2)}})(1+i))^3((\frac{1}{\sqrt{(2)}})(1+i))^* \\ + ((\frac{1}{\sqrt{(2)}})(1-i))^3((\frac{1}{\sqrt{(2)}})(1-i))^* + ((\frac{1}{\sqrt{(2)}})(-1+i))^3((\frac{1}{\sqrt{(2)}})(-1+i))^* \\ + ((\frac{1}{\sqrt{(2)}})(-1-i))^3((\frac{1}{\sqrt{(2)}})(-1-i))^*) - \frac{3}{64}(1^2 + (-1)^2 + i^2 + (-i)^2 \\ + ((\frac{1}{\sqrt{(2)}})(1+i))^2 + ((\frac{1}{\sqrt{(2)}})(1-i))^2 + ((\frac{1}{\sqrt{(2)}})(-1+i))^2 \\ + ((\frac{1}{\sqrt{(2)}})(-1-i))^2)(|1|^2 + |-1|^2 + |i|^2 + |-i|^2 + |(\frac{1}{\sqrt{(2)}})(1+i)|^2 \\ + |(\frac{1}{\sqrt{(2)}})(1-i)|^2 + |(\frac{1}{\sqrt{(2)}})(-1+i)|^2 + |(\frac{1}{\sqrt{(2)}})(-1-i)|^2) = 0. \end{aligned} \tag{3.35}$$

From the above analysis, we note the following:

Eqns. (3.20 – 3.26) show that the QPSK and OQPSK signals exhibit same fourth order cumulant values. Also, the $\frac{\pi}{4}$-QPSK and 8-PSK signals exhibit similar fourth-order cumulant values which is clear from Eqns. (3.29 – 3.31) and Eqns. (3.33 – 3.35). In the same way, it can

be shown that other HOC values of QPSK variants are also indistinguishable due to identical distribution of their constellation points.

In the following sections, we discuss the proposed cumulant features to classify the QPSK, OQPSK, $\frac{\pi}{4}$-QPSK and $8-PSK$ signals.

3.4 Proposed Cumulant Features

Features are proposed to distinguish between the QPSK and the OPSK signals and between the 8-PSK and the $\frac{\pi}{4}$ QPSK signals. They are described below:

A: Discrimination of QPSK and OQPSK

The RVs representing QPSK and OQPSK constellation have identical distribution. Thus the cumulants of these RVs are identical. Suppose $\nabla x_1(k) = x_1(k) - x_1(k-1)$ and $\nabla x_2(k) = x_2(k) - x_2(k-1)$, where $x_1(k)$ and $x_2(k)$ are as defined earlier. As illustrated in Table 3.2 and Table 3.4, the RVs ∇x_1 and ∇x_2 corresponding to these differences have non-identical distributions. Therefore, we analyse the 4^{th} order cumulants for these two RVs. Using Eqns. 2.48-2.50, Chapter 2, the 4^{th} order cumulants of ∇x_1 and ∇x_2 are obtained as

$$C_{40}(\nabla x_1) = \frac{1}{16}(2^4 + (-2)^4 + 2i^4 + (-2i)^4) + \frac{1}{8}((1+i)^4 + (1-i)^4 + (-1+i)^4 + (-1-i)^4) - 3(\frac{1}{16}(2^2 + (-2)^2 + 2i^2 + (-2i)^2) + \frac{1}{8}((1+i)^2 + (1-i)^2 + (-1+i)^2 + (-1-i)^2))^2 = 2, \tag{3.36}$$

$$C_{40}(\nabla x_2) = \frac{1}{8}((1+i)^4 + (1-i)^4 + (-1+i)^4 + (-1-i)^4) - 3(\frac{1}{8}((1+i)^2 + (1-i)^2 + (-1+i)^2 + (-1-i)^2))^2 = 2, \tag{3.37}$$

$$C_{42}(\nabla x_1) = \frac{1}{16}(|2|^4 + |-2|^4 + |2i|^4 + |-2i|^4) + \frac{1}{8}(|1+i|^4 + |1-i|^4 + |-1+i|^4 + |-1-i|^4) - |\frac{1}{16}(2^2 + (-2)^2 + 2i^2 + (-2i)^2) + \frac{1}{8}((1+i)^2 + (1-i)^2 + (-1+i)^2 + (-1-i)^2)|^2 - 2(\frac{1}{16}(|2|^2 + |-2|^2 + |2i|^2 + |-2i|^2) + \frac{1}{8}(|1+i|^2 + |1-i|^2 + |-1+i|^2 + |-1-i|^2))^2 = -2, \tag{3.38}$$

$$C_{42}(\nabla x_2) = \frac{1}{8}(|1+i|^4 + |1-i|^4 + |-1+i|^4 + |-1-i|^4) - |\frac{1}{8}((1+i)^2 + (1-i)^2 + (-1+i)^2 + (-1-i)^2)|^2 - 2(\frac{1}{8}(|1+i|^2 + |1-i|^2 + |-1+i|^2 + |-1-i|^2))^2 = 0, \tag{3.39}$$

$$C_{41}(\nabla x_1) = \frac{1}{16}(2^4 + (-2)^4 + (2i)^3(2i)^* + (-2i)^3(-2i)^*) + \frac{1}{8}((1+i)^3(1+i)^* + (1-i)^3(1-i)^* + (-1+i)^3(-1+i)^* + (-1-i)^3(-1-i)^*) - 3(\frac{1}{16}(2^2 + (-2)^2 + (2i)^2 + (-2i)^2) + \frac{1}{8}((1+i)^2 + (1-i)^2 + (-1+i)^2 + (-1-i)^2))(\frac{1}{16}(2^2 + |-2|^2 + |2i|^2 + |-2i|^2) + \frac{1}{8}(|1+i|^2 + |1-i|^2 + |-1+i|^2 + |-1-i|^2)) = 0 \tag{3.40}$$

and

$$C_{41}(\nabla x_2) = \frac{1}{8}((1+i)^3(1+i)^* + (1-i)^3(1-i)^* + (-1+i)^3(-1+i)^* + (-1-i)^3(-1-i)^*) - 3(\frac{1}{8}((1+i)^2 + (1-i)^2 + (-1+i)^2 + (-1-i)^2))(\frac{1}{8}(|1+i|^2 + |1-i|^2 + |-1+i|^2 + |-1-i|^2)) = 0. \tag{3.41}$$

It is noted from equations 3.36-3.41 that $C_{42}(\nabla x_1)$ and $C_{42}(\nabla x_2)$ are distinct. Therefore, $C_{42}(\nabla x)$ can be employed to discriminate the QPSK and OQPSK signals.

B: Discrimination of 8-PSK and $\pi/4$-QPSK

The constellation of $\pi/4$-shifted QPSK is given by

$$\mathbf{C}_3 = \{(\frac{1}{\sqrt{(2)}})(1+i), (\frac{1}{\sqrt{(2)}})(1-i), (\frac{1}{\sqrt{(2)}})(-1+i), (\frac{1}{\sqrt{(2)}})(-1-i)\}. \tag{3.42}$$

Consider a $\pi/4$-QPSK modulated signal $x_3(k)$. Suppose $x_3^o(k)$ and $x_3^e(k)$ denote the sequences of

Table 3.1: Backward Differences of a QPSK Signal

$x_1(k)$	$x_1(k-1)$	$\nabla x_1(k)$
1	1	0
-1	-1	0
i	i	0
$-i$	-i	0
1	-1	2
-1	1	-2
i	-i	2i
$-i$	i	-2i
1	i	1-i
1	-i	1+i
-1	i	-1-i
-1	-i	-1+i
i	1	-1+i
$-i$	1	-1-i
i	-1	1+i
$-i$	-1	1-i

Table 3.2: PMF of ∇x_1

$Difference$	$P_{\nabla x_1}$
0	$\frac{1}{4}$
2	$\frac{1}{16}$
-2	$\frac{1}{16}$
$2i$	$\frac{1}{16}$
$-2i$	$\frac{1}{16}$
$1+i$	$\frac{1}{8}$
$1-i$	$\frac{1}{8}$
$-1-i$	$\frac{1}{8}$
$-1+i$	$\frac{1}{8}$

odd and even symbols respectively. Then

$$x_3^o(k) = x_3(2k+1) \; and \; x_3^e(k) = x_3(2k), \;\; for \; k = 0, 1, 2, ... \tag{3.43}$$

The PMF of random variables x_3^o and x_3^e are given by

$$P_{x_3^o}(x) = \begin{cases} \frac{1}{4}, x \in \mathbf{C}_1 \end{cases} \tag{3.44}$$

and

$$P_{x_3^e}(x) = \begin{cases} \frac{1}{4}, x \in \mathbf{C}_3 \end{cases} . \tag{3.45}$$

Table 3.3: Backward Differences of an OQPSK Signal

$x_2(k)$	$x_2(k-1)$	$\nabla x_2(k)$
1	1	0
1	i	1-i
1	-i	1+i
-1	-1	0
-1	i	-1-i
-1	-i	-1+i
i	i	0
i	1	-1+i
i	-1	1+i
$-i$	-i	0
$-i$	1	-1-i
$-i$	-1	1-i

Table 3.4: PMF of ∇x_2

$Difference$	$P_{\nabla x_2}$
0	$\frac{1}{2}$
$1+i$	$\frac{1}{8}$
$1-i$	$\frac{1}{8}$
$-1-i$	$\frac{1}{8}$
$-1+i$	$\frac{1}{8}$

Now consider an 8-PSK signal $x_4(k)$. Suppose $x_4^o(k)$ and $x_4^e(k)$ denote the sequences of the odd and even symbols respectively. Then

$$x_4^o(k) = x_4(2k+1) \; and \; x_4^e(k) = x_4(2k), \; for \; k = 0, 1, 2, ... \tag{3.46}$$

The PMF of random variables x_4^o and x_4^e are then given by

$$P_{x_4^o}(x) = \left\{ \frac{1}{8}, x \in \mathbf{C}_2 \right. \tag{3.47}$$

and

$$P_{x_4^e}(x) = \left\{ \frac{1}{8}, x \in \mathbf{C}_2 \right. . \tag{3.48}$$

Using Eqns. 2.48-2.50, Chapter 2, the 4^{th}-order cumulants of $x_3^o(k)$, $x_3^e(k)$, $x_4^o(k)$ and $x_4^e(k)$ are given as

$$C_{40}(x_3^o) = \frac{1}{4}(1^4 + (-1)^4 + i^4 + (-i)^4) - 3(\frac{1}{4}(1^2 + (-1)^2 + i^2 + (-i)^2)^2 = 1, \tag{3.49}$$

$$C_{40}(x_3^e) = \frac{1}{4}(((\frac{1}{\sqrt{(2)}})(1+i))^4 + ((\frac{1}{\sqrt{(2)}})(1-i))^4 + ((\frac{1}{\sqrt{(2)}})(-1+i))^4 + ((\frac{1}{\sqrt{(2)}})(-1-i))^4) - 3(\frac{1}{4}(((\frac{1}{\sqrt{(2)}})(1+i))^2 + ((\frac{1}{\sqrt{(2)}})(1-i))^2 + ((\frac{1}{\sqrt{(2)}})(-1+i))^2 + ((\frac{1}{\sqrt{(2)}})(-1-i))^2))^2 = 1, \tag{3.50}$$

$$C_{40}(x_4^o) = \frac{1}{8}(1^4 + (-1)^4 + (i)^4 + (-i)^4 + ((\frac{1}{\sqrt{(2)}})(1+i))^4 + ((\frac{1}{\sqrt{(2)}})(1-i))^4 + ((\frac{1}{\sqrt{(2)}})(-1+i))^4 + ((\frac{1}{\sqrt{(2)}})(-1-i))^4) - 3(\frac{1}{8}(1^2 + (-1)^2 + i^2 + (-i)^2 + ((\frac{1}{\sqrt{(2)}})(1+i))^2 + ((\frac{1}{\sqrt{(2)}})(1-i))^2 + ((\frac{1}{\sqrt{(2)}})(-1+i))^2 + ((\frac{1}{\sqrt{(2)}})(-1-i))^2))^2 = 0, \tag{3.51}$$

$$C_{40}(x_4^e) = \frac{1}{8}(1^4 + (-1)^4 + (i)^4 + (-i)^4 + ((\frac{1}{\sqrt{(2)}})(1+i))^4 + ((\frac{1}{\sqrt{(2)}})(1-i))^4 + ((\frac{1}{\sqrt{(2)}})(-1+i))^4 + ((\frac{1}{\sqrt{(2)}})(-1-i))^4) - 3(\frac{1}{8}(1^2 + (-1)^2 + i^2 + (-i)^2 + ((\frac{1}{\sqrt{(2)}})(1+i))^2 + ((\frac{1}{\sqrt{(2)}})(1-i))^2 + ((\frac{1}{\sqrt{(2)}})(-1+i))^2 + ((\frac{1}{\sqrt{(2)}})(-1-i))^2))^2 = 0, \tag{3.52}$$

$$C_{42}(x_3^o) = \frac{1}{4}(1^4 + |-1|^4 + |i|^4 + |-i|^4) - \frac{1}{16}(|(1^2 + (-1)^2 + (i)^2 + (-i)^2|^2) - \frac{1}{8}(|1|^2 + |-1|^2 + |i|^2 + |-i|^2)^2 = -1, \tag{3.53}$$

$$C_{42}(x_3^e) = \frac{1}{4}(|(\frac{1}{\sqrt{(2)}})(1+i)|^4 + |(\frac{1}{\sqrt{(2)}})(1-i)|^4 + |(\frac{1}{\sqrt{(2)}})(-1+i)|^4 + |(\frac{1}{\sqrt{(2)}})(-1-i)|^4) - \frac{1}{16}(|((\frac{1}{\sqrt{(2)}})(1+i))^2 + ((\frac{1}{\sqrt{(2)}})(1-i))^2 + ((\frac{1}{\sqrt{(2)}})(-1+i))^2 + ((\frac{1}{\sqrt{(2)}})(-1-i))^2|^2) - \frac{1}{8}(|(\frac{1}{\sqrt{(2)}})(1+i)|^2 + |(\frac{1}{\sqrt{(2)}})(1+i)|^2 + |(\frac{1}{\sqrt{(2)}})(1+i)|^2 + |(\frac{1}{\sqrt{(2)}})(1+i)|^2)^2 = -1, \tag{3.54}$$

$$C_{42}(x_4^o) = \frac{1}{8}(1^4 + |-1|^4 + |i|^4 + |-i|^4 + |(\frac{1}{\sqrt{(2)}})(1+i)|^4 + |(\frac{1}{\sqrt{(2)}})(1-i)|^4 + |(\frac{1}{\sqrt{(2)}})(-1+i)|^4 + |(\frac{1}{\sqrt{(2)}})(-1-i)|^4) - \frac{1}{64}|(1)^2 + (-1)^2 + (i)^2 + (-i)^2 + ((\frac{1}{\sqrt{(2)}})(1+i))^2 + ((\frac{1}{\sqrt{(2)}})(1-i))^2 + ((\frac{1}{\sqrt{(2)}})(-1+i))^2 + ((\frac{1}{\sqrt{(2)}})(-1-i))^2|^2 - \frac{1}{32}(|1|^2 + |-1|^2 + |i|^2 + |-i|^2 + |(\frac{1}{\sqrt{(2)}})(1+i)|^2 + |(\frac{1}{\sqrt{(2)}})(1-i)|^2 + |(\frac{1}{\sqrt{(2)}})(-1+i)|^2 + |(\frac{1}{\sqrt{(2)}})(-1-i)|^2)^2 = -1, \tag{3.55}$$

$$C_{42}(x_4^e) = \frac{1}{8}(1^4 + |-1|^4 + |i|^4 + |-i|^4 + |(\frac{1}{\sqrt{(2)}})(1+i)|^4 + |(\frac{1}{\sqrt{(2)}})(1-i)|^4 + |(\frac{1}{\sqrt{(2)}})(-1+i)|^4 + |(\frac{1}{\sqrt{(2)}})(-1-i)|^4) - \frac{1}{64}|(1)^2 + (-1)^2 + (i)^2 + (-i)^2 + ((\frac{1}{\sqrt{(2)}})(1+i))^2 + ((\frac{1}{\sqrt{(2)}})(1-i))^2 + ((\frac{1}{\sqrt{(2)}})(-1+i))^2 + ((\frac{1}{\sqrt{(2)}})(-1-i))^2|^2 - \frac{1}{32}(|1|^2 + |-1|^2 + |i|^2 + |-i|^2 + |(\frac{1}{\sqrt{(2)}})(1+i)|^2 + |(\frac{1}{\sqrt{(2)}})(1-i)|^2 + |(\frac{1}{\sqrt{(2)}})(-1+i)|^2 + |(\frac{1}{\sqrt{(2)}})(-1-i)|^2)^2 = -1, \tag{3.56}$$

$$C_{41}(x_3^o) = \frac{1}{4}(1^4 + (-1)^4 + (i)^3 i^* + (-i)^3(-i)^*) - 3(\frac{1}{4}(1^2 + (-1)^2 + i^2 + (-i)^2)) (\frac{1}{4}(|1|^2 + |-1|^2 + |i|^2 + |-i|^2)) = 0, \tag{3.57}$$

$$C_{41}(x_3^e) = \frac{1}{4}(((\frac{1}{\sqrt{(2)}})(1+i))^3((\frac{1}{\sqrt{(2)}})(1+i))^* + ((\frac{1}{\sqrt{(2)}})(1-i))^3((\frac{1}{\sqrt{(2)}})(1-i))^* + ((\frac{1}{\sqrt{(2)}})(-1+i))^3((\frac{1}{\sqrt{(2)}})(-1+i))^* + ((\frac{1}{\sqrt{(2)}})(-1-i))^3((\frac{1}{\sqrt{(2)}})(-1-i))^*) - 3(\frac{1}{4}(((\frac{1}{\sqrt{(2)}})(1+i))^2 + ((\frac{1}{\sqrt{(2)}})(1-i))^2 + ((\frac{1}{\sqrt{(2)}})(-1+i))^2 + ((\frac{1}{\sqrt{(2)}})(-1-i))^2)) (\frac{1}{4}(|(\frac{1}{\sqrt{(2)}})(1+i)|^2 + |(\frac{1}{\sqrt{(2)}})(1-i)|^2 + |(\frac{1}{\sqrt{(2)}})(-1+i)|^2 + |(\frac{1}{\sqrt{(2)}})(-1-i)|^2)) = 0, \tag{3.58}$$

$$
\begin{aligned}
C_{41}(x_4^o) = \frac{1}{8}(1^4 + (-1)^4 + (i)^3(i)^* + (-i)^3(-i)^* + ((\frac{1}{\sqrt{(2)}})(1+i))^3((\frac{1}{\sqrt{(2)}})(1+i))^* \\
+ ((\frac{1}{\sqrt{(2)}})(1-i))^3((\frac{1}{\sqrt{(2)}})(1-i))^* + ((\frac{1}{\sqrt{(2)}})(-1+i))^3((\frac{1}{\sqrt{(2)}})(-1+i))^* \\
+ ((\frac{1}{\sqrt{(2)}})(-1-i))^3((\frac{1}{\sqrt{(2)}})(-1-i))^*) - \frac{3}{64}(1^2 + (-1)^2 + i^2 + (-i)^2 \\
+ ((\frac{1}{\sqrt{(2)}})(1+i))^2 + ((\frac{1}{\sqrt{(2)}})(1-i))^2 + ((\frac{1}{\sqrt{(2)}})(-1+i))^2 \\
+ ((\frac{1}{\sqrt{(2)}})(-1-i))^2)(|1|^2 + |-1|^2 + |i|^2 + |-i|^2 + |(\frac{1}{\sqrt{(2)}})(1+i)|^2 \\
+ |(\frac{1}{\sqrt{(2)}})(1-i)|^2 + |(\frac{1}{\sqrt{(2)}})(-1+i)|^2 + |(\frac{1}{\sqrt{(2)}})(-1-i)|^2) = 0,
\end{aligned}
\tag{3.59}
$$

and

$$
\begin{aligned}
C_{41}(x_4^e) = \frac{1}{8}(1^4 + (-1)^4 + (i)^3(i)^* + (-i)^3(-i)^* + ((\frac{1}{\sqrt{(2)}})(1+i))^3((\frac{1}{\sqrt{(2)}})(1+i))^* \\
+ ((\frac{1}{\sqrt{(2)}})(1-i))^3((\frac{1}{\sqrt{(2)}})(1-i))^* + ((\frac{1}{\sqrt{(2)}})(-1+i))^3((\frac{1}{\sqrt{(2)}})(-1+i))^* \\
+ ((\frac{1}{\sqrt{(2)}})(-1-i))^3((\frac{1}{\sqrt{(2)}})(-1-i))^*) - 3(\frac{1}{8}(1^2 + (-1)^2 + i^2 + (-i)^2 \\
+ ((\frac{1}{\sqrt{(2)}})(1+i))^2 + ((\frac{1}{\sqrt{(2)}})(1-i))^2 + ((\frac{1}{\sqrt{(2)}})(-1+i))^2 \\
+ ((\frac{1}{\sqrt{(2)}})(-1-i))^2)(\frac{1}{8}(|1|^2 + |-1|^2 + |i|^2 + |-i|^2 + |(\frac{1}{\sqrt{(2)}})(1+i)|^2 \\
+ |(\frac{1}{\sqrt{(2)}})(1-i)|^2 + |(\frac{1}{\sqrt{(2)}})(-1+i)|^2 + |(\frac{1}{\sqrt{(2)}})(-1-i)|^2)) = 0.
\end{aligned}
\tag{3.60}
$$

It is clear from Eqns.3.49- 3.60 that $C_{40}(x_3^o)$ (or $C_{40}(x_3^e)$) and $C_{40}(x_4^o)$ (or $C_{40}(x_4^e)$) are distinct. Therefore, $C_{40}(x^o)$ (or $C_{40}(x^e)$) can be employed to discriminate the 8-PSK and $\frac{\pi}{4}$-QPSK signals.

Based on the above discussion, we propose a distinct cumulant feature vector $\mathbf{v}^M$ to distinguish four modulation types, namely QPSK, OQPSK, $\frac{\pi}{4}$-QPSK and 8-PSK. This feature vector $\mathbf{v}^M$ is given as

$$
\mathbf{v}^M = [C_{40}(x), C_{42}(\nabla x), C_{40}(x^e)]. \tag{3.61}
$$

For the considered modulation types, $\mathbf{v}^M$ is given as

$$\mathbf{v}^M = \begin{cases} [1, -2, 1], M = 1 \\ [1, 0, 1], M = 2 \\ [0, -2, 1], M = 3 \\ [0, -2, 0], M = 4 \end{cases} \tag{3.62}$$

where $M = 1, 2, 3$ *and* 4 represents the modulation formats QPSK, OQPSK, $\frac{\pi}{4}$-QPSK and 8-PSK respectively. Clearly $\mathbf{v}^M$ is distinct for each of the modulation schemes considered.

Based on this cumualnt feature vector, we propose an AMC method which is described next.

3.5 Proposed AMC Method

The proposed AMC method is a three-step process comprising (1) extracting cumulant features, (2) combining cumulant features and (3) a classification rule. They are described below.

3.5.1 Extracting Cumulant Features

As discussed in Section 3.3, the receiver performs equalization to obtain the estimates of N_T transmitted streams $\hat{\mathbf{x}}_j$, $j = 1, ..., N_T$. The cumulant features are estimated from $\hat{\mathbf{x}}_j$ as follows:

$$\hat{C}_{40}(\hat{\mathbf{x}}_j) = \frac{1}{N}\sum_{k=1}^{N}(\hat{x}_j(k))^4 - 3(\frac{1}{N}\sum_{k=1}^{N}(\hat{x}_j(k))^2)^2, \tag{3.63}$$

$$\hat{C}_{40}(\hat{\mathbf{x}}_j^e) = \frac{1}{N}\sum_{k=1}^{N}(\hat{x}_j^e(k))^4 - 3(\frac{1}{N}\sum_{k=1}^{N}(\hat{x}_j^e(k))^2)^2 \tag{3.64}$$

and

$$\hat{C}_{42}(\nabla\hat{\mathbf{x}}_j) = \frac{1}{N}\sum_{k=1}^{N}|\nabla\hat{x}_j(k)|^4 - |\frac{1}{N}\sum_{k=1}^{N}(\nabla\hat{x}_j(k))^2|^2 - 2(\frac{1}{N}\sum_{k=1}^{N}|\nabla\hat{x}_j(k)|^2)^2 \tag{3.65}$$

where $\nabla\hat{x}_j(k) = \hat{x}_j(k) - \hat{x}_j(k-1)$ and $\hat{x}_j^e(k) = \hat{x}_j(2k), k = 0, 1, 2, ...$

3.5.2 Combining Cumulant Features

The accurate estimation of cumualnts depends on signal-to-noise ratio (SNR) and the observation length [4]. The estimated N_T streams may have different SNRs. This in turn will

affect the cumulant estimates. It is reported in [19, 35] that a better classification result can be obtained by combining these cumulant estimates in an efficient way. In this work, we employ the the maximal ratio combining (MRC) technique to combine the cumulant features.

In MRC, a weighting coefficient is applied to the individual cumulant estimates. The estimates that are affected by high noise carry a lower weight and the estimates that are affected by low noise carry a higher weight [35] . The similar cumulant features estimated from $\hat{\mathbf{x}}_j$, $j = 1, ..., N_T$ are MRC combined as follows

$$b_1 = \frac{\sum_{j=1}^{N_T} \alpha_j C_{40}(\hat{\mathbf{x}}_j)}{\sum_{j=1}^{N_T} \alpha_j}, \tag{3.66}$$

$$b_2 = \frac{\sum_{j=1}^{N_T} \alpha_j C_{42}(\hat{\nabla}\mathbf{x}_j)}{\sum_{j=1}^{N_T} \alpha_j} \tag{3.67}$$

and

$$b_3 = \frac{\sum_{j=1}^{N_T} \alpha_j C_{40}(\hat{\mathbf{x}}_j^e)}{\sum_{j=1}^{N_T} \alpha_j} \tag{3.68}$$

where

$$\alpha_j = \frac{snr_j}{snr_{max}}, \tag{3.69}$$

snr_j denotes the SNR of the j^{th} estimated stream and $snr_{max} = max(snr_1, snr_2, ..., snr_{N_T})$. The snr_j is obtained as

$$snr_j = \frac{\sigma_s^2}{\sigma_{\hat{\mathbf{x}}_j}^2 - \sigma_s^2} \tag{3.70}$$

where $\sigma_{\hat{\mathbf{x}}_j}^2$ is the power of equalized signal $\hat{\mathbf{x}}_j$ and σ_s^2 is the variance of transmit symbols. As the normalized constellation points are attained after equalization, we can assume $\sigma_s^2 = 1$.

The estimated feature $\hat{\mathbf{v}}$ is given by

$$\hat{\mathbf{v}} = [b_1\ b_2\ b_3]. \tag{3.71}$$

3.5.3 Classification Rule

The modulation class M^* is detected as

$$M^* = \underset{M=1,2,...,4}{argmin}(\|\hat{\mathbf{v}} - \mathbf{v}^M\|). \tag{3.72}$$

where ||.|| denotes the Euclidean norm.

We refer the above technique as ZF-modulation classification (MC) if the employed equalization technique is ZF. If the employed equalization technique is JADE, we refer it as JADE-MC.

3.6 Simulation Results and Discussion

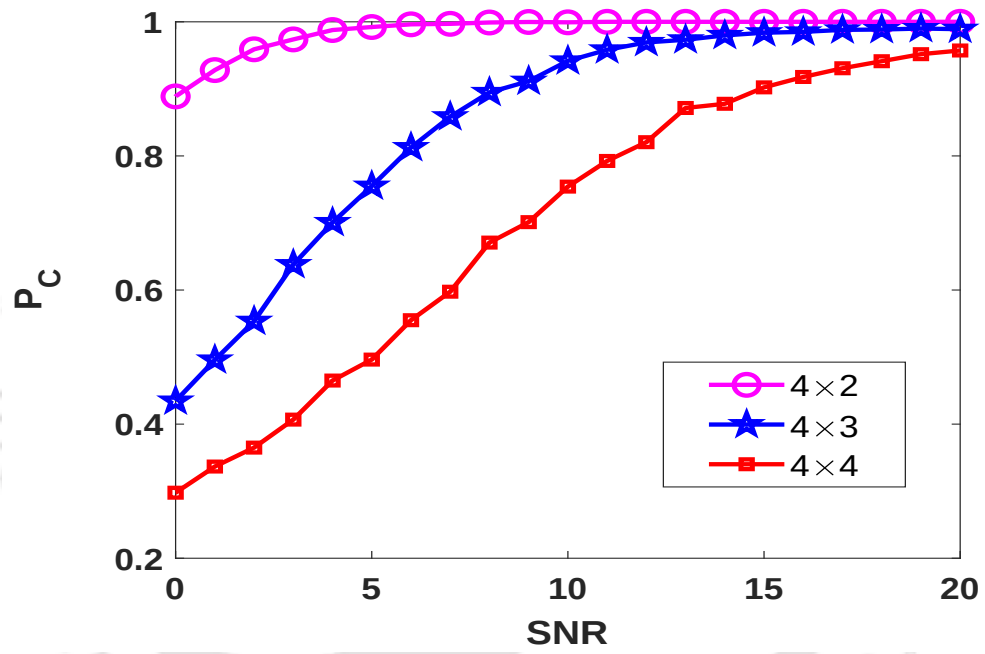

Figure 3.1: P_C versus SNR for for different MIMO antenna configurations ($N_R = 4, N_T = \{2, 3, 4\}$) with $N = 2000$

A set of experiments were carried out to evaluate the performance of the proposed method through the Monte-Carlo simulation. The performance of the proposed classifier was analysed by calculating the average probability of correct classification for different values of SNR. For each SNR value, 1000 Monte Carlo simulations were performed to calculate the average probability of correct classification. We generated a random channel matrix and a random source message for each trial. Two channel models were considered for the investigation, namely the Rayleigh flat fading channel and the Rician flat fading channel. The probability of correct

classification of the modulation types is given by

$$P_C = \sum_{i=1}^{M} P(R = B_i/T = B_i)P(T = B_i) \tag{3.73}$$

where $P(T = B_i)$ denotes the probability of occurrence of the modulation format B_i at the transmitter T and $P(R = B_i/T = B_i)$ denotes the probability that the modulation format is classified as B_i at the receiver R when the transmitted modulation format is B_i.

3.6.1 AMC Performance over Rayleigh Flat Fading Channel

A number of experiments were performed to study the performance of the proposed method by varying the sample length, N_T, and antenna correlation values. They are described below.

3.6.1.1 Performance of the ZF-MC Technique for Different Values of N_T Keeping N_R Fixed

Fig 3.1 shows P_C versus SNR for the ZF-MC technique in an uncorrelated Rayleigh channel for different values of N_T keeping N_R fixed. It is noted that increasing N_T and keeping N_R fixed result in a drop in the AMC performance. The reason for this is that SNR degrades as $N_R - N_T$ decreases [18]; and the accurate estimation of the HOC-features depends on the SNR of the equalized signal.

3.6.1.2 Effect of Sample Length and SNR

For the simulation results shown in Figs. 3.2-3.15, the number of transmitting and receiving antennas were set at $N_T = 2$ and $N_R = 4$ respectively.

Fig. 3.2 shows P_C versus SNR for the ZF-MC technique over an uncorrelated Rayleigh channel. It can be noted that with an increase in the sample size N and SNR, P_C also gradually increases. For instance, at an SNR value of 0 dB, the ZF-MC technique attains $P_C = 0.7370$ for $N = 500$, while at the same SNR, it attains $P_C = .9520$ for $N = 4000$. Table 3.5 shows the values of P_C attained by the ZF-MC technique at an SNR value of 0 dB for different sample lengths. For $N = 500$, the ZF-MC technique attains $P_C = 0.7370$ at an SNR value of 0 dB, while for the same sample length, it attains $P_C = .9962$ at an SNR value of 6 dB. Table 3.6 shows the values of P_C attained by the ZF-MC technique at different values of SNR with $N = 500$.

Fig. 3.3 shows P_C versus SNR for the JADE-MC technique over an uncorrelated Rayleigh

channel. At an SNR value of 0 dB, the JADE-MC technique attains $P_C = 0.7398$ for $N = 500$, while at the same SNR, it attains $P_C = 0.9567$ for $N = 4000$. Table 3.7 shows the values of P_C attained by the JADE-MC technique at an SNR value of 0 dB for different sample lengths. For $N = 500$, the JADE-MC technique attains $P_C = 0.7398$ at an SNR value of 0 dB, while for the same sample length, it attains $P_C = 0.9958$ at an SNR value of 6 dB. Table 3.8 shows the values of P_C attained by the JADE-MC technique at different values of SNR with $N = 500$.

The increase in P_C with an increase N and SNR is contributed by the fact that the accurate estimation of the cumulants depends on the SNR and the sample size. The higher the SNR and N, the cumulant estimates are closer to the theoretical values [4]. One can also note that the performance of the JADE-MC technique is close to that of the ZF-MC technique.

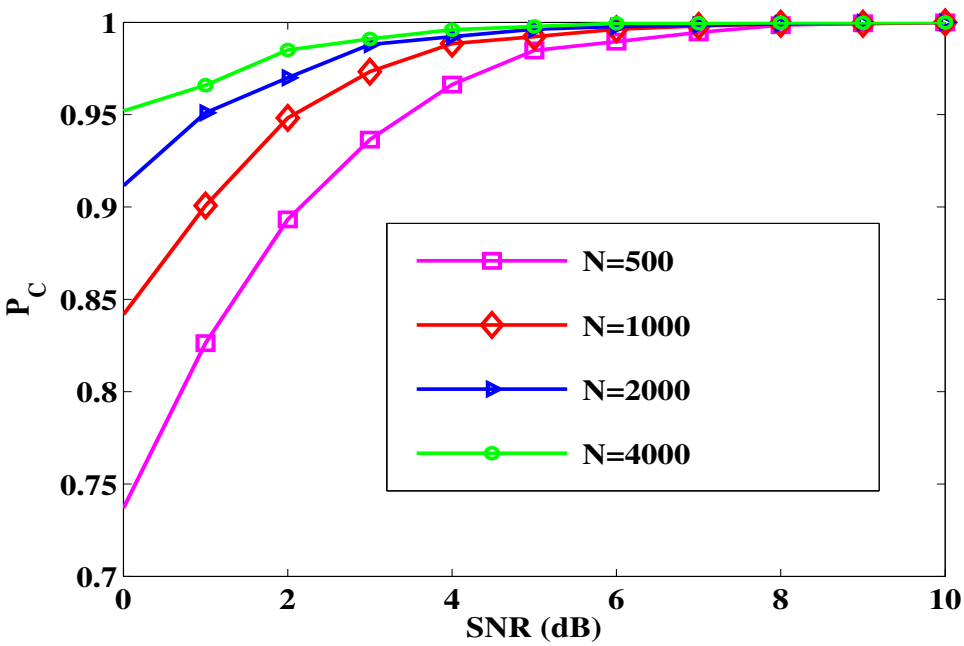

Figure 3.2: P_C versus SNR for ZF-MC in an uncorrelated Rayleigh channel

Table 3.5: P_C attained by ZF-MC at an SNR value of 0 dB for different sample lengths

N	P_C
500	0.7370
1000	0.8418
2000	0.9115
4000	0.9520

Table 3.6: P_C at different values of SNR for ZF-MC with N=500

SNR (dB)	P_C
0	0.7370
2	0.8932
4	0.9662
6	0.9962

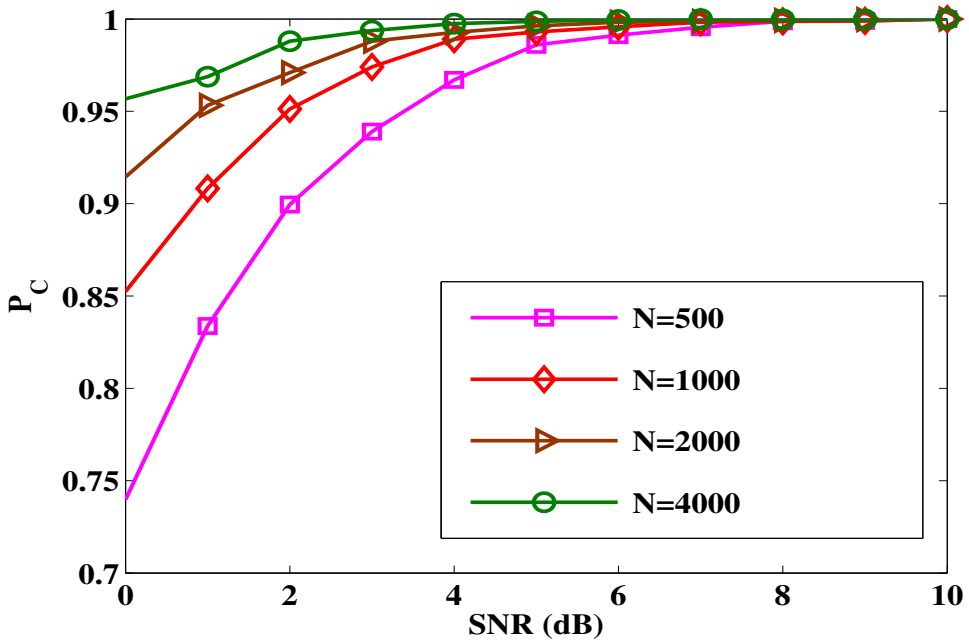

Figure 3.3: P_C versus SNR for JADE-MC in an uncorrelated Rayleigh channel

3.6.1.3 Effect of Antenna Correlation

Figs. 3.4-3.7 show the effect of antenna correlation on the ZF-MC technique. Figs. 3.8-3.11 show the effect of antenna correlation on the JADE-MC technique. It is observed that there is a decrease in P_C with an increase in the antenna correlation value. For instance, with an SNR value of 5 dB and $N = 500$, the ZF-MC technique attains $P_C = 0.9690$ for $|\rho_R| = |\rho_T| = 0.3$, while at the same SNR and the sample length, it attains $P_C = 0.9555$ for $|\rho_R| = |\rho_T| = 0.5$. Table 3.9 shows P_C attained by the ZF-MC technique for different antenna correlation values with an SNR value of 5 dB and $N = 500$. With an SNR value of 5 dB and $N = 500$, the JADE-MC technique attains $P_C = 0.9720$ for $|\rho_R| = |\rho_T| = 0.3$, while for the same SNR and the sample length, it attains $P_C = 0.9352$ for $|\rho_R| = |\rho_T| = 0.5$. Table 3.10 shows P_C attained by the JADE-

Table 3.7: P_C attained by JADE-MC at an SNR value of 0 dB for different sample lengths

N	P_C
500	0.7398
1000	0.8525
2000	0.9145
4000	0.9567

Table 3.8: P_C at different values of SNR for JADE-MC with N=500

SNR (dB)	P_C
0	0.7398
2	0.8995
4	0.9670
6	0.9958

MC technique for different antenna correlation values at an SNR value of 5 dB and $N = 500$. The decrease in P_C with an increase in the antenna correlation is attributed to the fact that the channel correlation amplifies the noise at the equalizer output [18]. One can also note that as SNR improves, P_C also improves for high antenna correlation value. For $|\rho_R| = |\rho_T| = 0.5$ and $N = 500$, the ZF-MC technique attains $P_C = 0.6400$ at an SNR value of 1 dB, while for the same antenna correlation value and sample size, it attains $P_C = 0.9352$ at an SNR value of 5 dB. Table 3.11 shows the values of P_C attained by the ZF-MC technique at different values of SNR for $|\rho_R| = |\rho_T| = 0.5$ and $N = 500$. For $|\rho_R| = |\rho_T| = 0.5$ and $N = 500$, the JADE-MC technique attains $P_C = 0.6745$ at an SNR value of 1 dB, while for the same antenna correlation value and sample size, it attains $P_C = 0.9352$ at an SNR value of 5 dB. Table 3.12 shows the values of P_C attained by the JADE-MC technique at different values of SNR for $|\rho_R| = |\rho_T| = 0.5$ and $N = 500$. It is also noted that as the sample length increases, P_C also improves for high antenna correlation value. For instance, with an SNR value of 3 dB and $|\rho_R| = |\rho_T| = 0.5$, the ZF-MC technique attains $P_C = 0.8225$ for $N = 500$, while at the same SNR and antenna correlation value, it attains $P_C = 0.9340$ for $N = 2000$. Table 3.13 shows the values of P_C attained by the ZF-MC technique for different values of N with an SNR value of 3 dB and $|\rho_R| = |\rho_T| = 0.5$. With an SNR value of 3 dB and $|\rho_R| = |\rho_T| = 0.5$, the JADE-MC technique attains $P_C = 0.8327$ for $N = 500$, while at the same SNR and antenna correlation value, it attains $P_C = 0.9417$ for $N = 2000$. Table 3.14 shows the values of P_C attained by the JADE-MC technique for different

values of N with an SNR value of 3 dB and $|\rho_R| = |\rho_T| = 0.5$.

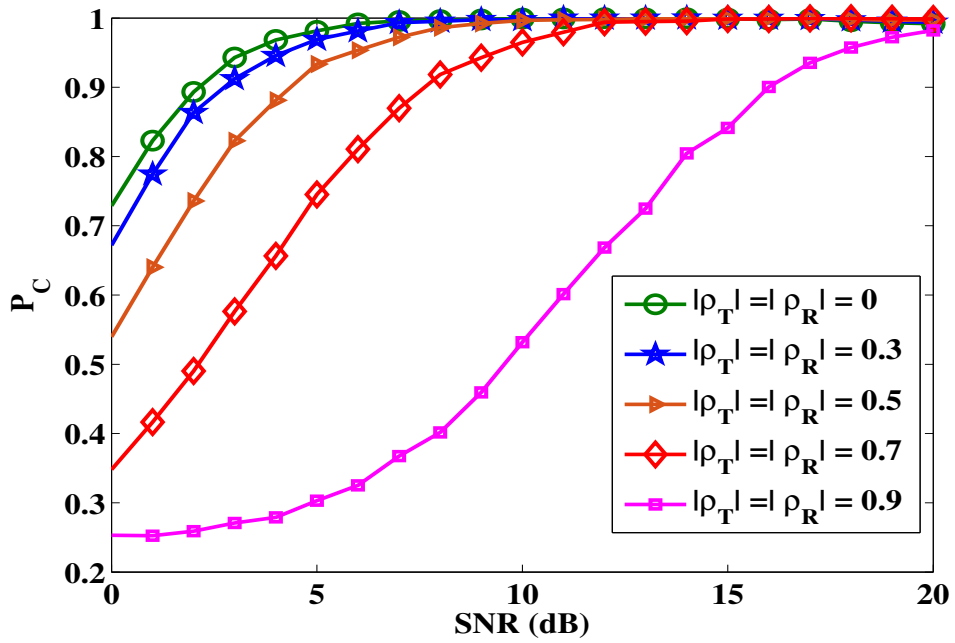

Figure 3.4: P_C versus SNR for ZF-MC with $N = 500$ in a correlated Rayleigh channel

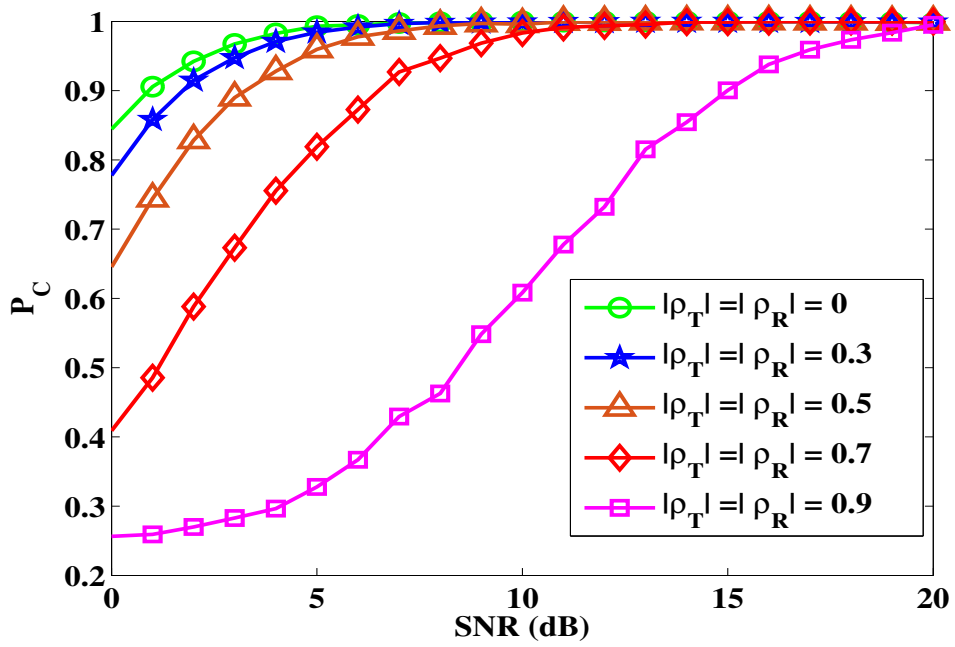

Figure 3.5: P_C versus SNR for ZF-MC with $N = 1000$ in a correlated Rayleigh channel

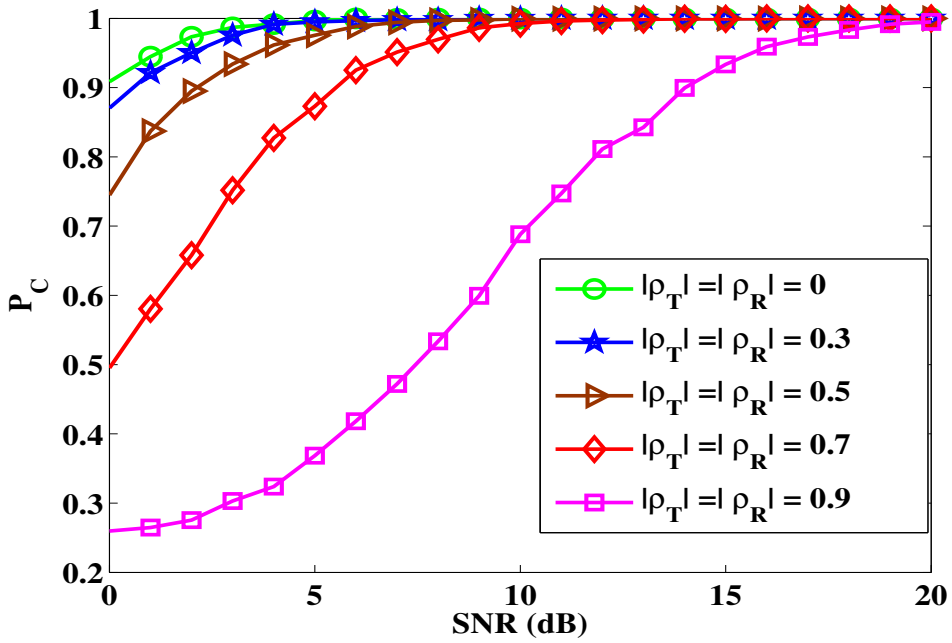

Figure 3.6: P_C versus SNR for ZF-MC with $N = 2000$ in a correlated Rayleigh channel

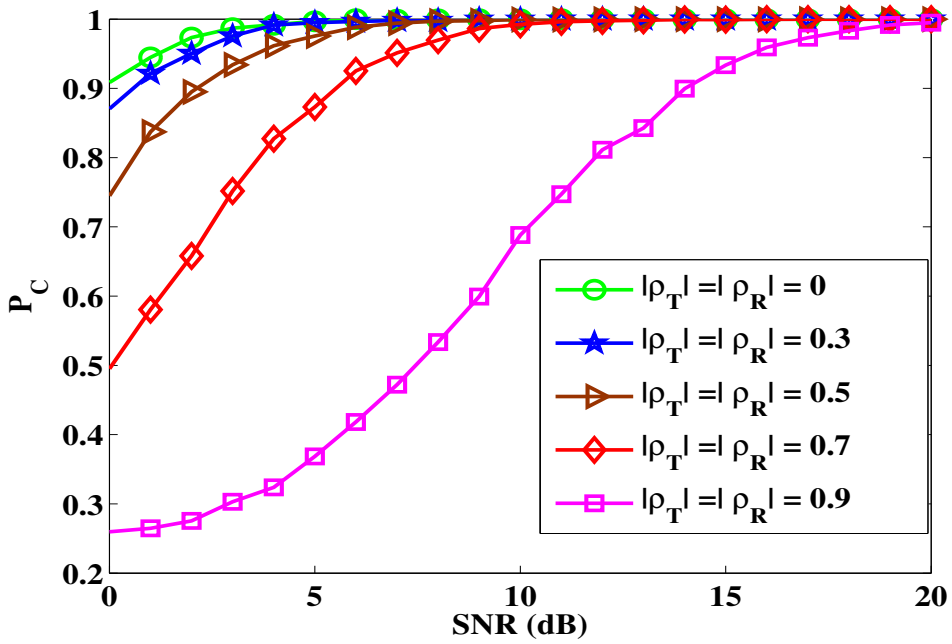

Figure 3.7: P_C versus SNR for ZF-MC with N=4000 in a correlated Rayleigh channel

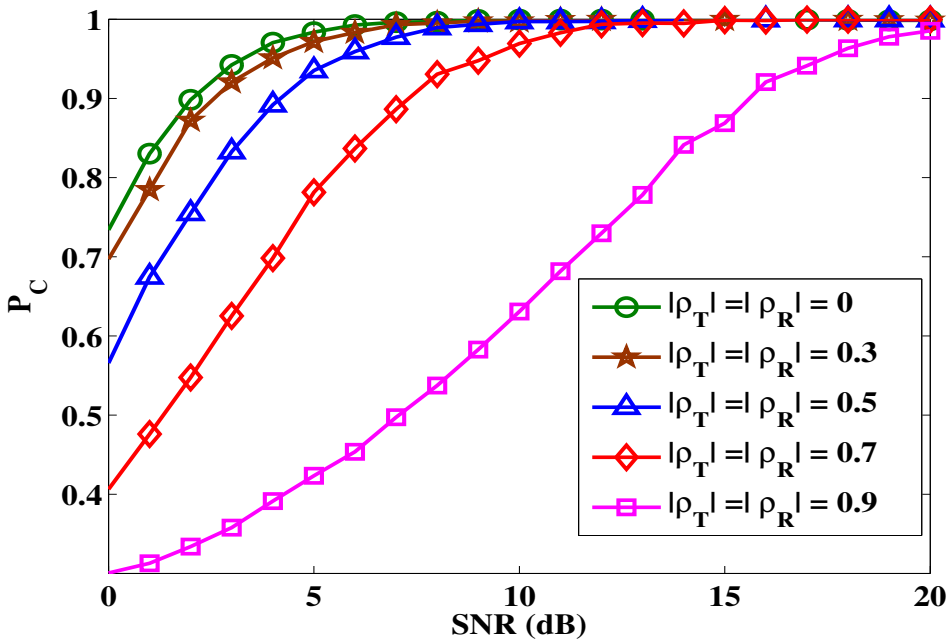

Figure 3.8: P_C versus SNR for JADE-MC with $N = 500$ in a correlated Rayleigh channel

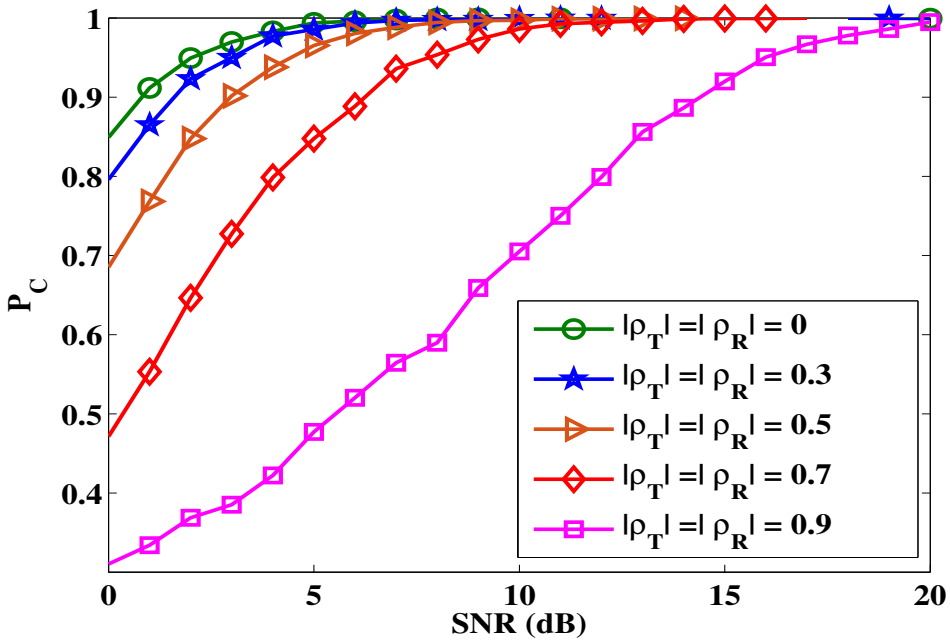

Figure 3.9: P_C versus SNR for JADE-MC with $N = 1000$ in a correlated Rayleigh channel

3.6.2 AMC Performance over the Rician Flat Fading Channel

Figs. 3.12-3.15 show P_C versus SNR for the JADE-MC technique over a correlated Rician channel. It can be noted that with an increase in the Rician factor K, P_C decreases. For instance,

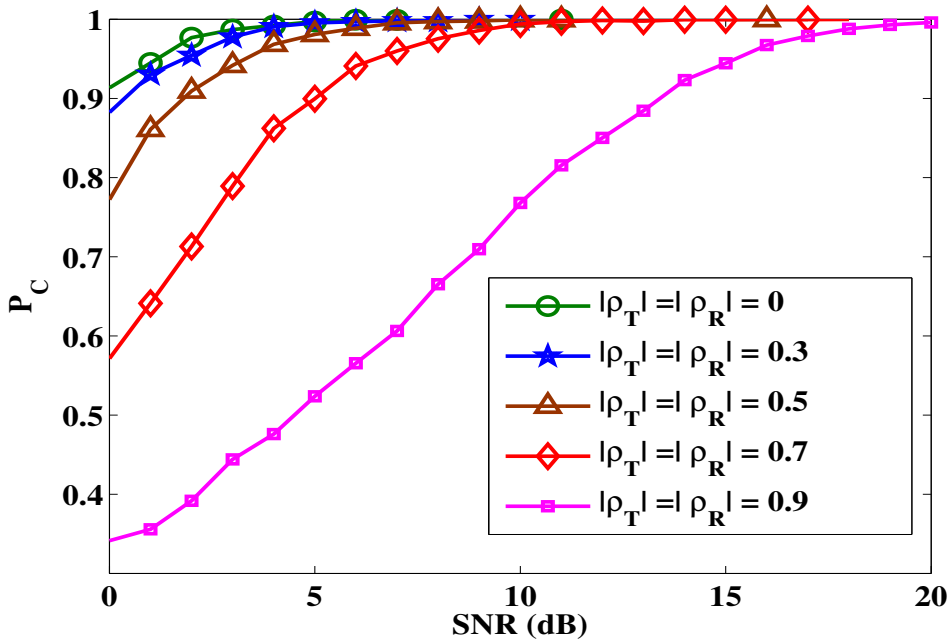

Figure 3.10: P_C versus SNR for JADE-MC with $N = 2000$ in a correlated Rayleigh channel

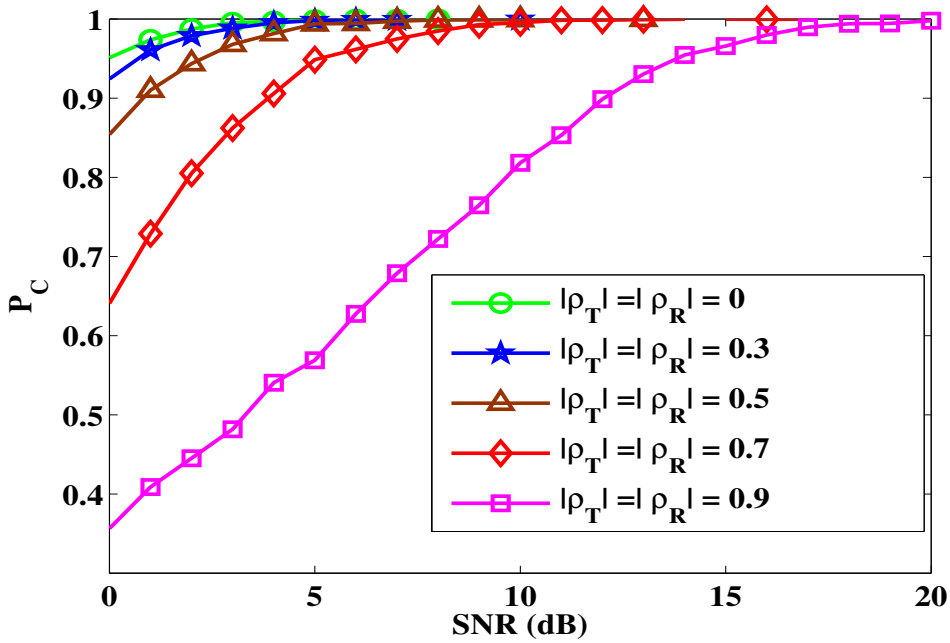

Figure 3.11: P_C versus SNR for JADE-MC with $N = 4000$ in a correlated Rayleigh channel

with an SNR value of 8 dB, $N = 2000$ and $|\rho_R| = |\rho_T| = 0.3$, the JADE-MC technique attains $P_C = 0.9670$ for $K = 3$, while for the same SNR, sample length and antenna correlation value, it attains $P_C = 0.7970$ for $K = 10$. Table 3.15 shows P_C attained by the JADE-MC technique for

Table 3.9: P_C attained by ZF-MC with an SNR value of 5 dB and $N = 500$ for different antenna correlation values ($|\rho| = |\rho_R| = |\rho_T|$)

$\|\rho\|$	P_C
0	0.9815
0.3	0.9690
0.5	0.9555
0.7	0.7452
0.9	0.3030

Table 3.10: P_C attained by JADE-MC with an SNR value of 5 dB and $N = 500$ for different antenna correlation values ($|\rho| = |\rho_R| = |\rho_T|$)

$\|\rho\|$	P_C
0	0.9837
0.3	0.9720
0.5	0.9352
0.7	0.7815
0.9	0.4233

different values of K with an SNR value of 8 dB, $N = 2000$ and $|\rho_R| = |\rho_T| = 0.3$. The decrease in P_C with an increase in K is attributed to the fact that with the increase in the Rician factor, the scattered component vanishes resulting into a highly correlated channel. This amplifies the noise at the equalizer output [18]. The performance improves as the SNR and sample length increases. For example, for $|\rho_R| = |\rho_T| = 0.3$, $N = 2000$ and $K = 10$, the JADE-MC technique attains $P_C = 0.7970$ at an SNR value of 8 dB, while for the same Rician factor, sample length and antenna correlation value, it attains $P_C = 0.9620$ at an SNR value of 12 dB. Table 3.16 shows P_C attained by the JADE-MC technique at different SNR values for $K = 10$, $N = 2000$ and $|\rho_R| = |\rho_T| = 0.3$. With an SNR value of 8 dB, $|\rho_R| = |\rho_T| = 0.3$ and $K = 10$, the JADE-MC technique attains $P_C = 0.7970$ for $N = 2000$ while for the same SNR, antenna correlation value and Rician factor, it attains $P_C = 0.8647$ for $N = 4000$.

Table 3.11: P_C at different values of SNR for ZF-MC with $N = 500$ and $|\rho_R| = |\rho_T| = 0.5$

SNR (dB)	P_C
1	0.6400
3	0.8228
5	0.9335
7	0.9772
9	0.9923

Table 3.12: P_C at different values of SNR for JADE-MC with $N = 500$ and $|\rho_R| = |\rho_T| = 0.5$

SNR (dB)	P_C
1	0.6745
3	0.8327
5	0.9352
7	0.9775
9	0.9938

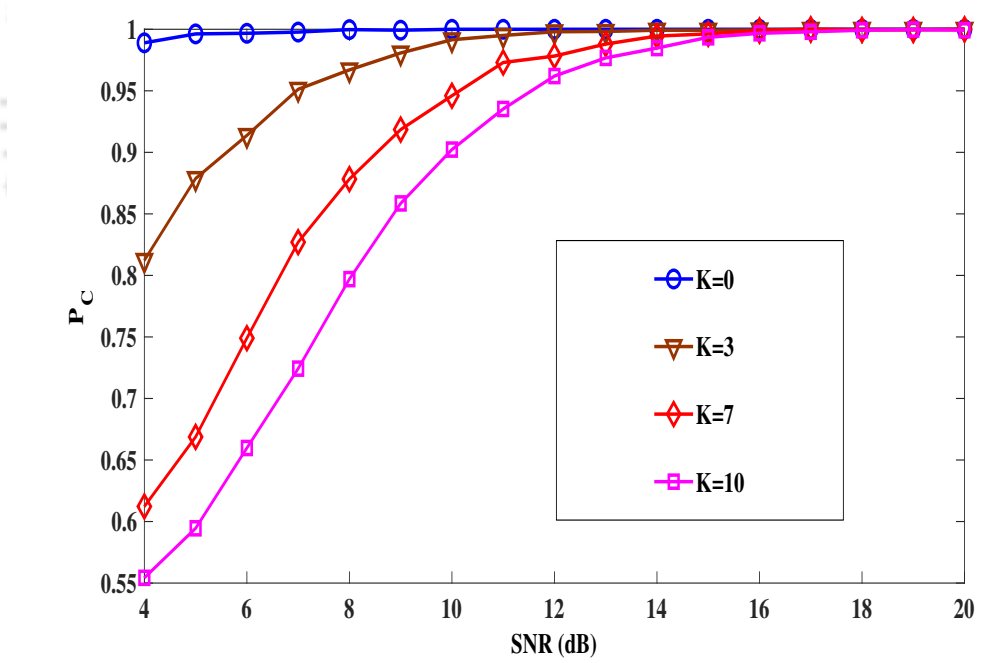

Figure 3.12: P_C versus SNR for JADE-MC with $N = 2000$ and $|\rho_R| = |\rho_T| = 0.3$ in a correlated Rician channel

Table 3.13: P_C attained by ZF-MC for different values of N with an SNR value of 3 dB and $|\rho_R| = |\rho_T| = 0.5$

N	P_C
500	0.8225
1000	0.8900
2000	0.9340
4000	0.9615

Table 3.14: P_C attained by JADE-MC for different values of N with an SNR value of 3 dB and $|\rho_R| = |\rho_T| = 0.5$

N	P_C
500	0.8327
1000	0.9017
2000	0.9417
4000	0.9680

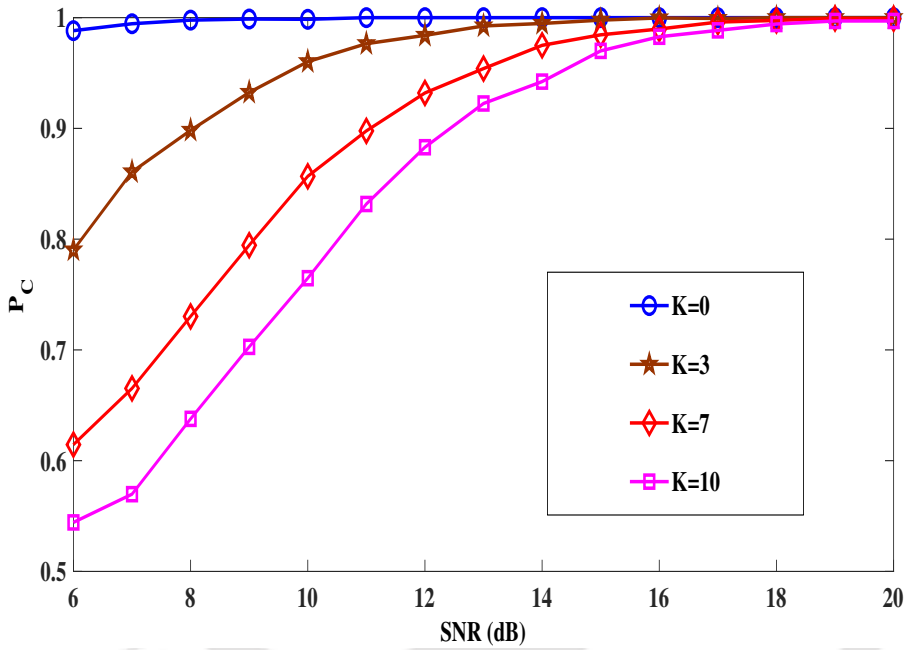

Figure 3.13: P_C versus SNR for JADE-MC with $N = 2000$ and $|\rho_R| = |\rho_T| = 0.5$ in a correlated Rician channel

Table 3.15: P_C attained by JADE-MC for different Rician factors with an SNR value of 8 dB, $N = 2000$ and $|\rho_R| = |\rho_T| = 0.3$

K	P_C
3	0.9670
7	0.8782
10	0.7970

Table 3.16: P_C attained by JADE-MC at different SNR values for $K = 10$, $N = 2000$ and $|\rho_R| = |\rho_T| = 0.3$

SNR (dB)	P_C
8	0.9670
10	0.9023
12	0.9620
14	0.9848

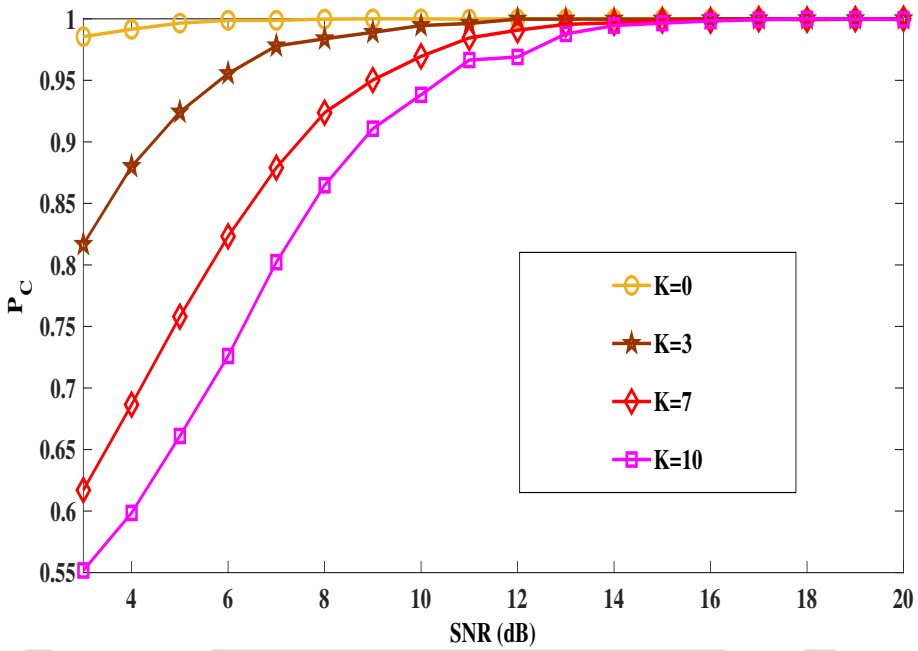

Figure 3.14: P_C versus SNR for JADE-MC with $N = 4000$ and $|\rho_R| = |\rho_T| = 0.3$ in a correlated Rician channel

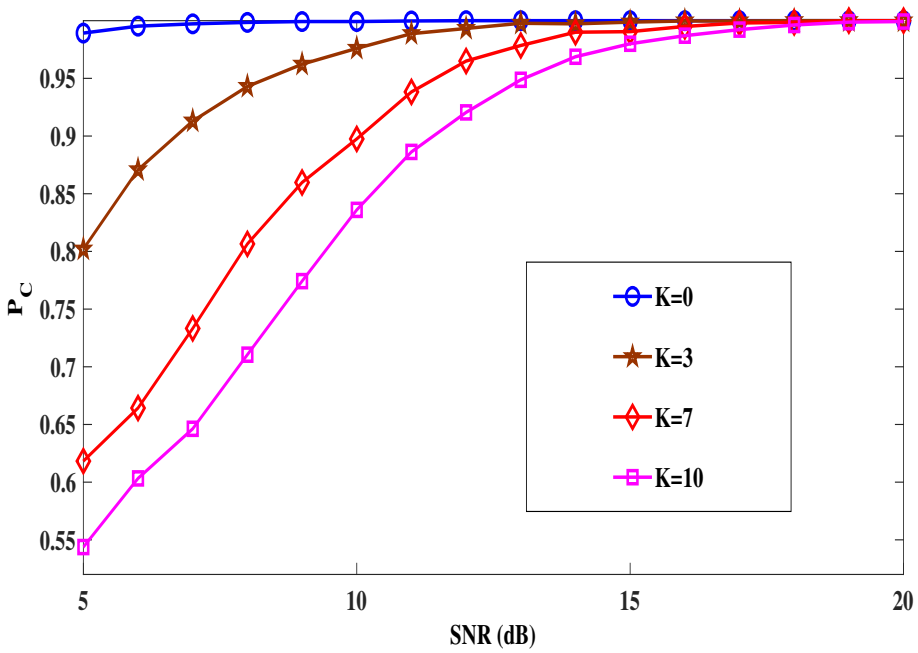

Figure 3.15: P_C versus SNR for JADE-MC with $N = 4000$ and $|\rho_R| = |\rho_T| = 0.5$ in a correlated Rician channel

3.7 Summary

This chapter dealt with the AMC of the QPSK-variant (QPSK, OQPSK and $\frac{\pi}{4}$-QPSK) and 8-PSK signals over a spatially correlated MIMO channel. The HOCs are popular as AMC features because they are resilient to the Gaussian noise. However, the HOCs estimated directly from the equalized signal failed to distinguish the QPSK-variant and 8-PSK signals. It was shown that the fourth-order cumulants of the QPSK and the OQPSK signals are identical, so also of $\frac{\pi}{4}$-QPSK and 8-PSK signals. We proposed a feature vector $\mathbf{v}^M = [C_{40}(x), C_{42}(\nabla x), C_{40}(x^e)]$ which was capable of distinguishing the above modulation types. The proposed method performed satisfactorily over a spatially correlated MIMO channel. For example, with an SNR value of 5 dB and $N = 500$, the JADE-MC technique attains $P_C = 0.9720$ for $|\rho_R| = |\rho_T| = 0.3$ over a Rayleigh channel.

4

Cooperative Automatic Modulation Classification for MIMO Systems in a Multi-Antenna Sensor Network

Contents

4.1 Introduction

In the earlier chapter, we addressed the AMC of MIMO signals in a single multi-antenna receiver situation. It was observed that the spatial fading and the spatial correlation affect the AMC performance. Ref. [35] reported that the deployment of cooperative multiple single-antenna sensors provides significant improvement in the AMC performance for the SISO signals over a multipath fading environment. However, the multiple receiver situation has not been explored by the existing works on the AMC for MIMO systems. The employment of multiple multi-antenna sensors increases the probability that signals received by some sensors are of better quality, which can be beneficial to AMC. Different copies of the same transmitted signal can be observed at the sensors on account of the varying propagations and transmission environments. These observations can be combined in an efficient way to improve the AMC performance.

The cooperative strategies are employed in a sensor network to address diverse communication and signal processing problems. Such strategies include *cooperative communication, cooperative localization and cooperative spectrum sensing* [35]. The emergence of wireless sensor networks (WSN) and coginitve radio (CR) networks makes cooperative classification an attractive strategy to improve the AMC performance. A better statistical estimate can be obtained by combining signals from multiple sensors, thereby enhancing the AMC performance.

In cooperative classification, spatially distributed autonomous sensors share data and/or classification decisions with each other to discriminate an unknown signal and make an overall decision. There are two kinds of cooperative architecture, namely *centralized cooperation* and *distributed cooperation* [42]. In a distributed signal sensing network, spatially distributed autonomous sensors track the channel environment in a cooperative manner for radio frequency (RF) spectrum monitoring. Each sensor is capable of collecting, analysing, and classifying the signal of interest independently. The sensors make soft-decisions and share the same among themselves for updating the estimates and decision fusion. Significant research has been carried out to develop cooperative modulation classifiers for SISO signals [35–44, 71, 72]. AMC based on distributed signal sensing is investigated in [71,72]. In the Centralized architectures, the spa-

tially distributed autonomous sensors transmit data to a fusion centre (FC). The FC combines the shared data and makes a final decision. The majority of the cooperative AMC algorithms proposed in the literature follow the centralized architecture [35–44].

This chapter presents a cooperative AMC method (CAMC) for MIMO signals in a distributed network. The proposed method employs a centralized cooperative classification framework with feature fusion to decide the modulation type. The rest of the chapter is organized as follows: Section 4.2 presents the system model. Section 4.3 presents the proposed CAMC method. The simulation results and the evaluation of the proposed method are presented in Section 4.4. Finally, a summary is presented in Section 4.5.

4.2 System Model

We consider a centralized cooperative system in a multi-antenna sensor network as shown in Fig. 4.1. It comprises a transmitter with N_T transmitting antennas, N_S spatially distributed autonomous multi-antenna sensors and an FC. Each multi-antenna sensor is equipped with N_R receiving antennas. We consider error free links between the sensor nodes and the FC with powerful error correcting codes. Suppose $\mathbf{x}(k) = [x_1(k)...x_{N_T}(k)]^T$ is an $N_T \times 1$ transmitted signal vector and $\mathbf{H}^l$ is the correlated channel matrix between transmitter and the l^{th} sensor node given by

$$\mathbf{H}^l = \begin{pmatrix} h^l_{11} & h^l_{12} & \cdots & h^l_{1N_T} \\ h^l_{21} & h^l_{22} & \cdots & h^l_{2N_T} \\ \vdots & \vdots & \ddots & \vdots \\ h^l_{N_R1} & h^l_{N_R2} & \cdots & h^l_{N_RN_T} \end{pmatrix}. \tag{4.1}$$

Then, the received signal vector $\mathbf{y}^l(k) = [y^l_1(k)...y^l_{N_R}(k)]^T$ at the l^{th} sensor node is given by

$$\mathbf{y}^l(k) = \mathbf{H}^l\mathbf{x}(k) + \boldsymbol{\eta}^l(k), \tag{4.2}$$

where $\boldsymbol{\eta}^l(k) = [\eta^l_1(k)...\eta^l_{N_R}(k)]^T$ is an $N_R \times 1$ vector of zero mean white circularly complex Gaussian noise.

As discussed in Chapter 3, $\boldsymbol{H}^l$ can be written as

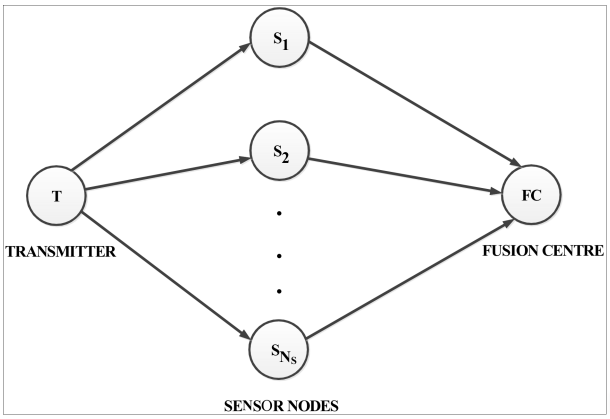

Figure 4.1: Cooperative AMC with Centralized Fusion

$$\boldsymbol{H}^l = \boldsymbol{\theta}_R^{1/2} \boldsymbol{H}_1^l \boldsymbol{\theta}_T^{1/2}, \tag{4.3}$$

where $\boldsymbol{H}_1^l$ is an $N_R \times N_T$ full rank complex channel matrix. The entries of $\boldsymbol{H}_1^l$ are i.i.d. and follow a circularly symmetric complex Gaussian distribution with zero mean and unit variance. $\boldsymbol{\theta}_T$ and $\boldsymbol{\theta}_R$ are the transmitter and the sensor correlation matrices of dimension $N_T \times N_T$ and $N_R \times N_R$ respectively. We consider the exponential antenna correlation model for this investigation. This model has been discussed in section 3.2.3 of chapter 3. An exponential correlation matrix $\boldsymbol{\theta}$ of size $L \times L$ is reproduced here.

$$\boldsymbol{\theta} = \begin{pmatrix} 1 & \rho & \cdots & \rho^{L-1} \\ \rho^* & 1 & \cdots & \rho^{L-2} \\ \vdots & \vdots & \ddots & \vdots \\ (\rho^*)^{L-1} & (\rho^*)^{L-2} & \cdots & 1 \end{pmatrix}, \tag{4.4}$$

where ρ is the correlation coefficient of adjacent antennas.

Let ρ_T and ρ_R denote the correlation coefficient of two adjacent antennas of the transmitter and the receiver respectively. Putting $\rho = \rho_T$ and $L = N_T$ in Eqn. 4.4, we get $\boldsymbol{\theta}_T$ matrix . Similarly substituting $\rho = \rho_R$ and $L = N_R$ gives $\boldsymbol{\theta}_R$ matrix.

4.3 Proposed CAMC Method

HOCs-based CAMC algorithms for SISO signals were presented in [35, 36, 38, 39]. The modulation types considered by these studies included BPSK, QPSK, 16 QAM and 64 QAM . These algorithms employ a centralized cooperative classification framework with the feature-level fusion. In such a centralized framework, each sensor node estimates a set of HOC features. These features are then combined at the FC using the maximum likelihood (ML) combining technique to decide the modulation type. The performance of such a feature-fusion method depends on the quality of the HOC estimates. Further, the decision making requires the prior knowledge of reference means and variances of the features at a given SNR. Ref. [41] reported a simple data fusion technique, where the FC takes the final decision on the modulation type based on maximum ratio combined (MRC) or equal gain combined (EGC) decision statistics.

We consider a pool of seven modulation types $Q = \{BPSK, OQPSK, QPSK, \frac{\pi}{4} - QPSK, 8 - PSK, 16 - QAM, 64QAM\}$ for this investigation. These modulation types are indexed by $M = 1, 2, 3, 4, 5, 6$ *and* 7, respectively.

4.3.1 Feature Selection

The following points are considered for selecting the features:

1) Swami et al., in [4], proposed a feature $f_1^M = C_{40}(x(k))$ to distinguish the modulation types BPSK, QPSK, 8-PSK and 16-QAM. However, f_1^M is identical for QPSK and OQPSK. It is also identical for $\frac{\pi}{4}$-QPSK and 8-PSK. The theoretical values of f_1^M for the considered modulation types are given by

$$f_1^M = \begin{cases} -2, M = 1 \\ 1, M = 2 \\ 1, M = 3 \\ 0, M = 4 \\ 0, M = 5 \\ -0.68, M = 6 \\ -0.619, M = 7 \end{cases} . \tag{4.5}$$

2) In Chapter 3, we proposed two cumualnt features $f_2^M = C_{42}(\nabla x(k)), \nabla x(k) = x(k) - x(k-1)$ and $f_3^M = C_{40}(x^e(k)), x^e(k) = x(2k), k = 0, 1, 2, \ldots$. f_2^M is capable of distinguishing QPSK and OQPSK and f_3^M is capable of distinguishing $\frac{\pi}{4}$-QPSK and 8-PSK. The theoretical values f_2^M and f_3^M for the considered modulation types are given by

$$f_2^M = \begin{cases} -4, M = 1 \\ -2, M = 2 \\ 0, M = 3 \\ -2, M = 4 \\ -2, M = 5 \\ -1.35, M = 6 \\ -1.24, M = 7 \end{cases} \tag{4.6}$$

and

$$f_3^M = \begin{cases} -2, M = 1 \\ 1, M = 2 \\ 1, M = 3 \\ 1, M = 4 \\ 0, M = 5 \\ -0.68, M = 6 \\ -0.619, M = 7 \end{cases} . \tag{4.7}$$

3) Ref. [13] proposed a feature $f_4^M = C_{63}(x(k))$ to distinguish the modulation BPSK, QPSK, 16-QAM and 64-QAM. Ref. [1] reported that in the case of discriminating BPSK and 16-QAM, the classification performance of f_4^M is better than that of the fourth-order cumualnts. However, f_4^M can not distinguish between QPSK and 8-PSK. The theoretical values f_4^M for the considered modulation types are given by

$$f_4^M = \begin{cases} 16, M = 1 \\ 4, M = 2 \\ 4, M = 3 \\ 4, M = 4 \\ 4, M = 5 \\ 2.08, M = 6 \\ 1.797, M = 7 \end{cases}. \tag{4.8}$$

Based on above discussions, we select the features f_1^M, f_2^M, f_3^M and f_4^M to distinguish the modulation types in Q. Concatenating f_1^M, f_2^M, f_3^M and f_4^M, we get the feature vector

$$\mathbf{f}^M = [f_1^M, f_2^M, f_3^M, f_4^M]. \tag{4.9}$$

For the considered modulation types, $\mathbf{f}^M$ is given as

$$\mathbf{f}^M = \begin{cases} [-2, -4, -2, 16], M = 1 \\ [1, -2, 1, 4], M = 2 \\ [1, 0, 1, 4], M = 3 \\ [0, -2, 1, 4], M = 4 \\ [0, -2, 0, 4], M = 5 \\ [-0.68, -1.35, -0.68, 2.08], M = 6 \\ [-0.619, -1.24, -0.619, 1.797], M = 7 \end{cases}. \tag{4.10}$$

It is clear from above that $\mathbf{f}^M$ is distinct for the modulation types in Q.

4.3.2 Cooperative Classification

The proposed CAMC method employs a centralized cooperative classification framework with feature-level fusion. The steps involved in the classification are (1) extraction of features, (2) combining cumulant features and (3) a classification rule. We describe these steps below.

Step 1: **Extraction of Features**

Each multi-antenna sensor node equalizes the received signal using the JADE equalization

technique. Suppose $\hat{\mathbf{x}}_j^l, j = 1, ..., N_T$, denotes the equalized signal vector of length N corresponding to N_T transmitted streams at the l^{th} sensor node. Each sensor node estimates a set of HOCs $\hat{C}_{40}(\hat{\mathbf{x}}_j^l)$, $\hat{C}_{42}(\nabla\hat{\mathbf{x}}_j^l)$, $\hat{C}_{40}(\hat{\mathbf{z}}_j^l)$ and $\hat{C}_{63}(\hat{\mathbf{x}}_j^l)$ from $\hat{\mathbf{x}}_j^l$ as follows

$$\hat{C}_{40}(\hat{\mathbf{x}}_j^l) = \frac{1}{N}\sum_{k=1}^{N}(x_j^l(k))^4 - 3(\frac{1}{N}\sum_{k=1}^{N}(x_j^l(k))^2)^2, \tag{4.11}$$

$$\hat{C}_{42}(\nabla\hat{\mathbf{x}}_j^l) = \frac{1}{N}\sum_{k=1}^{N}|\nabla x_j^l(k)|^4 - |\frac{1}{N}\sum_{k=1}^{N}(\nabla x_j^l(k))^2|^2 - 2(\frac{1}{N}\sum_{k=1}^{N}|\nabla x_j^l(k)|^2)^2, \tag{4.12}$$

$$\hat{C}_{40}(\hat{\mathbf{z}}_j^l) = \frac{1}{N}\sum_{k=1}^{N}(z_j^l(k))^4 - 3(\frac{1}{N}\sum_{k=1}^{N}(z_j^l(k))^2)^2 \tag{4.13}$$

and

$$\begin{aligned}\hat{C_{63}}(\hat{\mathbf{x}}_j^l) = &\frac{1}{N}\sum_{k=1}^{N}|x_j^l(k)|^6 - 9(\frac{1}{N}\sum_{k=1}^{N}|x_j^l(k)|^2)(\frac{1}{N}\sum_{k=1}^{N}|x_j^l(k)|^4) + 12(|\frac{1}{N}\sum_{k=1}^{N}(x_j^l(k))^2|^2) \\ &(\frac{1}{N}\sum_{k=1}^{N}|x_j^l(k)|^2) + 12(\frac{1}{N}\sum_{k=1}^{N}|x_j^l(k)|^2)^3\end{aligned}, \tag{4.14}$$

where $\nabla\hat{x}_j^l(k) = \hat{x}_j^l(k) - \hat{x}_j^l(k-1)$, $\hat{z}_j^l(k) = \hat{x}_j^l(2k), k = 0, 1, 2, ...$

The next step is to combine these estimates at the FC in an efficient way. Among the various diversity combining techniques, MRC is the best diversity combiner [73]. Ref. [35] employed the MRC technique to combine the decision statistics in the FB framework, while Ref. [41] employed the same technique to combine the decision statistics in the LB framework. In the FB framework, the HOC features are obtained as the weighted sum of those estimated from the equalized signals [35]. The weight coefficients are chosen in such a way that the estimates that are affected by high noise carry a lower weight and the estimates that are affected by low noise carry a higher weight. We employ the MRC technique to combine the similar cumulant features obtained from different sensor. The MRC requires the SNR estimate $\hat{snr}_j^l$ of the j^{th} estimated path of the l^{th}sensor [35]. The $\hat{snr}_j^l$ is obtained as

$$\hat{snr}_j^l = \frac{\sigma_s^2}{\sigma_{\hat{\mathbf{x}}_j^l}^2 - \sigma_s^2}, \tag{4.15}$$

where $\sigma_{\hat{\mathbf{x}}_j^l}^2$ is the power of equalized signal $\hat{\mathbf{x}}_j^l$ and σ_s^2 is the variance of transmit symbols . As the normalized constellation points are obtained after equalization, we can assume $\sigma_s^2 = 1$.

Now, each sensor node transmits the HOC estimates given by Eqns. 4.11-4.14 and the SNR estimate $\hat{snr}_j^l$ given by Eqn. 4.15 to the FC.

Step 2: **Combining Features at FC**

Suppose w_j^l denotes the weight coefficient for the j^{th} estimated path of the l^{th}sensor. The weight coefficients are given by [35]

$$w_j^l = \frac{\hat{snr}_j^l}{snr_{max}}, j = 1, ..., N_T, l = 1, ..., N_S, \tag{4.16}$$

where snr_{max} is the maximum local SNR value.

Now, suppose $\hat{f}_1$, $\hat{f}_2$, $\hat{f}_3$ and $\hat{f}_4$ are the estimates of f_1^M, f_2^M, f_3^M and f_4^M respectively computed at FC. These estimates are obtained by the MRC of the cumulant features as follows:

$$\hat{f}_1 = \frac{\sum_{l=1}^{N_S}\sum_{j=1}^{N_T} w_j^l \hat{C}_{40}(\hat{\mathbf{x}}_j^l)}{\sum_{l=1}^{N_S}\sum_{j=1}^{N_T} w_j^l}, \tag{4.17}$$

$$\hat{f}_2 = \frac{\sum_{l=1}^{N_S}\sum_{j=1}^{N_T} w_j^l \hat{C}_{42}(\nabla\hat{\mathbf{x}}_j^l)}{\sum_{l=1}^{N_S}\sum_{j=1}^{N_T} w_j^l}, \tag{4.18}$$

$$\hat{f}_3 = \frac{\sum_{l=1}^{N_S}\sum_{j=1}^{N_T} w_j^l \hat{C}_{40}(\hat{\mathbf{z}}_j^l)}{\sum_{l=1}^{N_S}\sum_{j=1}^{N_T} w_j^l} \tag{4.19}$$

and

$$\hat{f}_4 = \frac{\sum_{l=1}^{N_S}\sum_{j=1}^{N_T} w_j^l \hat{C}_{63}(\hat{\mathbf{x}}_j^l)}{\sum_{l=1}^{N_S}\sum_{j=1}^{N_T} w_j^l}, \tag{4.20}$$

.

Step 3: **Classification Rule**

The estimated feature vector $\hat{\mathbf{f}} = [\hat{f}_1, \hat{f}_2, \hat{f}_3, \hat{f}_4]$ is subjected to a minimum distance classifier that uses the Euclidean distance as the measure of feature similarity. The detected modulation class M^* is then given by

$$M^* = \underset{M=1,2,...,7}{argmin}(||\hat{\mathbf{f}} - \mathbf{f}^M||). \tag{4.21}$$

4.4 Simulation Results and Discussion

A set of experiments were carried out to evaluate the performance of the proposed method through the Monte-Carlo simulation. The average probability of correct classification P_C is employed as the performance measure. For each SNR value, 3000 Monte Carlo simulations were performed to calculate P_C. We generated a source message and a channel matrix randomly for each trail.

Figs. 4.2-4.4 show P_C versus SNR for the proposed CAMC method over an uncorrelated Rayleigh channel with $N_T = 2$ and $N_R = 4$. One can note that P_C increases with an increase in N_S. For instance, with an SNR value of 2 dB and $N = 500$, the CAMC method attains $P_C = 0.8163$ for $N_S = 1$, while at the same SNR and sample length, it attains $P_C = 0.8961$ for $N_S = 4$. With an SNR value of 2 dB and $N = 1000$, the CAMC method attains $P_C = 0.8736$ for $N_S = 1$, while at the same SNR and sample length, it attains $P_C = 0.9380$ for $N_S = 4$. Figs. 4.5-4.10 show P_C versus SNR for the proposed CAMC method over a correlated Rayleigh channel with $N_T = 2$ and $N_R = 4$. With an SNR value of 3 dB, $N = 1000$ and $|\rho_R| = |\rho_T| = 0.5$, the CAMC method attains $P_C = 0.8173$ for $N_S = 1$, while at the same SNR, sample length and antenna correlation value, it attains $P_C = 0.9325$ for $N_S = 8$. With an SNR value of 5 dB, $N = 1000$ and $|\rho_R| = |\rho_T| = 0.7$, the CAMC method attains $P_C = 0.7703$ for $N_S = 1$, while for the same SNR, sample length and antenna correlation value, it achieves $P_C = 0.9015$ for $N_S = 8$. Figs 4.11-4.13 show P_C versus SNR for the proposed CAMC method over a correlated Rayleigh channel with $N_T = 2$ and $N_R = 6$. With an SNR value of 4 dB, $N = 500$ and $|\rho_R| = |\rho_T| = 0.7$, the CAMC method attains $P_C = 0.8217$ for $N_S = 1$, while at the same SNR, sample length and antenna correlation value, it attains $P_C = 0.9306$ for $N_S = 8$. With an SNR value of 4 dB, $N = 1000$ and $|\rho_R| = |\rho_T| = 0.7$, the CAMC method attains $P_C = 0.8811$ for $N_S = 1$, while at the same SNR, sample length and antenna correlation value, it attains $P_C = 0.9599$ for $N_S = 8$. Figs. 4.14-4.15 show P_C versus SNR for the proposed CAMC

method over a correlated Rayleigh channel with $N_T = 2$ and $N_R = 8$. With an SNR value of 3 dB, $N = 500$ and $|\rho_R| = |\rho_T| = 0.5$, the CAMC method attains $P_C = 0.8621$ for $N_S = 1$, while at the same SNR, sample length and antenna correlation value, it attains $P_C = 0.9425$ for $N_S = 8$. With an SNR value of 3 dB, $N = 1000$ and $|\rho_R| = |\rho_T| = 0.7$, the CAMC method attains $P_C = 0.9093$ for $N_S = 1$, while at the same SNR, sample length and antenna correlation value, it attains $P_C = 0.9720$ for $N_S = 8$.

Table 4.1 shows the P_C attained by the CAMC method with an SNR value of 5 dB, $N_T = 2$, $N_R = 4$, $N = 500$ and $|\rho_R| = |\rho_T| = 0.5$ for different values N_S. Table 4.2 shows the P_C achieved by the CAC method with an SNR value of 5 dB, $N_T = 2$, $N_R = 4$, $N = 500$ and $|\rho_R| = |\rho_T| = 0.7$ for different values N_S. Table 4.3 shows the P_C attained by the CAMC method with an SNR value of 5 dB, $N_T = 2$,$N_R = 6$, $N = 500$ and $|\rho_R| = |\rho_T| = 0.7$ for different values N_S. It is clear from these tables that P_C increases with an increase in N_S. The increase in P_C with an increase in N_S is contributed by the increased diversity gain. A better statistical estimate is obtained by combining signals from multiple sensors, thereby enhancing the AMC performance.

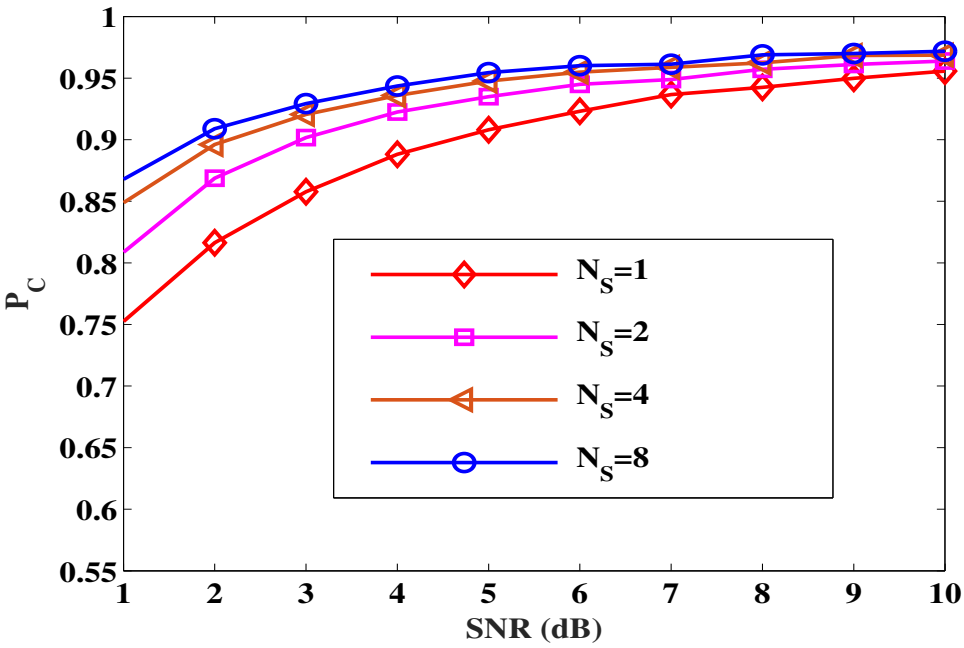

Figure 4.2: P_C versus SNR with $N_T = 2$, $N_R = 4$, $N = 500$ and $|\rho_R| = |\rho_T| = 0$

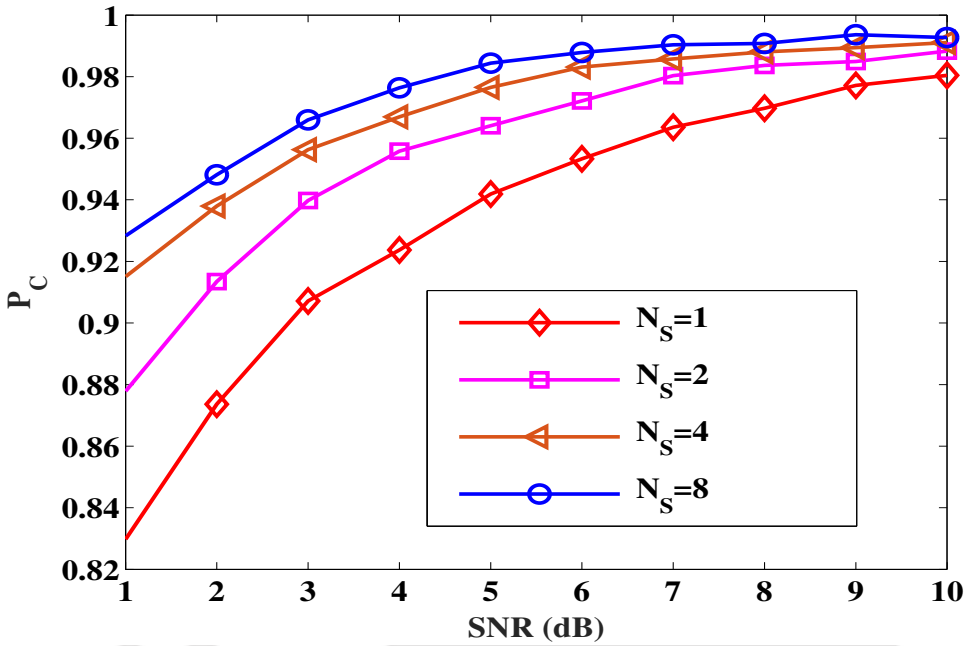

Figure 4.3: P_C versus SNR with $N_T = 2$, $N_R = 4$, $N = 1000$ and $|\rho_R| = |\rho_T| = 0$

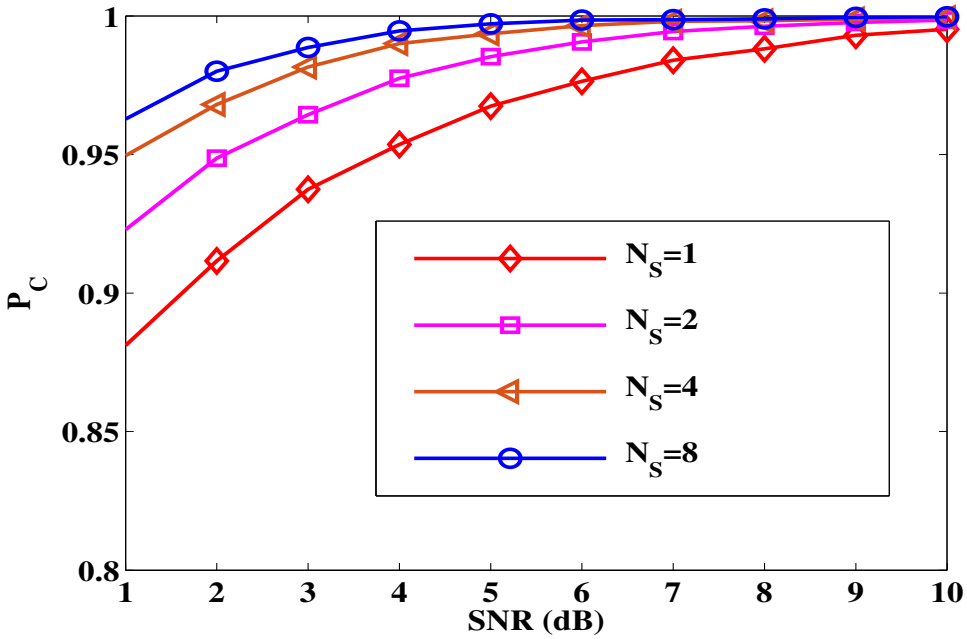

Figure 4.4: P_C versus SNR with $N_T = 2$, $N_R = 4$, $N = 2000$ and $|\rho_R| = |\rho_T| = 0$

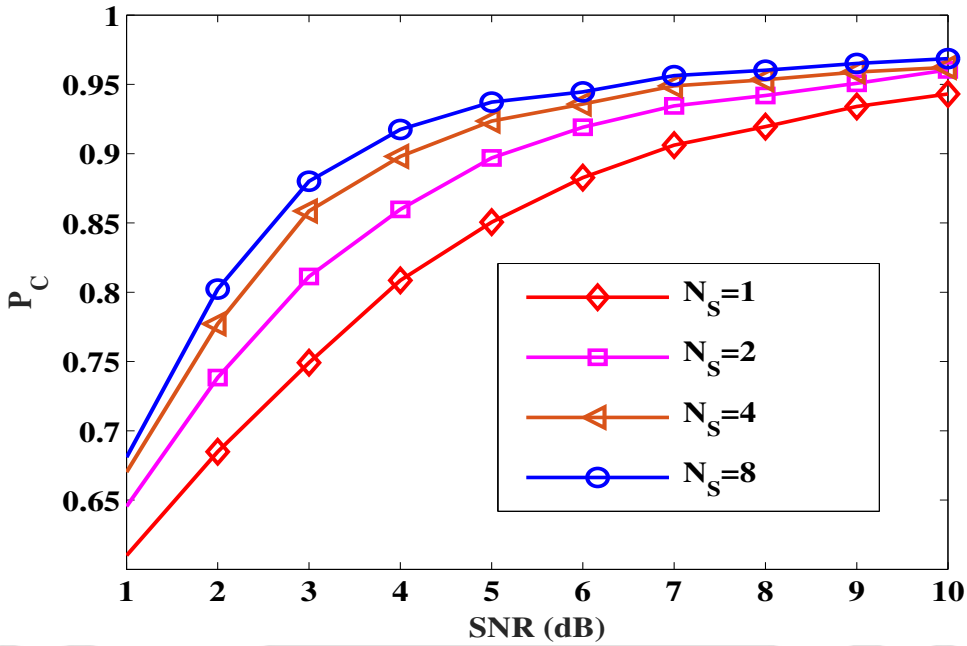

Figure 4.5: P_C versus SNR with $N_T = 2$, $N_R = 4$, $N = 500$ and $|\rho_R| = |\rho_T| = 0.5$

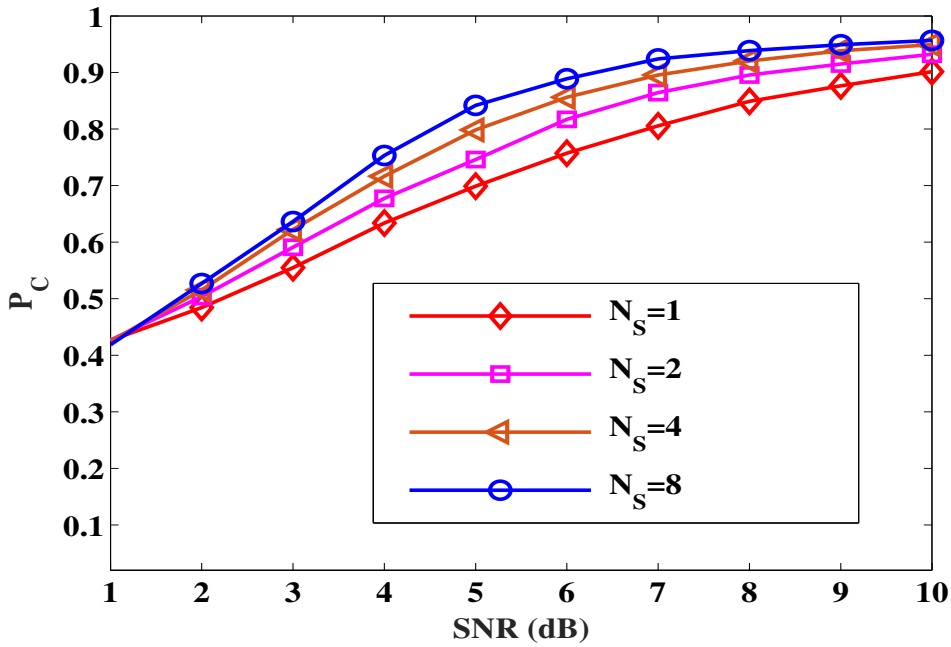

Figure 4.6: P_C versus SNR with $N_T = 2$, $N_R = 4$, $N = 500$ and $|\rho_R| = |\rho_T| = 0.7$

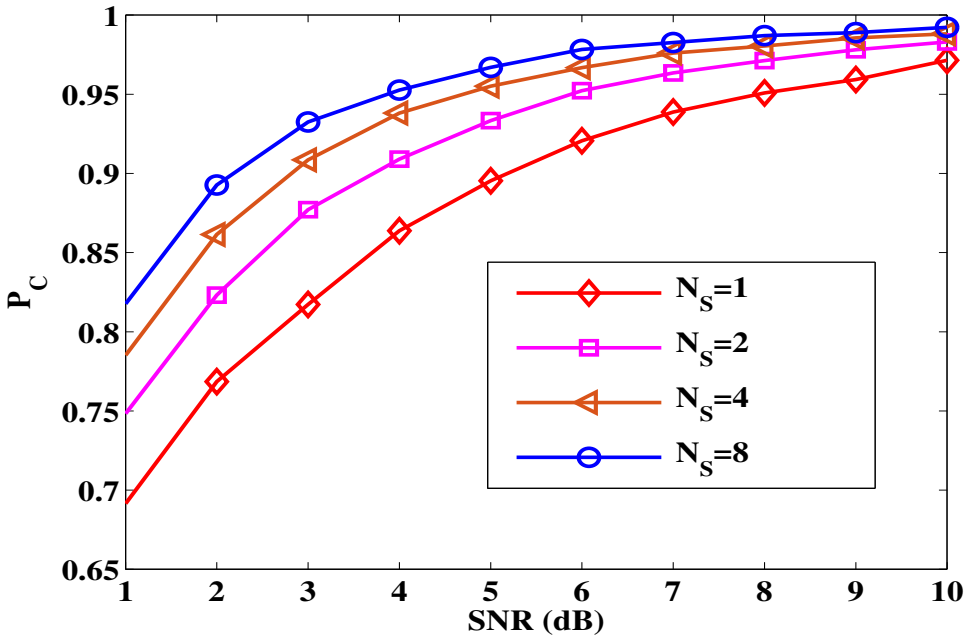

Figure 4.7: P_C versus SNR with $N_T = 2$, $N_R = 4$, $N = 1000$ and $|\rho_R| = |\rho_T| = 0.5$

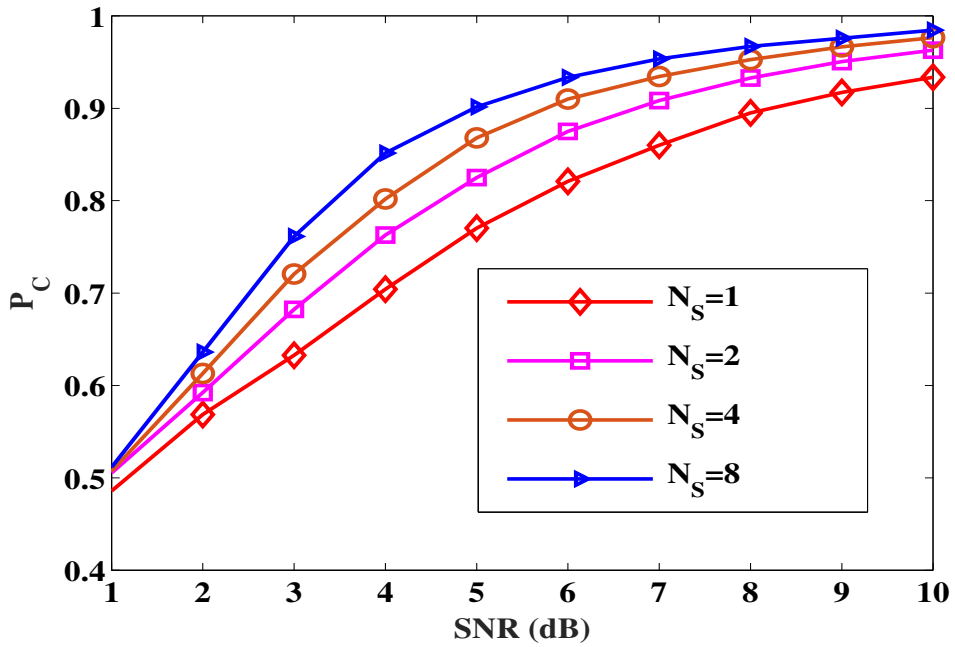

Figure 4.8: P_C versus SNR with $N_T = 2$, $N_R = 4$, $N = 1000$ and $|\rho_R| = |\rho_T| = 0.7$

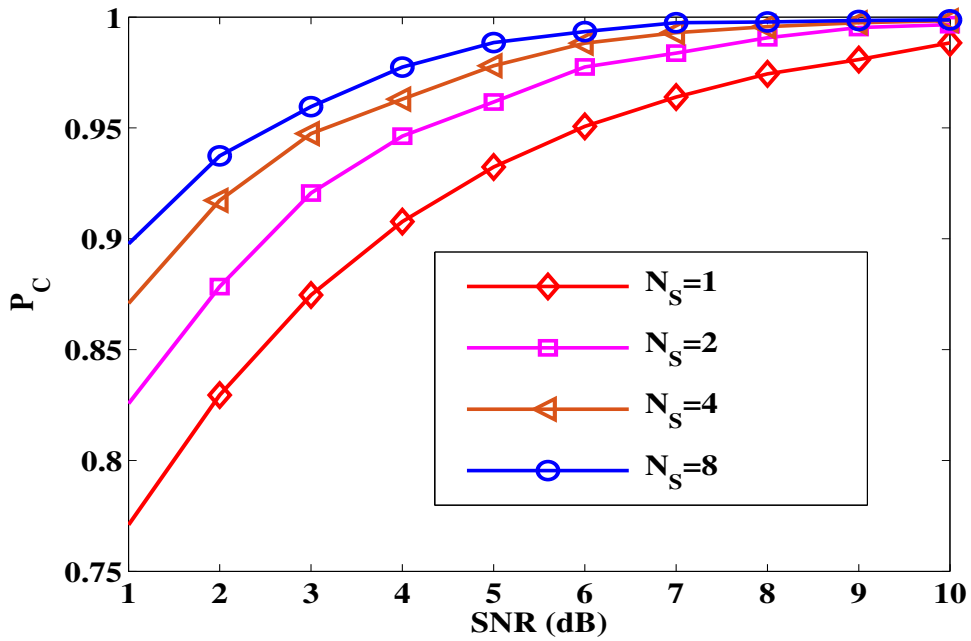

Figure 4.9: P_C versus SNR with $N_T = 2$, $N_R = 4$, $N = 2000$ and $|\rho_R| = |\rho_T| = 0.5$

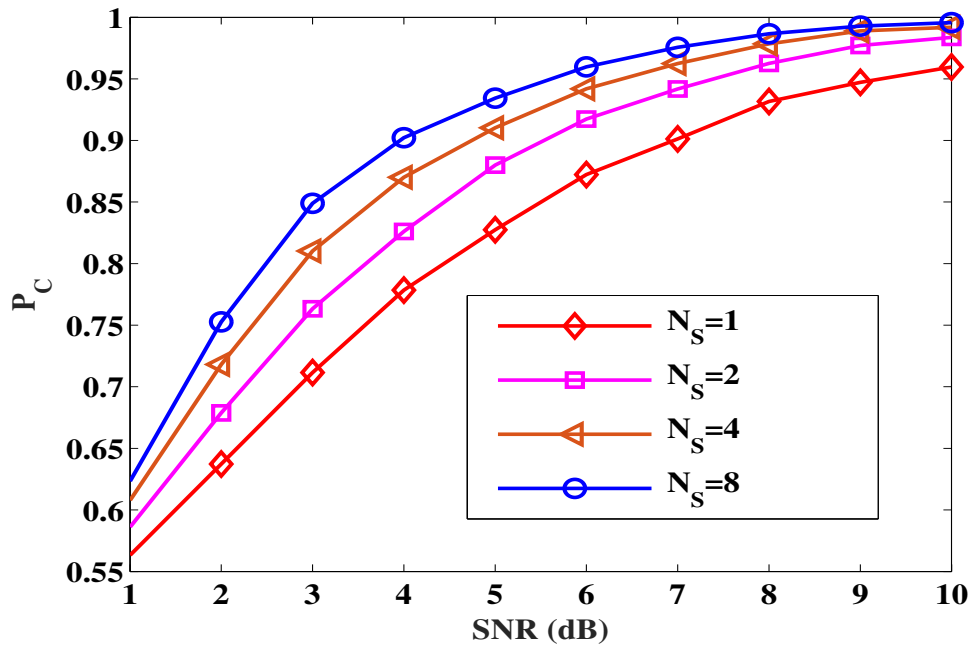

Figure 4.10: P_C versus SNR with $N_T = 2$, $N_R = 4$, $N = 2000$ and $|\rho_R| = |\rho_T| = 0.7$

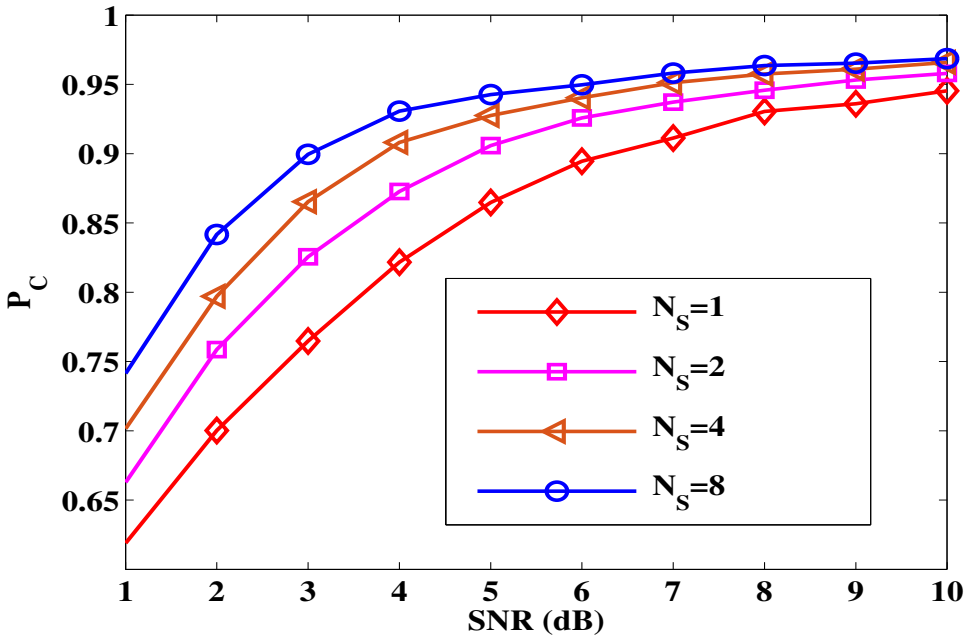

Figure 4.11: P_C versus SNR with $N_T = 2$, $N_R = 6$, $N = 500$ and $|\rho_R| = |\rho_T| = 0.7$

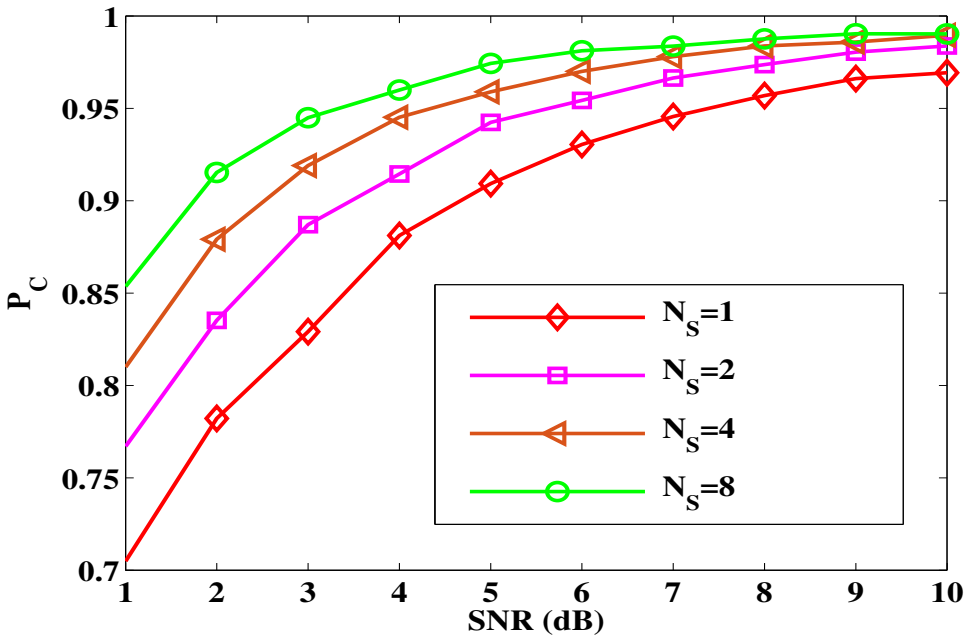

Figure 4.12: P_C versus SNR with $N_T = 2$, $N_R = 6$, $N = 1000$ and $|\rho_R| = |\rho_T| = 0.7$

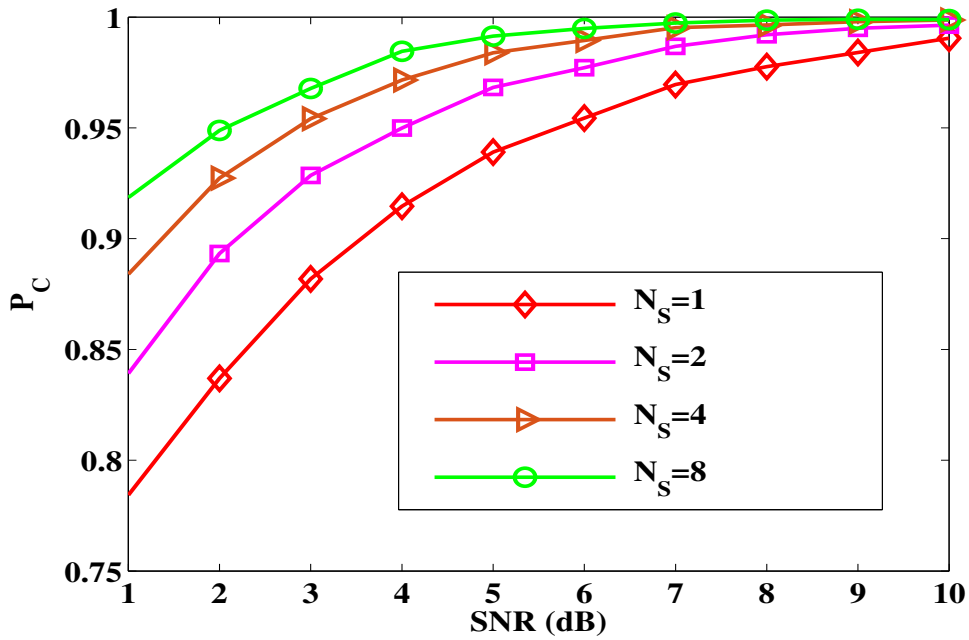

Figure 4.13: P_C versus SNR with $N_T = 2$, $N_R = 6$, $N = 2000$ and $|\rho_R| = |\rho_T| = 0.7$

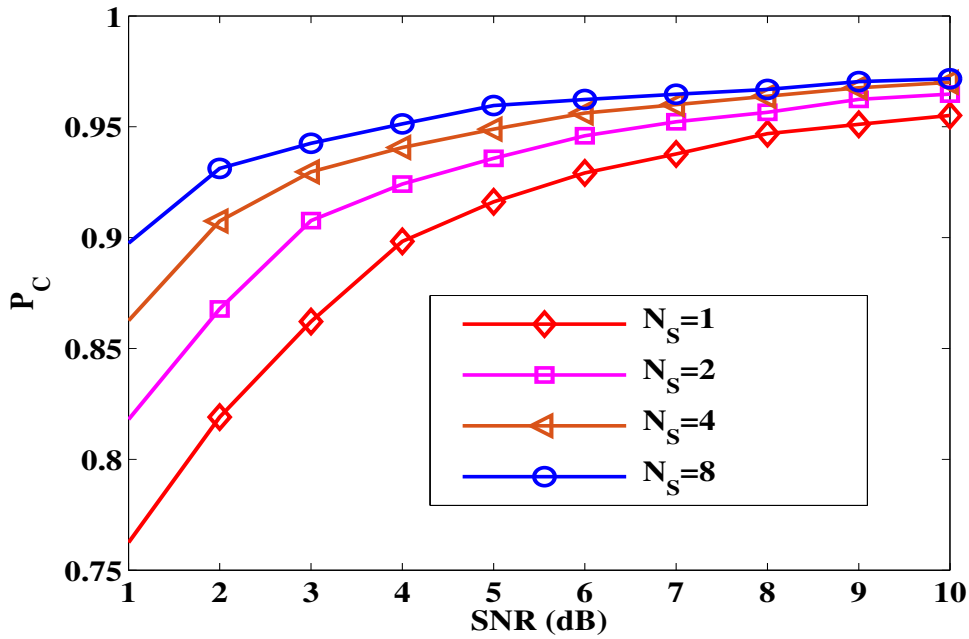

Figure 4.14: P_C versus SNR with $N_T = 2$, $N_R = 8$, $N = 500$ and $|\rho_R| = |\rho_T| = 0.7$

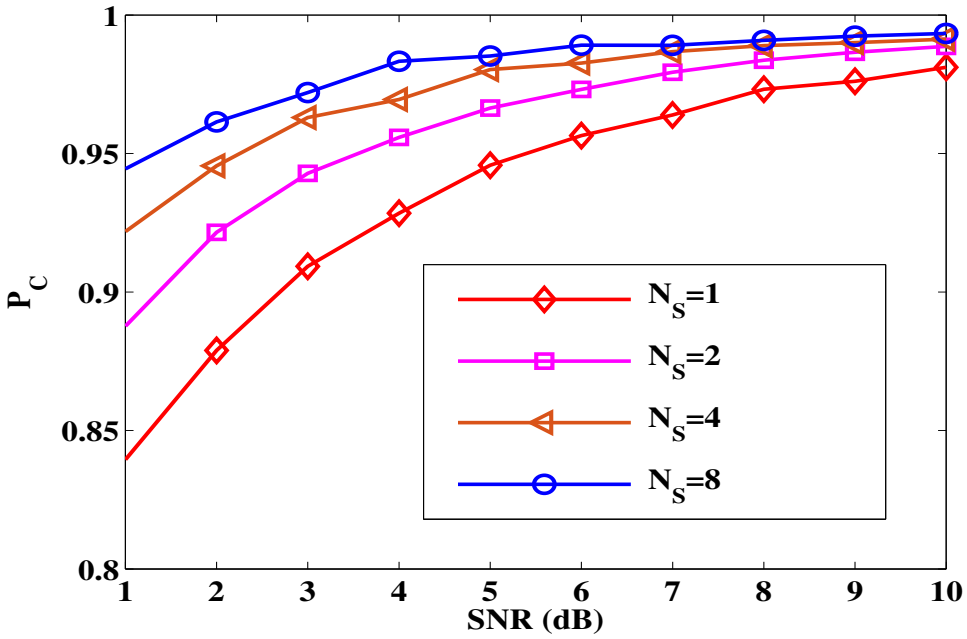

Figure 4.15: P_C versus SNR with $N_T = 2$, $N_R = 8$, $N = 1000$ and $|\rho_R| = |\rho_T| = 0.7$

Table 4.1: P_C at an SNR value of 5 dB with $N_T = 2$, $N_R = 4$, $N = 500$ and $|\rho_R| = |\rho_T| = 0.5$

N_S	P_C
1	0.8505
2	0.8970
4	0.9235
8	0.9371

Table 4.2: P_C at an SNR value of 5 dB with $N_T = 2$, $N_R = 4$, $N = 500$ and $|\rho_R| = |\rho_T| = 0.7$

N_S	P_C
1	0.6990
2	0.7460
4	0.7984
8	0.8418

Table 4.3: P_C at an SNR value of 5 dB with $N_T = 2$, $N_R = 6$, $N = 500$ and $|\rho_R| = |\rho_T| = 0.7$

N_S	P_C
1	0.8647
2	0.9058
4	0.9275
8	0.9427

4.5 Summary

This chapter proposed a CAMC method for the MIMO system in a distributed network. A better statistical estimation was obtained by combining signals from multiple sensors, thereby enhancing AMC performance. A feature vector $\mathbf{f}^M = [f_1^M, f_2^M, f_3^M, f_4^M]$ was employed to classify the modulation types BPSK, OQPSK, QPSK, $\frac{\pi}{4}$-QPSK, 8-PSK,16-QAM and 64-QAM. The proposed method employed a centralized cooperative classification framework with the feature-level fusion. The method performed reasonably well. For instance, with an SNR value of 3 dB, $N_T = 2$, $N_R = 4$, $N = 1000$ and $|\rho_R| = |\rho_T| = 0.5$, the CAMC method attained $P_C = 0.8173$ for $N_S = 1$, while for the same SNR, sample length and antenna correlation value, it attained $P_C = 0.9325$ for $N_S = 8$ with $N_T = 2$, $N_R = 4$.

4. Cooperative Automatic Modulation Classification for MIMO Systems in a Multi-Antenna Sensor Network

5

Automatic Modulation Classification over Spatially Correlated Keyhole MIMO Channels

Contents

5.1 Introduction

The MIMO spatial channel alters the statistical properties of the modulated signal, which makes AMC a challenging task. It is, therefore, necessary to cancel the channel mixing effect prior to AMC. It is observed in the literature that the most of the existing MIMO blind channel estimation techniques such as the JADE [31] and the constant modulus algorithm (CMA) [29, 30], require the channel matrix to be of full rank. The majority of the AMC algorithms for MIMO systems have considered the rich scattering environment that offers a full rank channel matrix [1, 15, 17–28]. In practice, MIMO systems can also operate in an insufficient scattering environment, which can lead to a rank deficient channel [14, 46, 47, 49, 50, 52, 56, 74]. For example, one may consider a scenario where a user device located indoor, transmits signals to a cell tower. The opaqueness of building walls to the signal transmitted by the user device allows the most of the signal energy to pass through keyholes like windows, doors etc [14]. The presence of a keyhole is also possible in outdoor scenarios, even under a rich scattering environment [50]. It can happen when the ring of scatterers around the transmitter and the receiver is small compared to the distance between the transmitter and the receiver. Therefore, rich scattering is only a necessary but not sufficient condition for full rank MIMO channels. A rank deficient channel, such as a keyhole channel can severely degrade the AMC performance. The entries of such a spatial channel matrix are no longer single Rayleigh distributed. It is shown in [46] that these channel entries are double Rayleigh distributed. Such low rank channel models have poor fading statistics because a double Rayleigh channel fades more than a single Rayleigh channel [75]. In addition to the keyhole effect, correlated transmitting and receiving antennas also affect the AMC performance [14]. The antenna correlation is attributed to the inadequate physical separation between antenna elements.

This chapter addresses the problem of AMC over a spatially-correlated keyhole MIMO channels. We propose a novel algorithm, namely the direct modulation recognition (DMR) algorithm, which is capable of classifying the lower order PSK constellations, namely BPSK, QPSK and OQPSK. The proposed algorithm employs the ratios of HOCs derived from the received signal and its backward difference as AMC features. These features are chosen so that

the contributions of the channel-coefficients are cancelled. Thus, the DMR algorithm does not require the CSI at the receiver.

The rest of the chapter is organized as follows: Section 5.2 presents the system model. The investigation of the fourth-order zero-conjugate cumulant based AMC algorithm over MIMO keyhole channels is presented in Section 5.3. Section 5.4 presents the proposed AMC method. The simulation results and the evaluation of the proposed method are presented in Section 5.5. Finally, a summary is presented in Section 5.6.

5.2 System Model

Consider a spatial multiplexing MIMO system with N_T transmitting and N_R receiving antennas as discussed in Chapter 1. The received signal model can be written as

$$\mathbf{y}(k) = \mathbf{H}\mathbf{x}(k) + \boldsymbol{\eta}(k), \tag{5.1}$$

where $\mathbf{x}(k) = [x_1(k)...x_{N_T}(k)]^T$ is an $N_T \times 1$ transmitted signal vector, $\mathbf{y}(k) = [y_1(k)...y_{N_R}(k)]^T$ is an $N_R \times 1$ received signal vector, $\boldsymbol{\eta}(k) = [\eta_1(k)...\eta_{N_R}(k)]^T$ is an $N_R \times 1$ vector of circularly complex white Gaussian noise with variance σ_η^2 and $\mathbf{H}$ is an $N_R \times N_T$ complex channel matrix.

It is generally assumed that the transmitter and the receiver are surrounded by quasi-static local scatters [49], leading to an uncorrelated Gaussian channel. Therefore, the channel coefficients in $\boldsymbol{H}$ can be modelled as i.i.d.complex Gaussian random variables. However, in some practical scenarios, the signal transmitted by a MIMO transmitter has to pass through a keyhole. The MIMO keyhole channel is described next.

5.2.1 MIMO Keyhole Channel

Figure 5.1 shows a MIMO system in the presence of a keyhole. The channel matrix of a MIMO keyhole channel can be represented as [49]

$$\mathbf{H_1} = \boldsymbol{d}\boldsymbol{g}^T = \begin{pmatrix} g_1 d_1 & g_2 d_1 & \cdots & g_{N_T} d_1 \\ g_1 d_2 & g_2 d_2 & \cdots & g_{N_T} d_2 \\ \vdots & \vdots & \ddots & \vdots \\ g_1 d_{N_R} & g_2 d_{N_R} & \cdots & g_{N_T} d_{N_R} \end{pmatrix}, \tag{5.2}$$

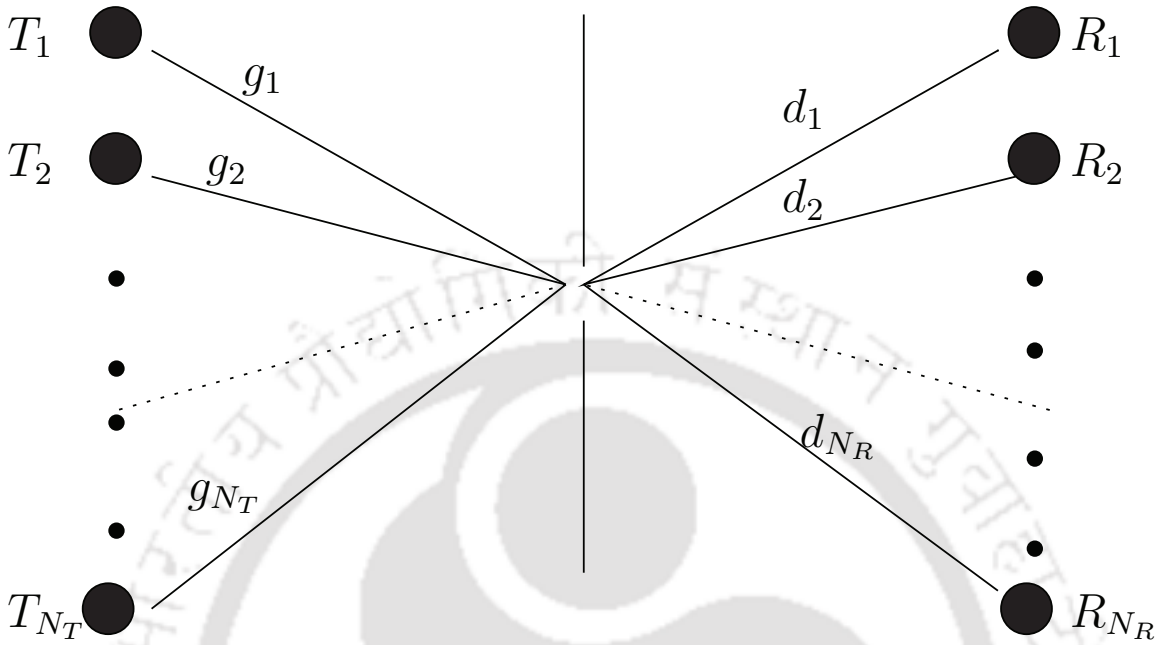

Figure 5.1: A MIMO system with keyhole

where $\boldsymbol{d} = [d_1 ... d_{N_R}]^T$ is the $N_R \times 1$ channel gain vector between the keyhole and the receiver and $\boldsymbol{g} = [g_1 ... g_{N_T}]^T$ is the $N_T \times 1$ channel gain vector between the transmitter and the keyhole. The rank of $\mathbf{H_1}$ is one. The amplitude of each element of $\mathbf{H_1}$ is double-Rayleigh distributed [46]. The probability density function (PDF) of double-Rayleigh variable is given by [75].

$$f(r) = \frac{r}{\sigma^4} K_0(\frac{2r}{\sigma^2}), \tag{5.3}$$

where $K_0(.)$ denotes the zeroth-order modified Bessel function of the second kind and σ^2 represents the average power of each channel path. A double Rayleigh channel fades more than the standard Rayleigh channel. The PDFs of Rayleigh and double-Rayleigh random variables are plotted in Fig. 5.2.

After incorporating the spatial correlation, the channel matrix $\boldsymbol{H}$ of a spatially correlated MIMO channel is given by

$$\boldsymbol{H} = \boldsymbol{\theta}_R^{1/2} \mathbf{H_1} \boldsymbol{\theta}_T^{1/2}, \tag{5.4}$$

where $\boldsymbol{\theta}_R$ and $\boldsymbol{\theta}_T$ are the receiver and the transmitter correlation matrices. The exponential

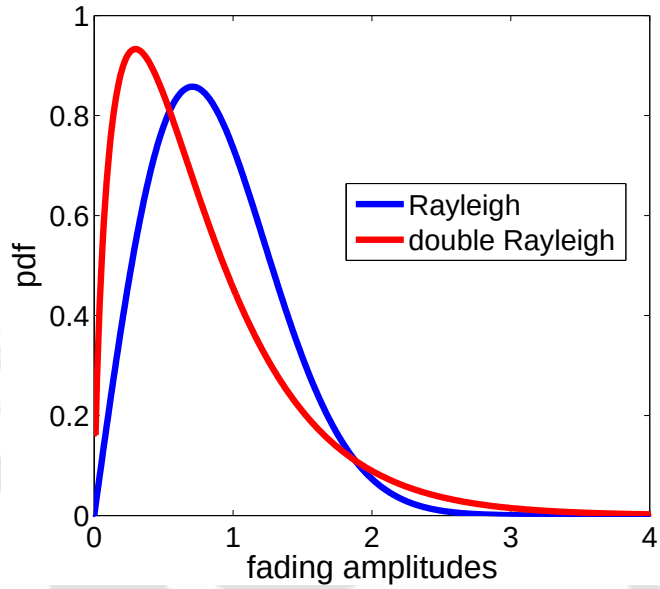

Figure 5.2: PDFs of Rayleigh and Double-Rayleigh Channel Amplitude

antenna correlation model is considered for this investigation.

5.3 Investigation of the Fourth-Order Zero-Conjugate Cumulant based AMC technique over MIMO Keyhole Channels

Swami et al., in [4], reported that different digitally modulated signals exhibit distinct fourth-order cumulant values. The fact that the fourth-order cumulants offer resistance to the Gaussian noise makes them attractive AMC features. In [15], Muhlhaus et al. proposed a fourth-order zero-conjugate cumulant (FZC) based AMC algorithm over an uncorrelated Rayleigh MIMO channel. Here, we investigate the performance of this algorithm over a spatially correlated MIMO keyhole channel. For this investigation, we consider two modulation types, namely BPSK and QPSK. These two modulation types are indexed by $M = 1$ *and* 2 respectively. The algorithm involves following steps [15]:

Step 1: Equalize the received signal (using ZF or JADE) $\mathbf{y}(k)$ to obtain N_T transmitted streams $\hat{\mathbf{x}}_j$, $j = 1, ..., N_T$.

step 2: Estimate the 4^{th}-order zero-conjugate cumualnt from $\hat{\mathbf{x}}_j$, $j = 1, ..., N_T$.

Step 3: Combine the cumulant estimates as

$$\hat{f} = \frac{\sum_{j=1}^{N_T} (snr_j)^2 C_{42}(\hat{\mathbf{x}}_j)}{\sum_{j=1}^{N_T} (snr_j)^2} \tag{5.5}$$

where snr_j is the SNR of the jth path.

Step 3: Decide M^* as

$$M^* = \underset{M=1,2}{argmin}(|\hat{f} - f^M|). \tag{5.6}$$

where f^M is the theoretical FZC value for the M^{th} modulation type.

Although the algorithm performs very well under a rich scattering environment, it performs poorly in the presence of a keyhole. This is because under the keyhole condition both the ZF and JADE equalizers fail to equalize the received signal. This is validated by the simulation results presented in Fig. 5.3 and Fig. 5.4. We refer the above technique as ZF-FZC if the employed equalization technique is ZF. If the employed equalization technique is JADE, we refer it as JADE-FZC. For the simulation, the number of transmitting and receiving antennas were set at $N_T = 2$ and $N_R = 4$, respectively. For each trial, we generated a random channel matrix and a random source message. For each SNR value, 3000 Monte Carlo simulations were performed to calculate the average probability of correct classification P_C.

Table 5.1: Fourth-Order Zero-Conjugate Cumulant Values for BPSK and QPSK

M	f^M
1	- 2
2	1

5.3.1 Effect of a Keyhole on Channel Equalization

The equalized signal at the ZF equalizer output can be written as

$$\begin{aligned}\hat{\mathbf{y}}(k) &= (\mathbf{H}^H\mathbf{H})^{-1}\mathbf{H}^H\mathbf{H}\mathbf{x}(k) + (\mathbf{H}^H\mathbf{H})^{-1}\mathbf{H}^H\boldsymbol{\eta}(k) \\ &= \mathbf{x}(k) + \mathbf{z}(k),\end{aligned} \tag{5.7}$$

where $\mathbf{z}(k) = (\mathbf{H}^H\mathbf{H})^{-1}\mathbf{H}^H\boldsymbol{\eta}(k)$.

The total noise variance at the ZF equalizer output can be written as [14]

$$\sigma_{\mathbf{z}}^2 = N_R\sigma_\eta^2 Tr[(\mathbf{H}^H\mathbf{H})^{-1}]. \tag{5.8}$$

As stated earlier, the rank of the keyhole channel is one. It is clear from Eqn. 5.8 that the noise amplification takes place at the ZF output whenever the rank of $\mathbf{H}^H\mathbf{H}$ is low [14]. When $N_S = 1$

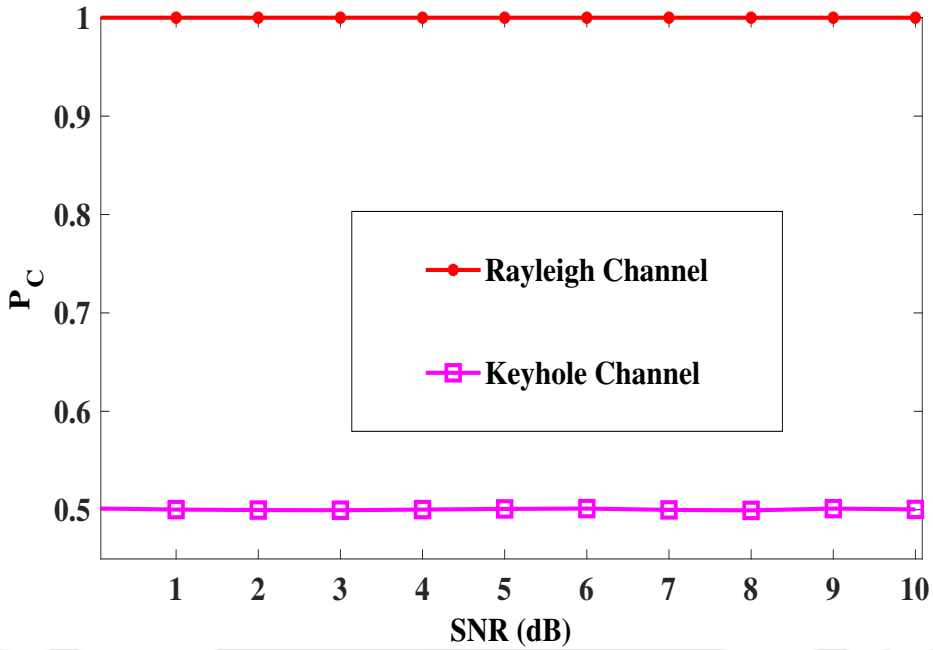

Figure 5.3: P_C versus SNR for ZF-FZC with $N_T = 2$, $N_R = 4$, $N = 2000$ and $|\rho_R| = |\rho_T| = 0$

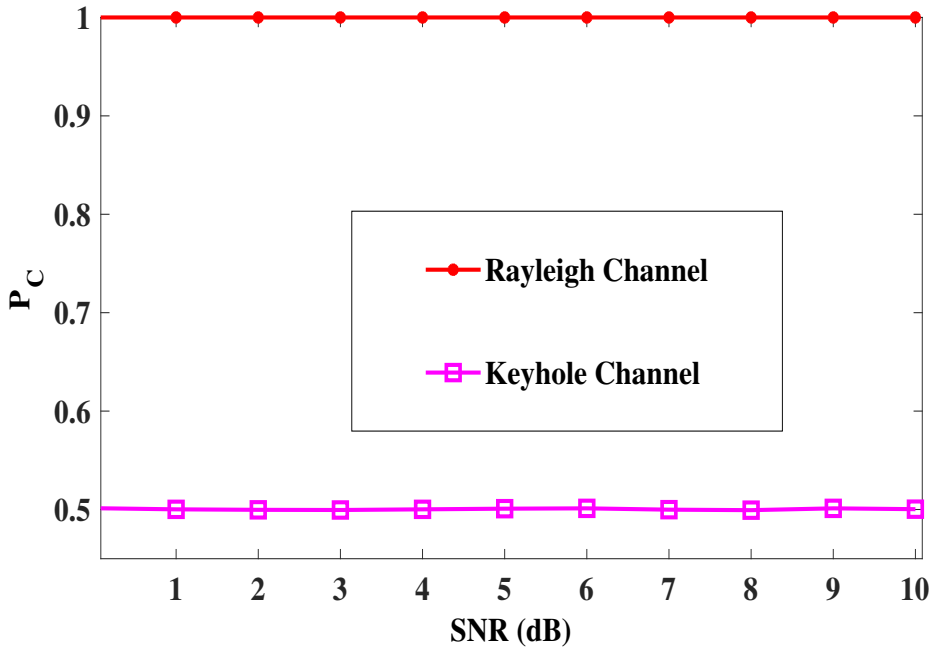

Figure 5.4: P_C versus SNR for JADE-FZC with $N_T = 2$, $N_R = 4$, $N = 2000$ and $|\rho_R| = |\rho_T| = 0$

, the channel model becomes akin to the keyhole or pinhole MIMO channel. Therefore, the ZF equalizer suffers from noise amplification under the keyhole condition. The JADE technique too fails to equalize the received signal as it requires the channel matrix to be of rank one for

the separation of independent components [31] .

5.4 Proposed AMC Method

Before going into the details of the proposed AMC algorithm, we revisit two important properties of the cumulants which will be useful in deriving the proposed cumualnt features:

1) Additive Property : If $y_1(k)$ and $y_2(k)$ are two independent random processes and $y(k) = y_1(k) + y_2(k)$, then the n^{th} order m conjugate cumulant of $y(k)$ is the sum of individual cumulants of $y_1(k)$ and $y_2(k)$ i.e.

$$C_{n,m}(y(k)) = C_{n,m}(y_1(k)) + C_{n,m}(y_2(k)). \tag{5.9}$$

2) Scaling Property : if $y(k) = ax(k)$, then n^{th} order m conjugate cumulant of $y(k)$ is given as

$$C_{n,m}(y(k)) = a^{n-m}(a^*)^m C_{n,m}(x(k)). \tag{5.10}$$

Now, consider a received signal at the k^{th} instant at the i^{th} receiving antenna as

$$y_i(k) = h_{i1}x_1(k) + h_{i2}x_2(k) + ... + h_{iN_T}x_{N_T}(k) + \eta_i(k), i = 1, ..., N_R. \tag{5.11}$$

The backward difference of $y_i(k)$ gives

$$\nabla y_i(k) = h_{i1}\nabla x_1(k) + ... + h_{iN_T}\nabla x_{N_T}(k) + \nabla\eta_i(k) \tag{5.12}$$

where $\nabla x_i(k) = x_i(k) - x_i(k-1)$ and $\nabla\eta_i(k) = \eta_i(k) - \eta_i(k-1)$.

Using the additive and the scaling properties of the cumulants given by Eqn. 5.9 and Eqn. 5.10 respectively, the n^{th} order m conjugate cumulant of $y_i(k)$ and $\nabla y_i(k)$ are respectively given as

$$C_{n,m}(y_i(k)) = h_{i1}^{n-m}(h_{i1}^*)^m C_{n,m}(x_1(k)) + ... + h_{iN_T}^{n-m}(h_{iN_T}^*)^m C_{n,m}(x_{N_T}(k)) + C_{n,m}(\eta_i(k)) \tag{5.13}$$

and

$$C_{n,m}(\nabla y_i(k)) = h_{i1}^{n-m}(h_{i1}^*)^m C_{n,m}(\nabla x_1(k)) + ... + h_{iN_T}^{n-m}(h_{iN_T}^*)^m C_{n,m}(x_{N_T}(k)) + C_{n,m}(\nabla\eta_i(k)). \tag{5.14}$$

As $x_1(k)$,...,$x_{N_T}(k)$ belong to the same modulation constellation, we have $C_{n,m}(x_1(k)) = ... = C_{n,m}(x_{N_T}(k))$ and $C_{n,m}(\nabla x_1(k)) = ... = C_{n,m}(\nabla x_{N_T}(k))$. Note that $C_{n,m}(\eta_i(k)) = C_{n,m}(\nabla \eta_i(k)) = 0$, for $n \geq 3$. Therefore, we can rewrite the Eqns. (5.13) and (5.14) respectively as

$$C_{n,m}(y_i(k)) = (h_{i1}^{n-m}(h_{i1}^*)^m + ... + h_{iN_T}^{n-m}(h_{iN_T}^*)^m)C_{n,m}(x_1(k)) \tag{5.15}$$

and

$$C_{n,m}(\nabla y_i(k)) = (h_{i1}^{n-m}(h_{i1}^*)^m + ... + h_{iN_T}^{n-m}(h_{iN_T}^*)^m)C_{n,m}(\nabla x_1(k)). \tag{5.16}$$

Taking the ratio of $C_{n,m}(\nabla y_i(k))$ and $C_{n,m}(y_i(k))$,we obtain

$$\frac{C_{n,m}(\nabla y_i(k))}{C_{n,m}(y_i(k))} = \frac{C_{n,m}(\nabla x_1(k))}{C_{n,m}(x_1(k))}, \ provided\ C_{n,m}(x_1(k)) \neq 0. \tag{5.17}$$

It is clear that the above ratio is capable of cancelling out the contribution of the channel coefficients. We analyse this ratio for the 4^{th}-order and 6^{th}-order cumulants for the modulation types BPSK, QPSK, OQPSK and 16-QAM. We derive this ratio analytically for the BPSK, QPSK, OQPSK and 16-QAM signals. These values are tabulated in Table 5.2. One can note from Table that this ratio exists for 4^{th}-order zero conjugate, 4^{th}-order two conjugate, 6^{th}-order one conjugate and 6^{th}-order three conjugate cumulants.

Table 5.2: Ratio-cumulant values of RV x (associated with transmitted data sequence $x(k)$) for different modulation types

Modulation Type	$\frac{C_{40}(\nabla x)}{C_{40}(x)}$	$\frac{C_{42}(\nabla x)}{C_{42}(x)}$	$\frac{C_{61}(\nabla x)}{C_{61}(x)}$	$\frac{C_{63}(\nabla x)}{C_{63}(x)}$
BPSK	2	2	2	5
QPSK	2	2	2	2
OQPSK	2	0	1.5	0.5
16-QAM	2	2	2	2

It is observed from Table 5.2 that $\frac{C_{63}(\nabla x)}{C_{63}(x)}$ is distinct for BPSK, OQPSK and QPSK (or 16-QAM) and $\frac{C_{42}(\nabla x)}{C_{42}(x)}$ is distinct for BPSK (or QPSK or 16-QAM) and OQPSK. The details of derivation of these ratios are presented next.

Consider a BPSK signal $x_1(k)$ at an instant k. The 6^{th}-order three-conjugate cumulant and the 4^{th}-order two-conjugate cumulant of RVs x_1 (associated with transmitted data sequence $x_1(k)$)

and ∇x_1 (associated with data sequence $\nabla x_1(k)$) are given by

$$\begin{aligned} C_{63}(x_1) &= E(|x_1|^6) - 9E(|x_1|^2)E(|x_1|^4) + 12|E(x_1)^2|^2E(|x_1|^2) \\ &\quad + 12(E(|x_1|^2))^3 \\ &= \frac{1}{2}(1^6 + |-1|^6) - 9(\frac{1}{2}(1^2 + |-1|^2))(\frac{1}{2}(1^4 + |-1|^4)) + 12(|\frac{1}{2}(1^2 + (-1)^2)|^2) \\ &(\frac{1}{2}(1^2 + |-1|^2)) + 12(\frac{1}{2}(1^2 + |-1|^2))^3 = 16, \end{aligned} \tag{5.18}$$

$$\begin{aligned} C_{63}(\nabla x_1) &= E(|\nabla x_1|^6) - 9E(|\nabla x_1|^2)E(|\nabla x_1|^4) + 12|E(\nabla x_1^2)|^2E(|\nabla x_1|^2) \\ &\quad + 12(E(|\nabla x_1|^2))^3 \\ &= \frac{1}{4}(2^6 + |-2|^6) - 9(\frac{1}{4}(2^2 + |-2|^2))(\frac{1}{4}(2^4 + |-2|^4)) + 12(|\frac{1}{4}(2^2 + (-2)^2)|^2) \\ &(\frac{1}{4}(2^2 + |-2|^2)) + 12(\frac{1}{4}(2^2 + |-2|^2))^3 = 80, \end{aligned} \tag{5.19}$$

$$C_{42}(x_1) = \frac{1}{2}(1^4 + (-1)^4) - |\frac{1}{2}(1^2 + (-1)^2)|^2 - 2(\frac{1}{2}(|1|^2 + |-1|^2))^2 = -2 \tag{5.20}$$

and

$$C_{42}(\nabla x_1) = \frac{1}{4}(2^4 + (-2)^4) - \frac{1}{16}|2^2 + (-2)^2|^2 - 2(\frac{1}{4}(|2|^2 + |-2|^2))^2 = -4. \tag{5.21}$$

Now, incorporating the above cumulant values in Eqn. 5.17, we obtain

$$\frac{C_{42}(\nabla x_1)}{C_{42}(x_2)} = \frac{-4}{-2} = 2 \tag{5.22}$$

and

$$\frac{C_{63}(\nabla x_1)}{C_{63}(x_1)} = \frac{80}{16} = 5. \tag{5.23}$$

For a QPSK signal $x_2(k)$, the 6^{th}-order three-conjugate cumulant and the 4^{th}-order two-conjugate cumulant of RVs x_2 (associated with transmitted data sequence $x_2(k)$) and ∇x_2 (asso-

ciated with data sequence $\nabla x_2(k)$) are given by

$$\begin{aligned} C_{63}(x_2) = \frac{1}{4}(1^6 + |-1|^6 + |i|^6 + |-i|^6) - 9(\frac{1}{4}(1^2 + |-1|^2 + |i|^2 + |-i|^2)) \\ (\frac{1}{4}(1^4 + |-1|^4 + |i|^4 + |-i|^4)) + 12(|\frac{1}{4}(1^2 + (-1)^2 + (i)^2 + (-i)^2)|^2) \\ (\frac{1}{4}(1^2 + |-1|^2 + |i|^2 + |-i|^2)) + 12(\frac{1}{4}(1^2 + |-1|^2 + |i|^2 + |-i|^2))^3 = 4, \end{aligned} \tag{5.24}$$

$$\begin{aligned} C_{63}(\nabla x_2) = \frac{1}{16}(2^6 + |-2|^6 + |2i|^6 + |-2i|^6) + \frac{1}{8}(|1+i|^6 + |1-i|^6 + |-1-i|^6 + |-1+i|^6) \\ - 9(\frac{1}{16}(2^2 + |-2|^2 + |2i|^2 + |-2i|^2) + \frac{1}{8}(|1+i|^2 + |1-i|^2 + |-1-i|^2 + |-1+i|^2)) \\ (\frac{1}{16}(2^4 + |-2|^4 + |2i|^4 + |-2i|^4) + \frac{1}{8}(|1+i|^4 + |1-i|^4 + |-1-i|^4 + |-1+i|^4)) \\ + 12(|\frac{1}{16}(2^2 + (-2)^2 + (2i)^2 + (-2i)^2) + \frac{1}{8}((1+i)^2 + (1-i)^2 + (-1-i)^2 + (-1+i)^2)|^2) \\ (\frac{1}{16}(2^2 + |-2|^2 + |2i|^2 + |-2i|^2) + \frac{1}{8}(|1+i|^2 + |1-i|^2 + |-1-i|^2 + |-1+i|^2)) + 12 \\ (\frac{1}{16}(2^2 + |-2|^2 + |2i|^2 + |-2i|^2) + \frac{1}{8}(|1+i|^2 + |1-i|^2 + |-1-i|^2 + |-1+i|^2))^3 = 8, \end{aligned} \tag{5.25}$$

$$\begin{aligned} C_{42}(x_2) = \frac{1}{4}(1^4 + (|-1|^4 + |i|^4 + |-i|^4) - \frac{1}{16}|(1^2 + (-1)^2 + (i)^2 + (-i)^2|^2 \\ - \frac{1}{8}(|1|^2 + |-1|^2 + |i|^2 + |-i|^2)^2 = -1 \end{aligned} \tag{5.26}$$

and

$$\begin{aligned} C_{42}(\nabla x_2) = \frac{1}{16}(|2|^4 + |-2|^4 + |2i|^4 + |-2i|^4) + \frac{1}{8}(|1+i|^4 + |1-i|^4 + |-1+i|^4 + |-1-i|^4) \\ - |\frac{1}{16}(2^2 + (-2)^2 + 2i^2 + (-2i)^2) + \frac{1}{8}((1+i)^2 + (1-i)^2 + (-1+i)^2 + (-1-i)^4)|^2 \\ - 2(\frac{1}{16}(|2|^2 + |-2|^2 + |2i|^2 + |-2i|^2) + \frac{1}{8}(|1+i|^2 + |1-i|^2 + |-1+i|^2 + |-1-i|^2))^2 \\ = -2. \end{aligned} \tag{5.27}$$

Now, incorporating the above cumulant values in Eqn. 5.17, we obtain

$$\frac{C_{42}(\nabla x_2)}{C_{42}(x_2)} = \frac{2}{-1} = 2 \tag{5.28}$$

and

$$\frac{C_{63}(\nabla x_2)}{C_{63}(x_2)} = \frac{8}{4} = 2. \tag{5.29}$$

For an OQPSK signal $x_3(k)$, the 6^{th}-order three-conjugate cumulant and the 4^{th}-order two-conjugate cumulant of RVs x_3 (associated with transmitted data sequence $x_3(k)$) and ∇x_3 (associated with data sequence $\nabla x_3(k)$) are given by

$$\begin{aligned} C_{63}(x_3) = \frac{1}{4}(1^6 + |-1|^6 + |i|^6 + |-i|^6) - 9(\frac{1}{4}(1^2 + |-1|^2 + |i|^2 + |-i|^2)) \\ (\frac{1}{4}(1^4 + |-1|^4 + |i|^4 + |-i|^4)) + 12(|\frac{1}{4}(1^2 + (-1)^2 + (i)^2 + (-i)^2)|^2) \\ (\frac{1}{4}(1^2 + |-1|^2 + |i|^2 + |-i|^2)) + 12(\frac{1}{4}(1^2 + |-1|^2 + |i|^2 + |-i|^2))^3 = 4, \end{aligned} \tag{5.30}$$

$$\begin{aligned} C_{63}(\nabla x_3) = \frac{1}{8}(|1+i|^6 + |1-i|^6 + |-1-i|^6 + |-1+i|^6) - 9(\frac{1}{8}(|1+i|^2 + |1-i|^2 \\ + |-1-i|^2 + |-1+i|^2))(\frac{1}{8}(|1+i|^4 + |1-i|^4 + |-1-i|^4 + |-1+i|^4)) \\ + 12(|\frac{1}{8}((1+i)^2 + (1-i)^2 + (-1-i)^2 + (-1+i)^2)|^2)(\frac{1}{8}(|1+i|^2 + |1-i|^2 \\ + |-1-i|^2 + |-1+i|^2)) + 12(\frac{1}{8}(|1+i|^2 + |1-i|^2 + |-1-i|^2 + |-1+i|^2))^3 \\ = 2, \end{aligned} \tag{5.31}$$

$$\begin{aligned} C_{42}(x_3) = \frac{1}{4}(1^4 + (|-1|^4 + |i|^4 + |-i|^4) - \frac{1}{16}|(1^2 + (-1)^2 + (i)^2 + (-i)^2|^2 \\ - \frac{1}{8}(|1|^2 + |-1|^2 + |i|^2 + |-i|^2)^2 = -1 \end{aligned} \tag{5.32}$$

and

$$\begin{aligned} C_{42}(\nabla x_3) = \frac{1}{8}(|1+i|^4 + |1-i|^4 + |-1+i|^4 + |-1-i|^4) - |\frac{1}{8}((1+i)^2 + (1-i)^2 + (-1+i)^2 \\ + (-1-i)^2)|^2 - 2(\frac{1}{8}(|1+i|^2 + |1-i|^2 + |-1+i|^2 + |-1-i|^2))^2 = 0. \end{aligned} \tag{5.33}$$

Now, incorporating the above cumulant values in Eqn. 5.17, we obtain

$$\frac{C_{42}(\nabla x_3)}{C_{42}(x_3)} = \frac{0}{-1} = 0 \tag{5.34}$$

and

$$\frac{C_{63}(\nabla x_3)}{C_{63}(x_3)} = \frac{2}{4} = 0.5. \tag{5.35}$$

Based on above discussion, we propose to employ the following cumualnt feature vector to classify BPSK,QPSK and OQPSK:

$$\mathbf{u}^M = [u_1, u_2] \tag{5.36}$$

where

$$u_1 = \frac{C_{63}(\nabla x)}{C_{63}(x)}$$

and

$$u_2 = \frac{C_{42}(\nabla x)}{C_{42}(x)}.$$

For the considered modulation types, $\mathbf{u}^M$ is given as

$$\mathbf{u}^M = \begin{cases} [5, 2], M = 1 \\ [2, 2], M = 2 \\ [0.5, 0], M = 3 \end{cases} \tag{5.37}$$

where $M = 1, 2$ *and* 3 represents the modulation formats BPSK, QPSK and OQPSK respectively. Now, the proposed cumulant vector can be estimated as

$$\hat{\mathbf{u}}^M = [\hat{u}_1, \hat{u}_2] \tag{5.38}$$

where

$$\hat{u}_1 = \frac{\sum_{i=1}^{N_R} \hat{C_{63}}(\nabla \mathbf{y}_i)}{\sum_{i=1}^{N_R} \hat{C_{63}}(\mathbf{y}_i)} \tag{5.39}$$

and

$$\hat{u}_2 = \frac{\sum_{i=1}^{N_R} \hat{C}_{42}(\nabla \mathbf{y}_i)}{\sum_{i=1}^{N_R} \hat{C}_{42}(\mathbf{y}_i)}. \tag{5.40}$$

The fourth and sixth order cumulants are estimated using the following equations:

$$\hat{C}_{42}(\mathbf{y}_i) = \frac{1}{N}\sum_{k=1}^{N} |y_i(k)|^4 - |\frac{1}{N}\sum_{k=1}^{N} (y_i(k))^2|^2 - 2(\frac{1}{N}\sum_{k=1}^{N} |y_i(k)|^2)^2, \tag{5.41}$$

$$\hat{C}_{42}(\nabla \mathbf{y}_i) = \frac{1}{N}\sum_{k=1}^{N} |\nabla y_i(k)|^4 - |\frac{1}{N}\sum_{k=1}^{N} (\nabla y_i(k))^2|^2 - 2(\frac{1}{N}\sum_{k=1}^{N} |\nabla y_i(k)|^2)^2, \tag{5.42}$$

$$\hat{C_{63}}(\mathbf{y}_i) = \frac{1}{N}\sum_{k=1}^{N}|y_i(k)|^6 - 9(\frac{1}{N}\sum_{k=1}^{N}|y_i(k)|^2)(\frac{1}{N}\sum_{k=1}^{N}|y_i(k)|^4) + 12(|\frac{1}{N}\sum_{k=1}^{N}(y_i(k))^2|^2) \\ (\frac{1}{N}\sum_{k=1}^{N}|y_i(k)|^2) + 12(\frac{1}{N}\sum_{k=1}^{N}|y_i(k)|^2)^3 \tag{5.43}$$

and

$$\hat{C_{63}}(\nabla\mathbf{y}_i) = \frac{1}{N}\sum_{k=1}^{N}|\nabla y_i(k)|^6 - 9(\frac{1}{N}\sum_{k=1}^{N}|\nabla y_i(k)|^2)(\frac{1}{N}\sum_{k=1}^{N}|\nabla y_i(k)|^4) + 12(|\frac{1}{N}\sum_{k=1}^{N}(\nabla y_i(k))^2|^2) \\ (\frac{1}{N}\sum_{k=1}^{N}|\nabla y_i(k)|^2) + 12(\frac{1}{N}\sum_{k=1}^{N}|\nabla y_i(k)|^2)^3. \tag{5.44}$$

The detected modulation class M^* is given by

$$M^* = \underset{M=1,2,3}{argmin}(\|\hat{\mathbf{u}}^M - \mathbf{u}^M\|). \tag{5.45}$$

5.5 Simulation Results and Discussion

A set of experiments were carried out to evaluate the performance of the proposed method through the Monte-Carlo simulation. The performance of the proposed classifier is analysed by calculating the average probability of correct classification P_C against a range of SNRs. For the simulation, the number of transmitting and receiving antennas were set at $N_T = 2$ and $N_R = 4$ respectively. The modulation types considered for the classification were BPSK, QPSK and OQPSK. For each SNR value, 3000 Monte Carlo simulations were performed to calculate P_C. For each trial, we generated a random channel matrix and a random source message. We illustrate the effects of sample length (N), SNR and antenna correlation on the proposed algorithm next.

5.5.1 Performance Comparison of the DMR Technique and the JADE-FZC Technique

Fig. 5.5 shows P_C versus SNR for the JADE-FZC technique and the DMR technique over a correlated keyhole channel. Fig. 5.6 shows the same over a correlated Rician channel. The modulation types considered for classification were BPSK and QPSK. One can note that the DMR technique outperforms the JADE-FZC technique in both the scenarios. For instance,

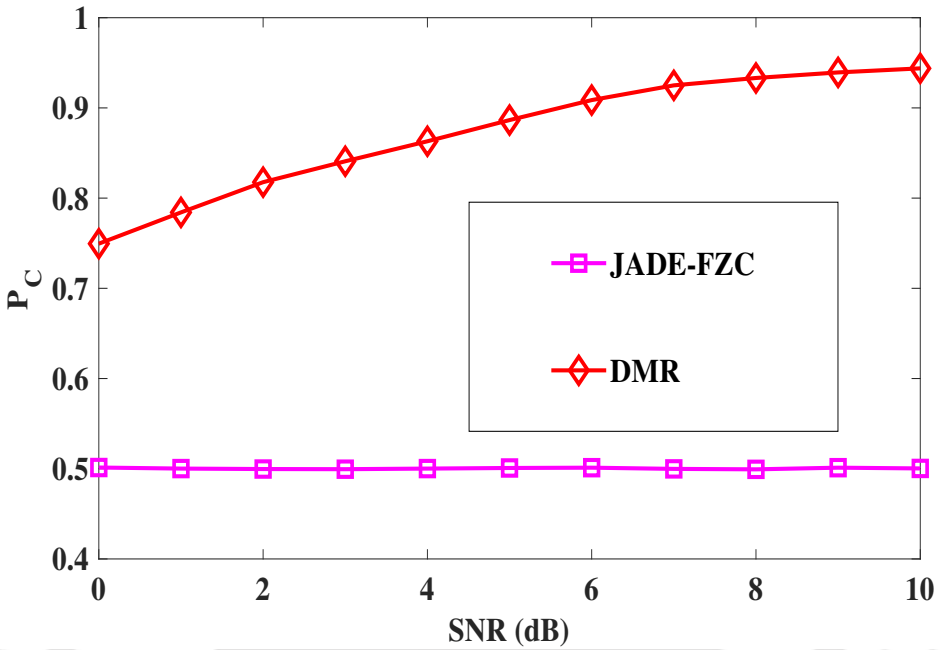

Figure 5.5: P_C versus SNR for JADE-FZC and DMR over a Keyhole channel with $N = 2000$ and $|\rho_R| = |\rho_T| = 0.5$

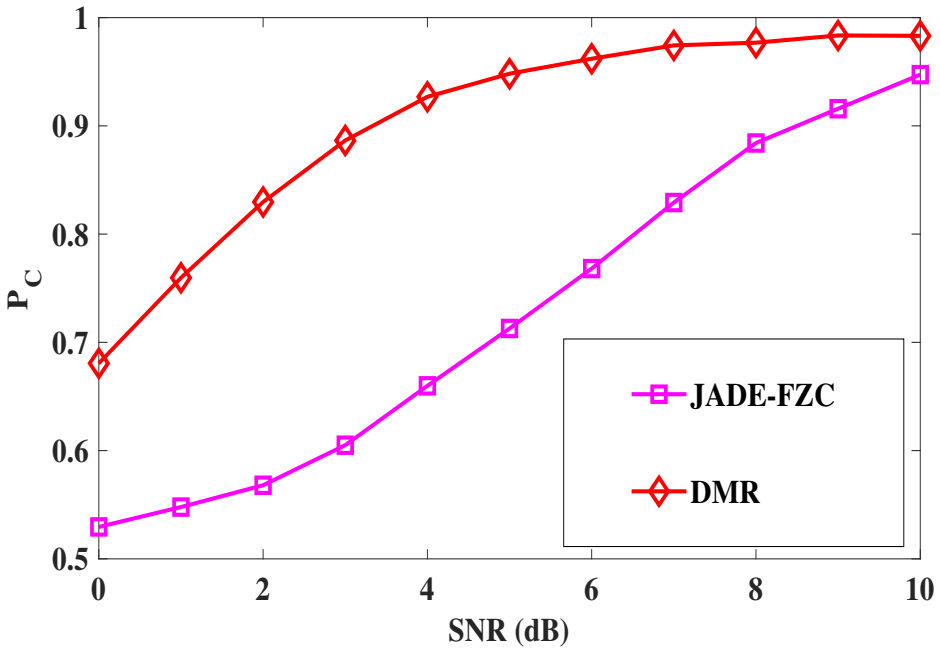

Figure 5.6: P_C versus SNR for JADE-FZC and DMR over a Rician channel with $N = 2000$, $K = 10$ and $|\rho_R| = |\rho_T| = 0.5$

at an SNR value of 6 dB, the DMR technique attains P_C=0.9000 for $N = 2000$ and $|\rho_R| = |\rho_T| = 0.5$ while for the same antenna correlation value and sample length, the JADE-FZC technique attains P_C=0.5000 at an SNR value of 6 dB. Under correlated Rician channel, the DMR technique attains P_C=0.9482 at an SNR value of 6 dB for $N = 2000$, $|\rho_R| = |\rho_T| = 0.5$ and $K = 10$ while for the same antenna correlation, sample length and Rician factor, the JADE-FZC technique attains P_C=0.7682 at an SNR value of 6 dB.

5.5.2 Effect of Antenna Correlation on the Performance of the DMR Technique

Figs. 5.7-5.9 show the effect of antenna correlation on the DMR technique over a Rayleigh Channel and Figs. 5.10-1.12 show the same over a keyhole Channel. It can be observed that with an increase in the antenna correlation value, there is a decrease in P_C. For instance, with an SNR value of 5 dB and $N = 2000$, the DMR technique attains P_C=0.9692 for $|\rho_R| = |\rho_T| = 0.5$, while for the same SNR and sample length, it attains P_C=0.9309 for $|\rho_R| = |\rho_T| = 0.7$ over a Rayleigh channel. Table 5.3 shows P_C for different antenna correlation values with an SNR value of 7 dB and $N = 2000$ over the Rayleigh channel. Under the keyhole channel, with an SNR value of 7 dB and $N = 2000$, the DMR technique attains P_C=0.8882 for $|\rho_R| = |\rho_T| = 0.5$, while for the same SNR and sample length, it attains P_C=0.8537 for $|\rho_R| = |\rho_T| = 0.7$. Table 5.4 shows P_C for different antenna correlation values with an SNR value of 7 dB and $N = 2000$ under keyhole channel. The decrease in P_C with an increase in the antenna correlation value is attributed to the reduced diversity gain as a correlated low rank channel model yields only receiver array gain.

It is noted that with an increase in SNR, P_C improves. For instance, under the Rayleigh Channel, the DMR technique attains $P_C = 0.8214$ at an SNR value of 2 dB for $N = 2000$ and $|\rho_R| = |\rho_T| = 0.5$, while for the same sample size and the antenna correlation value, it attains $P_C = 0.9692$ at an SNR value of 6 dB. Table 5.5 shows P_C attained by the DMR technique at different SNRs for $N = 2000$ and $|\rho_R| = |\rho_T| = 0.5$ under the Rayleigh channel. Under the Keyhole Channel, the DMR technique attains $P_C = 0.7337$ at an SNR value of 2 dB for $N = 2000$ and $|\rho_R| = |\rho_T| = 0.5$, while for the same sample size and the antenna correlation value, it attains $P_C = 0.8658$ at an SNR value of 6 dB. Table 5.6 shows P_C attained by the

DMR technique at different SNRs for $N = 2000$ and $|\rho_R| = |\rho_T| = 0.5$ under the Keyhole channel. It is also noted that with an increase in the sample size, P_C improves. For instance, with an SNR value of 5 dB and $|\rho_R| = |\rho_T| = 0.5$, the DMR technique attains $P_C = 0.9246$ for $N = 1000$ under the Rayleigh channel, while at the same SNR and the antenna correlation value, it attains $P_C = 0.9749$ for $N = 4000$. Table 5.7 shows P_C attained by the DMR technique with an SNR value of 5 dB and $|\rho_R| = |\rho_T| = 0.5$ for different sample lengths under the Rayleigh channel. Under the keyhole channel, with an SNR value of 5 dB and $|\rho_R| = |\rho_T| = 0.5$, the DMR technique attains $P_C = 0.8033$ for $N = 1000$, while at the same SNR and the antenna correlation value, it attains $P_C = 0.8736$ for $N = 4000$. Table 5.8 shows P_C attained by the DMR technique with an SNR value of 5 dB and $|\rho_R| = |\rho_T| = 0.5$ for different sample lengths under the Keyhole channel. The increase in P_C with an increase in SNR and N is attributed to the fact that the accurate estimation of the cumulants depends on SNR and N. The higher the SNR and N, the cumulant estimates are closer to the theoretical values [4].

Table 5.3: P_C attained by the DMR technique with an SNR value of 7 dB and $N = 2000$ for different antenna correlation values ($|\rho| = |\rho_R| = |\rho_T|$) in a correlated Rayleigh channel

$\|\rho\|$	P_C
0	0.9825
0.5	0.9720
0.7	0.9391
0.9	0.8221

Table 5.4: P_C attained by the DMR technique with an SNR value of 7 dB and $N = 2000$ for different antenna correlation values ($|\rho| = |\rho_R| = |\rho_T|$) in a correlated keyhole channel

$\|\rho\|$	P_C
0	0.9071
0.5	0.8882
0.7	0.8537
0.9	0.7430

Table 5.5: P_C attained by the DMR technique at different SNRs for $N = 2000$ and $|\rho_R| = |\rho_T| = 0.5$ in a Rayleigh channel

SNR (dB)	P_C
2	0.8214
4	0.9476
6	0.9692
8	0.9768

Table 5.6: P_C attained by the DMR technique at different SNRs for $N = 2000$ and $|\rho_R| = |\rho_T| = 0.5$ in a keyhole channel

SNR (dB)	P_C
2	0.7337
4	0.8122
6	0.8658
8	0.9059

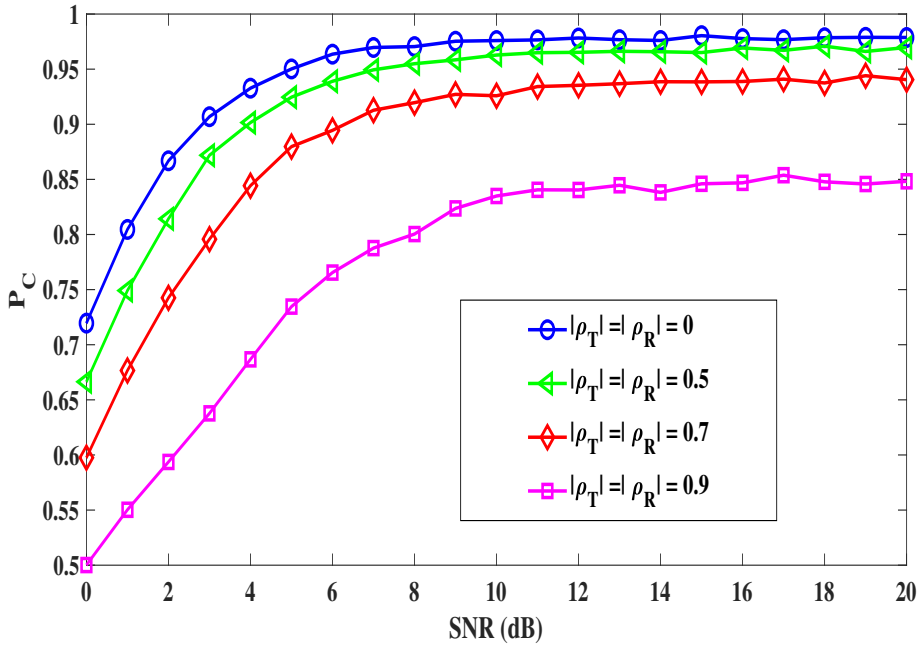

Figure 5.7: P_C versus SNR for the DMR technique in a correlated Rayleigh channel with $N = 1000$

Table 5.7: P_C attained by the DMR technique with an SNR value of 5 dB and $|\rho_R| = |\rho_T| = 0.5$ for different sample lengths in a Rayleigh channel

N	P_C
1000	0.9246
2000	0.9597
4000	0.9749

Table 5.8: P_C attained by the DMR technique with an SNR value of 5 dB and $|\rho_R| = |\rho_T| = 0.5$ for different sample lengths in a Keyhole channel

N	P_C
1000	0.8033
2000	0.8405
4000	0.8736

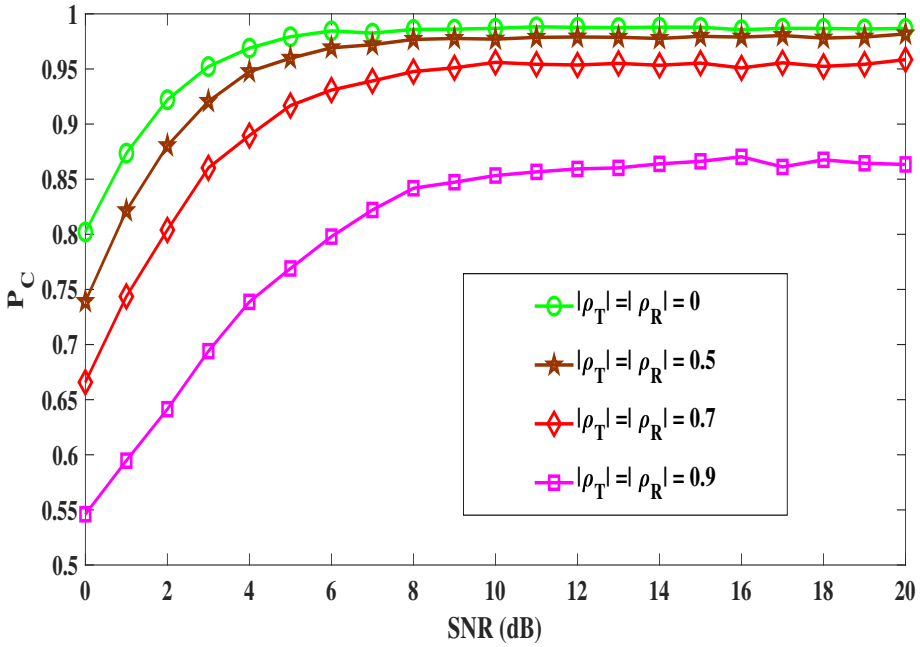

Figure 5.8: P_C versus SNR for the DMR technique in a correlated Rayleigh channel with $N = 2000$

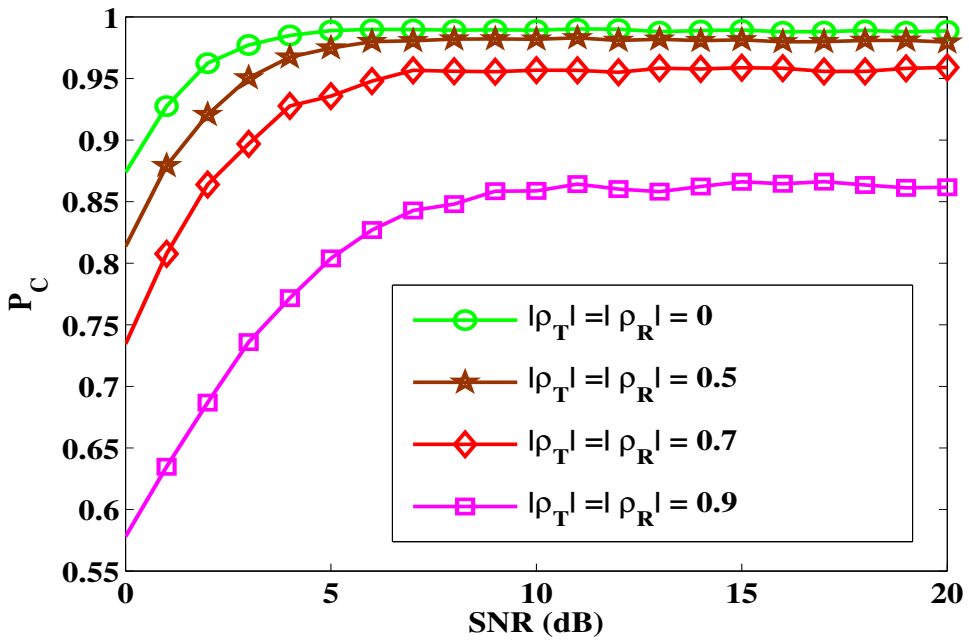

Figure 5.9: P_C versus SNR for the DMR technique in a correlated Rayleigh channel with $N = 4000$

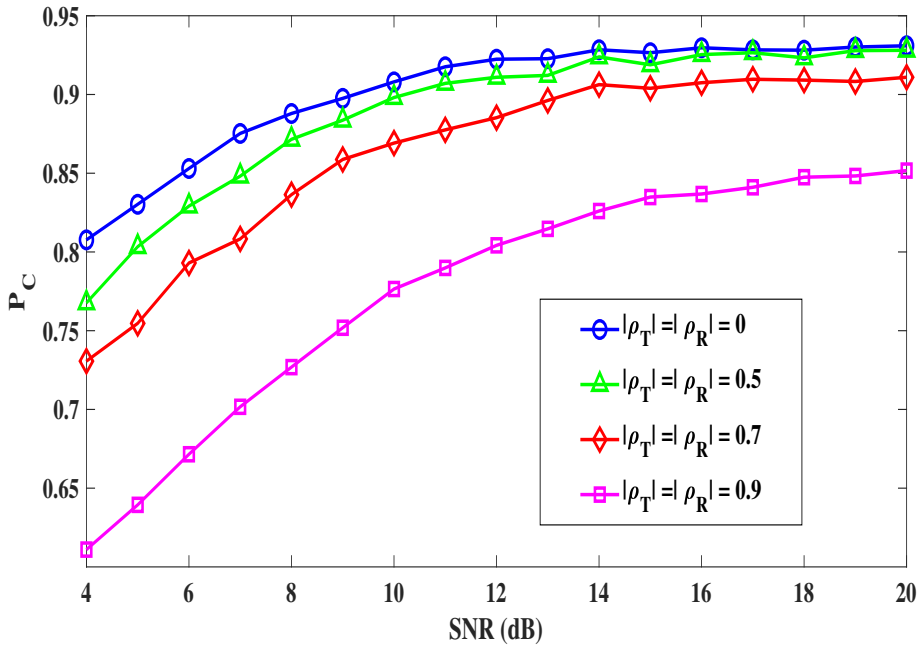

Figure 5.10: P_C versus SNR for the DMR technique in a correlated Keyhole channel with $N = 1000$

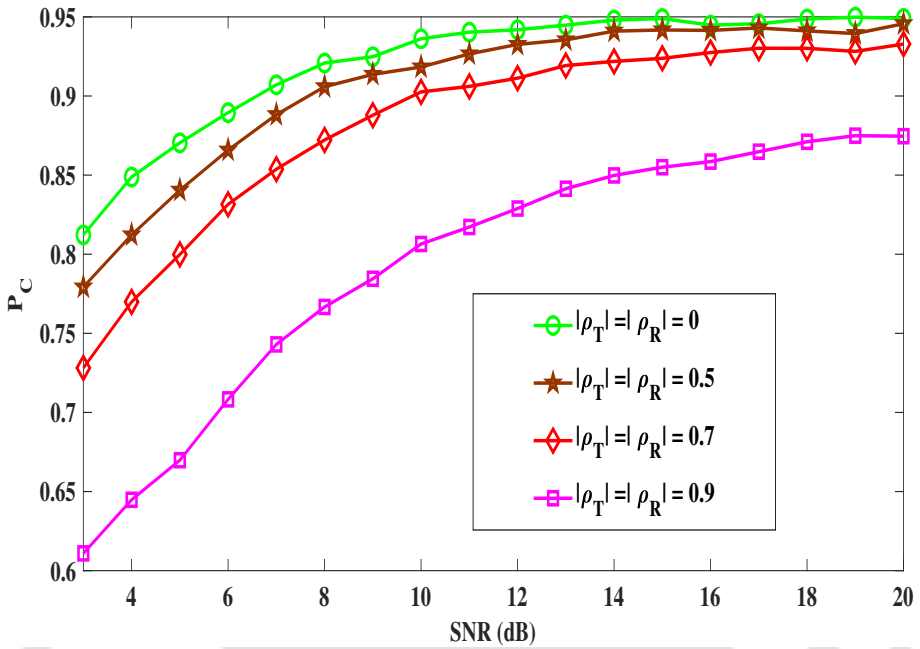

Figure 5.11: P_C versus SNR for the DMR technique in a correlated Keyhole channel with $N = 2000$

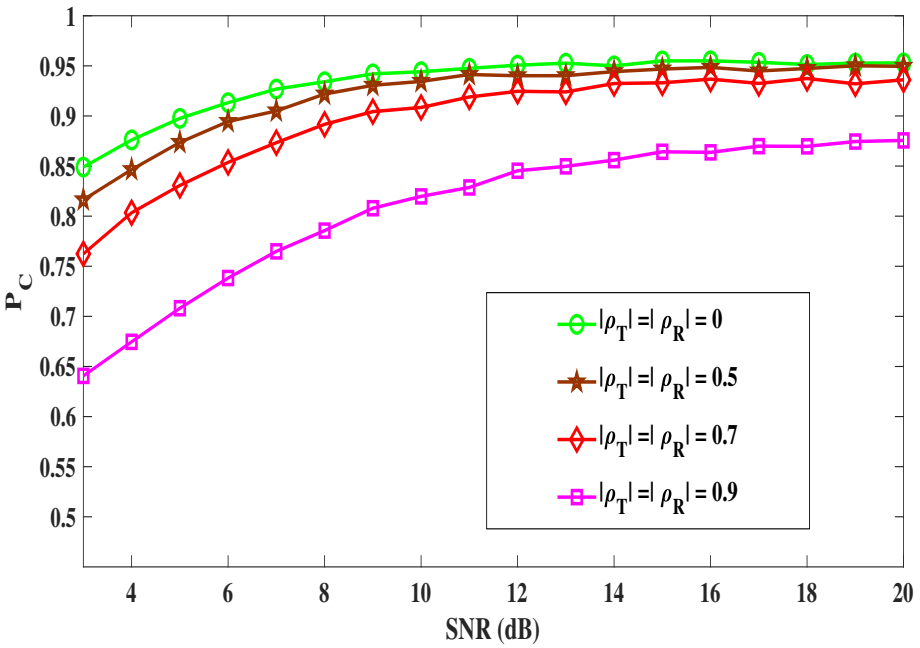

Figure 5.12: P_C versus SNR for the DMR technique in a correlated Keyhole channel with $N = 4000$

5.6 Summary

This chapter addressed the problem of AMC over correlated Keyhole MIMO channels. A novel algorithm, namely DMR, was proposed to distinguish the modulation types BPSK, QPSK and OQPSK. The proposed algorithm employed the ratios of HOCs derived from the received signal and its backward difference as AMC features. These features were chosen so that the contributions of the channel-coefficients are cancelled. Thus, the DMR algorithm does not require the CSI at the receiver. The simulation results showed that the proposed method performed satisfactorily under the keyhole channel. For instance, with an SNR value of 4 dB, $N = 2000$,$N_T = 2$, $N_R = 4$ and $|\rho_R| = |\rho_T| = 0.5$, the proposed method attained $P_C = 0.9476$.

6

Automatic Modulation Classification over a Correlated MIMO Amplify and Forward (AF)-Relay Fading Channel

Contents

6.1 Introduction

In the previous chapter, we discussed that MIMO systems can operate in an insufficient scattering environment, which can lead to a rank deficient channel. A rank deficient channel, such as a keyhole channel severely affects the AMC performance. It is necessary to cancel the channel mixing effect prior to AMC as the MIMO spatial channel alters the statistical properties of the modulated signal. A keyhole channel makes AMC a challenging task as the existing blind channel equalization techniques such as the JADE algorithm [31] and the constant modulus algorithm (CMA) [29, 30] require the channel matrix to be of full rank.

It is reported in [54, 58], that cooperative relaying is an attractive solution to overcome the rank deficiency of MIMO channels. These cooperative relays (CRs) act as active scatterers, which eventually turns the keyhole channel into a multi-keyhole channel [53]. The use of relay networks offers throughput enhancement, power reduction and network coverage [53–61]. There are two popular relaying strategies. They are : 1) decode-and-forward (DF)- the relays decode the received signals then re-encode before retransmitting and 2) amplify-and-forward (AF)- the relays apply linear signal processing to the signal before forwarding [76]. The AF relaying technique provides lower baseband complexity and fast signal processing as it does not require to decode the received signal. Additionally, in heterogeneous networks, where many nodes of diverse complexity and different standards exist, the AF relays are more suitable [76].

This chapter addresses the AMC of MIMO signals over an AF-relay fading channel. We propose an AMC method, namely relay assisted (RA)-AMC, which is capable of classifying a pool of modulation types, namely BPSK, OQPSK, QPSK, $\frac{\pi}{4}$-QPSK, 8-PSK and 16-QAM. The proposed method involves two steps. In the first step, the method employs a cumulant feature vector derived directly from the received signal to distinguish BPSK, OQPSK and the sub-pool $Q_1 = \{QPSK, \frac{\pi}{4} - QPSK, 8 - PSK, 16 - QAM\}$ as a whole. This cumulant feature offers resistance against noise amplification which occurs in a correlated AF-relay system. In the second step, it employs a cumulant feature vector derived from the equalized signal to distinguish the modulation types in Q_1.

The rest of the chapter is organized as follows: Section 6.2 presents the system model.

Section 6.3 presents the proposed AMC method. The simulation results and the evaluation of the proposed method are presented in Section 6.4. Finally, a summary is presented in Section 6.5.

6.2 AF- Relay Assisted MIMO System

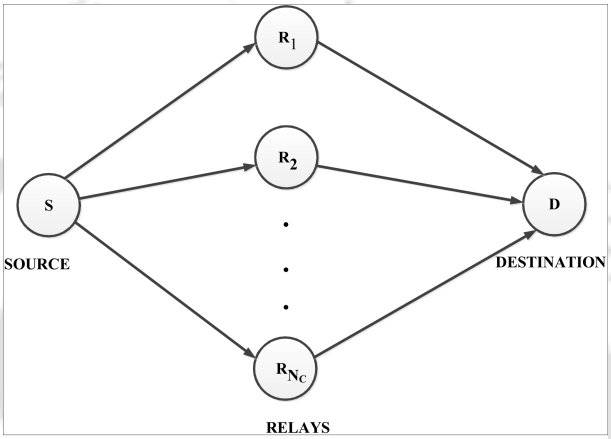

Figure 6.1: Cooperative Relay Assisted MIMO System

Consider a two-hop MIMO relay communication system shown in Fig. 6.1. The system consists of a source node equipped with N_T antennas, N_C parallel relay nodes, each equipped with a single antenna, and a destination node equipped with N_R antennas. The relays act as active scatterers. We assume that there is no direct communication link between the source and the destination. For instance, there may be no direct communication link when the distance between the source and the destination is large or the location of destination is inside a building and the location of source is outside the building [77]. The communication between the source and the destination takes place over two time slots. In the first time slot, the AF-relay nodes receive the signal transmitted by the source node and process the received signals. In the second slot, the relay nodes simultaneously forward the processed data to the destination node. During the second time slot, the source node remains idle. The received signal at the destination can be written as [53]

$$\mathbf{y} = \boldsymbol{\theta}_R^{1/2} \boldsymbol{H}_1 \boldsymbol{G} (\boldsymbol{H}_2 \boldsymbol{\theta}_T^{1/2} \mathbf{x} + \boldsymbol{g}_1) + \boldsymbol{g}_2, \tag{6.1}$$

where $\mathbf{x} = [x_1 ... x_{N_T}]^T$ is an $N_T \times 1$ transmitted signal vector, $\mathbf{H}_1$ is an $N_R \times N_C$ complex

channel matrix between the CRs and the destination , $\mathbf{H}_2$ is an $N_C \times N_T$ complex channel matrix between the source and the CRs, $\boldsymbol{\theta}_R$ and $\boldsymbol{\theta}_T$ are the correlation matrices of the destination and the source, respectively, $\mathbf{G}$ is an $N_C \times N_C$ gain matrix, and $\boldsymbol{g}_1$ and $\boldsymbol{g}_2$ are complex Gaussian noise vectors contributed by the CRs and the receiver, respectively. We assume that the gain of each CR is constant and is normalized to the number of CRs N_C. The gain matrix is given as

$$G = \frac{1}{\sqrt{N_C}} \boldsymbol{I}_{N_C \times N_C}. \tag{6.2}$$

In the absence of the relay noise and antenna correlation, the equivalent channel matrix $\mathbf{H}$ can be written as [56, 78, 79]

$$\mathbf{H} = \frac{1}{\sqrt{N_C}} \mathbf{H}_1 \mathbf{H}_2, \tag{6.3}$$

where the channel coefficients of both $(\boldsymbol{H}_1)_{N_R \times N_C}$ and $(\boldsymbol{H}_2)_{N_C \times N_T}$ are i.i.d and follow a circularly symmetric complex Gaussian distribution with zero-mean and unit variance.

Suppose

$$\mathbf{H}_1 = \begin{pmatrix} a_{11} & a_{12} & \cdots & a_{1N_C} \\ a_{21} & a_{22} & \cdots & a_{2N_C} \\ \vdots & \vdots & \ddots & \vdots \\ a_{N_R1} & a_{N_R2} & \cdots & a_{N_RN_C} \end{pmatrix} \tag{6.4}$$

and

$$\mathbf{H}_2 = \begin{pmatrix} b_{11} & b_{12} & \cdots & b_{1N_T} \\ b_{21} & b_{22} & \cdots & b_{2N_T} \\ \vdots & \vdots & \ddots & \vdots \\ b_{N_C1} & b_{N_C2} & \cdots & b_{N_CN_T} \end{pmatrix}. \tag{6.5}$$

Then Eqn. 6.3 can be rewritten as

$$\mathbf{H} = \begin{pmatrix} h_{11} & h_{12} & \cdots & h_{1N_T} \\ h_{21} & h_{22} & \cdots & h_{2N_T} \\ \vdots & \vdots & \ddots & \vdots \\ h_{N_R1} & h_{N_R2} & \cdots & h_{N_RN_T} \end{pmatrix} \tag{6.6}$$

where

$$h_{ij} = \frac{1}{\sqrt{N_C}} \sum_{k=1}^{N_C} a_{ik} b_{kj}, i = 1, ..., N_R \; and \; j = 1, ..., N_T. \tag{6.7}$$

Using central limit theorem, one can note that the h_{ij} is complex Gaussian distributed for large N_C. Thus, the magnitudes of channel coefficients of **H** follow single Rayleigh distribution [79].

Furthermore, the condition for attaining full rank is given as [61, 80]

$$N_C \geqslant min(N_T, N_R). \tag{6.8}$$

In addition to spatial fading, the spatial correlation also affects practical MIMO systems. For this investigation, we consider the exponential antenna correlation model.

6.3 Proposed AMC Algorithm over AF-Relay Fading Channel

A pool of six modulation types $Q = \{BPSK, OQPSK, QPSK, \frac{\pi}{4} - QPSK, 8 - PSK, 16 - QAM\}$ is considered for classification in this investigation. These modulation types are indexed by $M = 1, 2, 3, 4, 5 \; and \; 6$, respectively.

Traditionally, the FB-AMC algorithms for MIMO systems involve three steps. First, the received signal is equalized to mitigate the channel mixing effect. In the second step, features are extracted from the equalized signal and finally, these features are subjected to a classifier that distinguishes the modulation type. The HOMs and HOCs are widely employed AMC features for MIMO systems. Swami et al., in [4], reported that different digitally modulated signals exhibit distinct 4^{th}-order cumulant values. The robustness of 4^{th}-order cumulants against Gaussian noise makes them attractive AMC features. In [15], Muhlhaus et al. proposed an AMC algorithm based on 4^{th}-order cumulants over uncorrelated MIMO channels.

The accurate estimation of the 4^{th}-order cumulants depends on SNR of the equalized signal [4]. However, in an AF-MIMO relay network, the equalizer suffers from both the relay noise amplification and the noise amplification due to antenna correlation [14, 18, 55]. As a result, the AMC performance will be affected.

It will be useful if we are able to make the AMC classifier naturally resilient against channel conditions. In the previous chapter, we proposed an algorithm, namely DMR, with such

resilience. It is capable of classifying the modulation types BPSK,QPSK and OQPSK. In the DMR algorithm, the ratios of HOCs derived directly from the received signal and its backward difference are used as the AMC features. These features are chosen so that the contribution of the channel-coefficients is cancelled. Thus, the DMR algorithm avoids the equalization operation. The feature vector employed by the DMR algorithm is given by

$$\mathbf{u}^M = [u_1, u_2], \tag{6.9}$$

where

$$u_1 = \frac{C_{63}(\nabla x(k))}{C_{63}(x(k))}$$

and

$$u_2 = \frac{C_{42}(\nabla x(k))}{C_{42}(x(k))}.$$

For the considered modulation types, $\mathbf{u}^M$ is given as

$$\mathbf{u}^M = \begin{cases} [5,2], M = 1 \\ [.5,0], M = 2 \\ [2,2], M = 3 \\ [2,2], M = 4 \\ [2,2], M = 5 \\ [2,2], M = 6 \end{cases}. \tag{6.10}$$

$\mathbf{u}^M$ is distinct for BPSK, OQPSK. Thus, $\mathbf{u}^M$ can distinguish BPSK, OQPSK and the sub-pool $Q_1 = \{QPSK, \frac{\pi}{4} - QPSK, 8-PSK, 16-QAM\}$ as a whole. The previous chapter showed that the DMR algorithm outperforms the equalizer based JADE-FZC algorithm in classifying the BPSK, OQPSK and QPSK signals over the correlated keyhole channel. In an AF-MIMO relay network,

the equalizer suffers from both the relay noise amplification and the noise amplification due to antenna correlation. Therefore, in an AF-MIMO relay network, the DMR algorithm has potential to perform better for the same AMC task as it avoids the equalization operation.

In this work, we propose to employ $\mathbf{u}^M$ to distinguish BPSK, OQPSK and Q_1.

6.3.1 Feature Selection for Distinguishing the Modulation Types in Q_1

The following points are considered for selecting the features to distinguish the modulation types in Q_1:

1) Consider the 4^{th}-order cumualnt features $f_1^M = C_{40}(x(k))$ and $f_2^M = C_{42}(x(k))$ [4]. The theoretical values of f_1^M and f_2^M for the considered modulation types are given by

$$f_1^M = \begin{cases} 1, M = 3 \\ 0, M = 4 \\ 0, M = 5 \\ -0.68, M = 6 \end{cases} \tag{6.11}$$

and

$$f_2^M = \begin{cases} -1, M = 3 \\ -1, M = 4 \\ -1, M = 5 \\ -0.68, M = 6 \end{cases}. \tag{6.12}$$

The feature f_1^M is distinct for QPSK, 8-PSK and 16-QAM. It is not distinguishable for $\frac{\pi}{4}$-QPSK and 8-PSK. The feature f_2^M is distinct for QPSK and 16-QAM. However, it is not distinguishable for QPSK, $\frac{\pi}{4}$-QPSK and 8-PSK. In the case of discriminating QPSK and 16-QAM, the classification performance of f_2^M is better than that of f_1^M.

(2) In chapter 3, we proposed a cumualnt feature $f_3^M = C_{40}(x^e(k))(x^e(k) = x(2k), k = 0, 1, 2, ...)$ to distinguish $\frac{\pi}{4}$-QPSK and 8-PSK. It may be mentioned that one can also employ $f_3^M = C_{40}(x^o(k)), x^o(k) = x(2k+1), k = 0, 1, 2, ...$ The theoretical values of f_3^M for the considered modulation types are given by

$$f_3^M = \begin{cases} 1, M = 3 \\ 1, M = 4 \\ 0, M = 5 \\ -0.68, M = 6 \end{cases}. \tag{6.13}$$

Based on above discussion, we select the features f_1^M, f_2^M and f_3^M to distinguish the modulation types in $Q1$. Concatenating f_1^M, f_2^M and f_3^M, we get the feature vector

$$\mathbf{v}^M = [f_1^M, f_2^M, f_3^M]. \tag{6.14}$$

For the considered modulation types, $\mathbf{v}^M$ is given as

$$\mathbf{v}^M = \begin{cases} [1, -1, 1], M = 3 \\ [0, -1, 1], M = 4 \\ [0, -1, 0], M = 5 \\ [-0.68, -0.68, -.68], M = 6 \end{cases}. \tag{6.15}$$

It is clear from above that $\mathbf{v}^M$ is distinct for the modulation types in Q_1. Note that $\mathbf{v}^M$ can not be obtained directly from the received signal as the channel affects the cumulant values. Therefore, $\mathbf{v}^M$ needs to be estimated from the equalized MIMO signal. In this work, we employ the JADE equalization technique.

Based on above discussion, we propose an AMC method, namely RA-AMC, for an AF-relay fading channel with $\mathbf{u}^M$ and $\mathbf{v}^M$as feature vectors. The steps involved in the classification are described below.

Step 1: **Classification of BPSK, OQPSK and Q_1 using $\mathbf{u}^M$**

Suppose $\hat{\mathbf{u}} = [\hat{u}_1, \hat{u}_2]$ is the estimate of $\mathbf{u}$. $\hat{u}_1$ and $\hat{u}_2$ are obtained from the estimated HOCs as follows:

$$\hat{u}_1 = \frac{\sum_{i=1}^{N_R} \hat{C}_{6,3}(\nabla \mathbf{y}_i)}{\sum_{i=1}^{N_R} \hat{C}_{6,3}(\mathbf{y}_i)} \tag{6.16}$$

and

$$\hat{u}_2 = \frac{\sum_{i=1}^{N_R} \hat{C}_{4,2}(\nabla \mathbf{y}_i)}{\sum_{i=1}^{N_R} \hat{C}_{4,2}(\mathbf{y}_i)}, \tag{6.17}$$

where $\mathbf{y}_i$ is the received signal vector at the i^{th} receiving antenna,

$$\hat{C}_{42}(\mathbf{y}_i) = \frac{1}{N}\sum_{k=1}^{N}|y_i(k)|^4 - |\frac{1}{N}\sum_{k=1}^{N}(y_i(k))^2|^2 - 2(\frac{1}{N}\sum_{k=1}^{N}|y_i(k)|^2)^2, \tag{6.18}$$

$$\hat{C}_{42}(\nabla \mathbf{y}_i) = \frac{1}{N}\sum_{k=1}^{N}|\nabla y_i(k)|^4 - |\frac{1}{N}\sum_{k=1}^{N}(\nabla y_i(k))^2|^2 - 2(\frac{1}{N}\sum_{k=1}^{N}|\nabla y_i(k)|^2)^2, \tag{6.19}$$

$$\begin{aligned}\hat{C_{63}}(\mathbf{y}_i) = \frac{1}{N}\sum_{k=1}^{N}|y_i(k)|^6 - 9(\frac{1}{N}\sum_{k=1}^{N}|y_i(k)|^2)(\frac{1}{N}\sum_{k=1}^{N}|y_i(k)|^4) + 12(|\frac{1}{N}\sum_{k=1}^{N}(y_i(k))^2|^2) \\ (\frac{1}{N}\sum_{k=1}^{N}|y_i(k)|^2) + 12(\frac{1}{N}\sum_{k=1}^{N}|y_i(k)|^2)^3\end{aligned} \tag{6.20}$$

and

$$\begin{aligned}\hat{C_{63}}(\nabla \mathbf{y}_i) = \frac{1}{N}\sum_{k=1}^{N}|\nabla y_i(k)|^6 - 9(\frac{1}{N}\sum_{k=1}^{N}|\nabla y_i(k)|^2)(\frac{1}{N}\sum_{k=1}^{N}|\nabla y_i(k)|^4) + 12(|\frac{1}{N}\sum_{k=1}^{N}(\nabla y_i(k))^2|^2) \\ (\frac{1}{N}\sum_{k=1}^{N}|\nabla y_i(k)|^2) + 12(\frac{1}{N}\sum_{k=1}^{N}|\nabla y_i(k)|^2)^3.\end{aligned} \tag{6.21}$$

The detected modulation class M^* is given by

$$M^* = \underset{M=1,2,3}{argmin}(\|\hat{\mathbf{u}} - \mathbf{u}^M\|). \tag{6.22}$$

Now, If the estimated $M^* = 3$, the modulation type belongs to the pool $Q_1 = \{QPSK, \frac{\pi}{4} - QPSK, 8 - PSK, 16 - QAM\}$. To distinguish these modulation types, we go to step 2.

Step 2: **Classification of QPSK, $\frac{\pi}{4}$-QPSK, 8-PSK, 16-QAM** using $\mathbf{v}^M$

Suppose $\hat{\mathbf{v}} = [\hat{f}_1\hat{f}_2\hat{f}_3]$ is the estimate of $\mathbf{v}$. $\hat{f}_1$ $\hat{f}_2$ and $\hat{f}_3$ can be obtained from the 4^{th}-order cumulants estimated from the equalized signal.

Let $\hat{\mathbf{x}}_j$, $j = 1, ..., N_T$ denote the equalized signals corresponding to N_T transmitted streams.

The 4^{th}-order cumulant features are estimated from $\hat{\mathbf{x}}_j$ as

$$\hat{C}_{40}(\hat{\mathbf{x}}_j) = \frac{1}{N}\sum_{k=1}^{N}(\hat{x}_j(k))^4 - 3(\frac{1}{N}\sum_{k=1}^{N}(\hat{x}_j(k))^2)^2, \tag{6.23}$$

$$\hat{C}_{40}(\hat{\mathbf{x}}_j^e) = \frac{1}{N}\sum_{k=1}^{N}(\hat{x}_j^e(k))^4 - 3(\frac{1}{N}\sum_{k=1}^{N}(\hat{x}_j^e(k))^2)^2 \tag{6.24}$$

and

$$\hat{C}_{42}(\hat{\mathbf{x}}_j) = \frac{1}{N}\sum_{k=1}^{N}|\hat{x}_j(k)|^4 - |\frac{1}{N}\sum_{k=1}^{N}(\hat{x}_j(k))^2|^2 - 2(\frac{1}{N}\sum_{k=1}^{N}|\hat{x}_j(k)|^2)^2, \tag{6.25}$$

where $\hat{x}_j^e(k) = \hat{x}_j(2k), k = 0, 1, 2, ...$

As discussed in Chapter 3 a better classification results can be obtained by combining the above cumulant estimates using the MRC technique. In MRC, the cumulant features are obtained as the weighted sum of the cumulants estimated from N_T equalized signals [35]. Thus the cumulant features are given by

$$\hat{f}_1 = \frac{\sum_{j=1}^{N_T}\alpha_j C_{40}(\hat{\mathbf{x}}_j)}{\sum_{j=1}^{N_T}\alpha_j}, \tag{6.26}$$

$$\hat{f}_2 = \frac{\sum_{j=1}^{N_T}\alpha_j C_{42}(\hat{\mathbf{x}}_j)}{\sum_{j=1}^{N_T}\alpha_j}, \tag{6.27}$$

and

$$\hat{f}_3 = \frac{\sum_{j=1}^{N_T}\alpha_j C_{40}(\hat{\mathbf{x}}_j^e)}{\sum_{j=1}^{N_T}\alpha_j}, \tag{6.28}$$

where

$$\alpha_j = \frac{snr_j}{snr_{max}}, \tag{6.29}$$

snr_j denotes the SNR of the j^{th} estimated stream and $snr_{max} = max(snr_1, snr_2, ..., snr_{N_T})$. The snr_j is obtained as

$$snr_j = \frac{\sigma_s^2}{\sigma_{\hat{\mathbf{x}}_j}^2 - \sigma_s^2}, \tag{6.30}$$

where $\sigma_{\hat{\mathbf{x}}_j}^2$ is the power of equalized signal $\hat{\mathbf{x}}_j$ and σ_s^2 is the variance of transmit symbols. As

the normalized constellation points are attained after equalization, we can assume $\sigma_s^2 = 1$.

The estimates that are affected by high noise carry lower weights and the estimates that are affected by low noise carry higher weights.

Now, the detected modulation class M^* is given by

$$M^* = \underset{M=3,4,5,6}{argmin}(\|\hat{\mathbf{v}} - \mathbf{v}^M\|). \tag{6.31}$$

6.4 Simulation Results and Discussion

A set of experiments were carried out to evaluate the performance of the proposed method through the Monte-Carlo simulation. For the simulation, the number of transmitting and receiving antennas were set at $N_T = 2$ and $N_R = 4$, respectively. For all the experiments, we considered that the SNR over source-relays links (say SNR_{SR}) and the SNR over relays-destination links (say SNR_{RD}) were equal. The performance of the proposed classifier is analysed by calculating the average probability of correct classification P_C for different values of SNR (SNR=SNR_{SR}=SNR_{RD}). For each SNR value, 3000 Monte Carlo simulations were performed to calculate the average probability of correct classification. For each trial, we generated a random channel matrix and a random source message.

6.4.1 Classification Performance of the DMR technique and the JADE-FZC technique

A set of experiments were conducted to study the comparative performance of the DMR technique and the JADE-FZC technique over an AF-relay fading channel. BPSK and QPSK were the considered modulation types for classification. Figs. 6.2-6.5 show P_C versus SNR for the JADE-FZC technique and the DMR technique over an AF- relay fading channel. One can note that the DMR technique outperforms the JADE-FZC technique. For instance, the DMR technique attains $P_C = 0.9210$ at an SNR value of 8 dB for $N_C = 2$ and $|\rho_R| = |\rho_T| = 0.5$, while the JADE-FZC technique attains $P_C = 0.5427$ at an SNR value of 8 dB for the same values N_C, $|\rho_R|$ and $|\rho_T|$. It is because the JADE-FZC technique suffers from both the relay noise amplification and the noise amplification due to antenna correlation. On the other hand, the DMR technique avoids the equalization operation. It employs a feature vector which is obtained directly from the received signal. This set of experiments establishes the justification

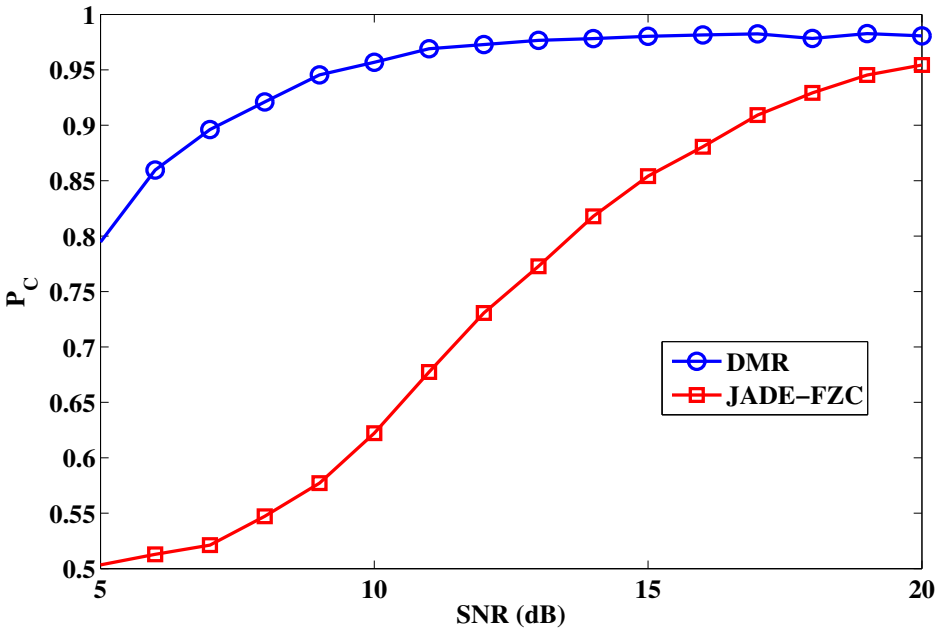

Figure 6.2: P_C versus SNR for JADE-FZC and DMR in the case of classifying BPSK and QPSK with $N = 2000$, $N_C = 2$ and $|\rho_R| = |\rho_T| = 0.5$

for the two step classification.

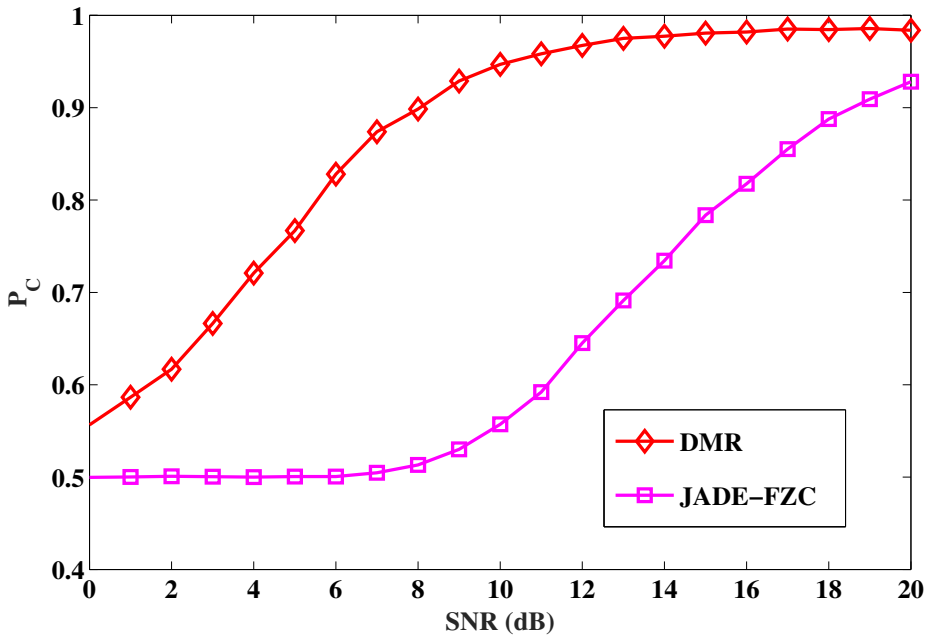

Figure 6.3: P_C versus SNR for JADE-FZC and DMR in the case of classifying BPSK and QPSK with $N = 2000$, $N_C = 2$ and $|\rho_R| = |\rho_T| = 0.7$

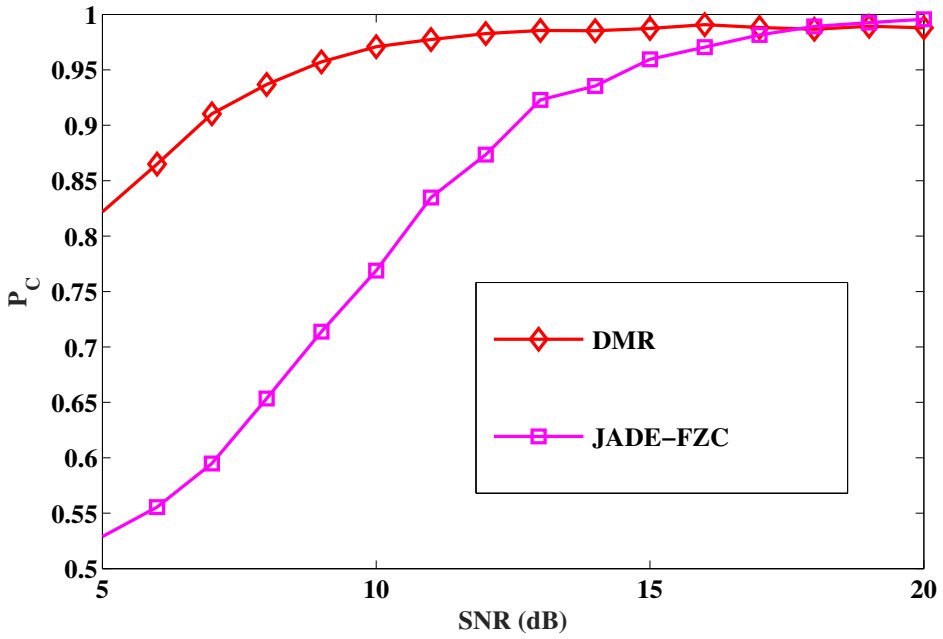

Figure 6.4: P_C versus SNR for JADE-FZC and DMR in the case of classifying BPSK and QPSK with $N = 2000$, $N_C = 5$ and $|\rho_R| = |\rho_T| = 0.5$

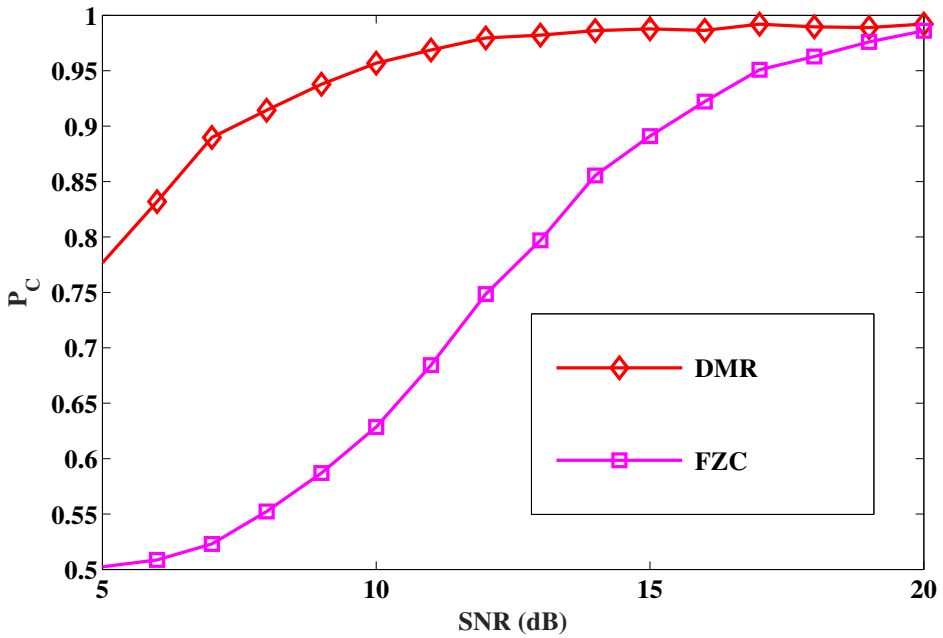

Figure 6.5: P_C versus SNR for JADE-FZC and DMR in the case of classifying BPSK and QPSK with $N = 2000$, $N_C = 5$ and $|\rho_R| = |\rho_T| = 0.7$

6.4.2 Effect of Number of Relays

In this set of experiments, we studied the effect of number of relays N_C on the proposed method. The sample size considered for this set of experiments is $N = 2000$. The considered values of N_C for the investigation were 2, 4 and 10.

Fig. 6.6 shows P_C versus SNR in the case of classifying BPSK, OQPSK and Q_1 using the feature vector $\mathbf{u}^M$ over an uncorrelated AF- relay fading channel for different values of N_C. Note that there is an increase in P_C with an increase in N_C. For instance, with an SNR value of 12 dB and $N = 2000$, the classifier with $\mathbf{u}^M$ as feature vector attains $P_C = 0.9638$ for $N_C = 2$, while at the same SNR and sample length, it attains $P_C = 0.9827$ for $N_C = 10$. Table 6.1 shows P_C attained by the classifier with $\mathbf{u}^M$ as feature vector with an SNR value of 12 dB and $N = 2000$ for different values of N_C. It is clear from Table 6.1 that there is an increase in P_C with an increase in N_C. Fig. 6.7 shows P_C versus SNR in the case of classifying QPSK, $\frac{\pi}{4}$-QPSK, 8-PSK and 16-QAM using the feature vector $\mathbf{v}^M$ over an AF- relay fading channel for different values of N_C. It is observed that P_C increases with an increase in N_C. For instance, with an SNR value of 12 dB and $N = 2000$, the classifier with $\mathbf{v}^M$ as feature vector attains $P_C = 0.7732$ for $N_C = 2$, while at the same SNR and sample length, it attains $P_C = 0.9732$ for $N_C = 10$. Table 6.2 shows P_C attained by the classifier with $\mathbf{v}^M$ as feature vector with an SNR value of 12 dB and $N = 2000$ for different values of N_C. It is clear from Table 6.2 that P_C increases with an increase in N_C. Fig. 6.8 shows P_C versus SNR in the case of classifying BPSK, OQPSK, QPSK, $\frac{\pi}{4}$-QPSK, 8-PSK and 16-QAM using the RA-AMC technique (two-step classification) over an AF- relay fading channel for different values of N_C. It is noted that there is an increase in P_C with an increase in N_C. For instance,with an SNR value of 12 dB and $N = 2000$, the RA-AMC technique attains $P_C = 0.7850$ for $N_C = 2$, while at the same SNR and sample length, it attains $P_C = 0.9125$ for $N_C = 10$. Table 6.3 shows P_C attained by the RA-AMC technique with an SNR value of 12 dB and $N = 2000$ for different values of N_C. It is clear from Table 6.3 that that P_C increases with an increase in N_C . The increase in P_C with an increase in N_C is contributed by the fact that the magnitudes of channel coefficients of $\mathbf{H}$ follow single Rayleigh distribution for large N_C.

It is also observed from Figs 6.6-6.8 that P_C increases with an increase in SNR. For example, one can note from Fig. 6.8 that for $N_C = 4$, the RA-AMC technique attains $P_C = 0.7105$ at an SNR value of 8 dB while for the same value of N_C, the RA-AMC technique attains $P_C = 0.8620$ at an SNR value of 12 dB.

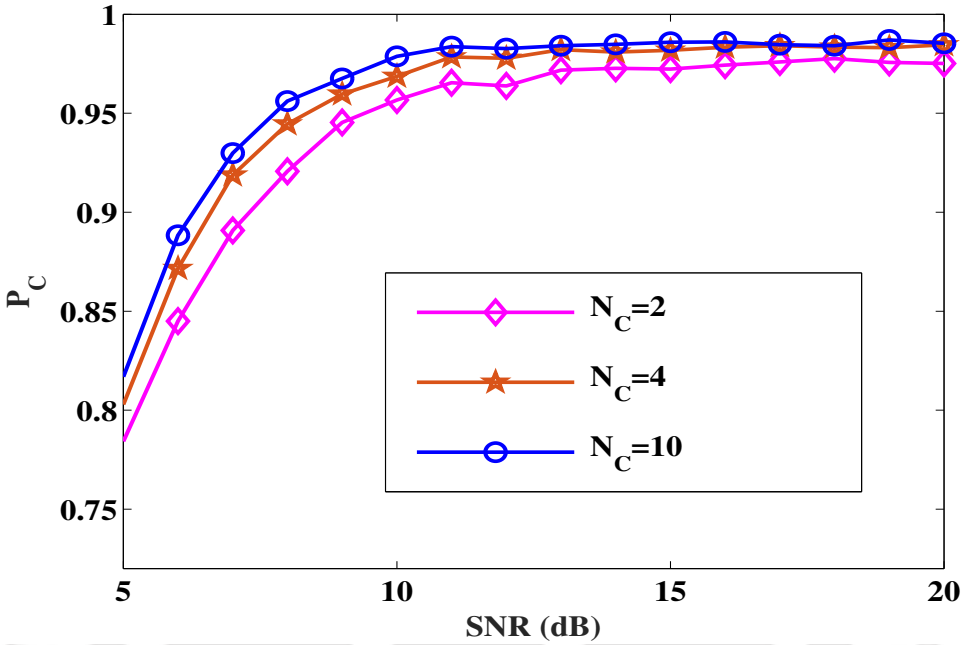

Figure 6.6: P_C versus SNR in the case of classifying BPSK, OQPSK and Q_1 using the feature vector $\mathbf{u}^M$ with $N = 2000$ and $|\rho_R| = |\rho_T| = 0$

Table 6.1: P_C with an SNR value of 12 dB, $N = 2000$ and $|\rho_R| = |\rho_T| = 0$ in the case of classifying BPSK, OQPSK and Q_1 using the feature vector $\mathbf{u}^M$ for different values of N_C

N_C	P_C
2	0.9638
4	0.9778
10	0.9827

6.4.3 Effect of Antenna Correlation

Figs. 6.9-6.11 show P_C versus SNR in the case of classifying BPSK, OQPSK and Q_1 using the feature vector $\mathbf{u}^M$ over an AF- relay fading channel for different antenna correlation values. It is observed that P_C decreases with an increase in the antenna correlation value. For instance, with an SNR value of 12 dB, $N = 2000$ and $N_C = 4$, the classifier with $\mathbf{u}^M$ as feature vector

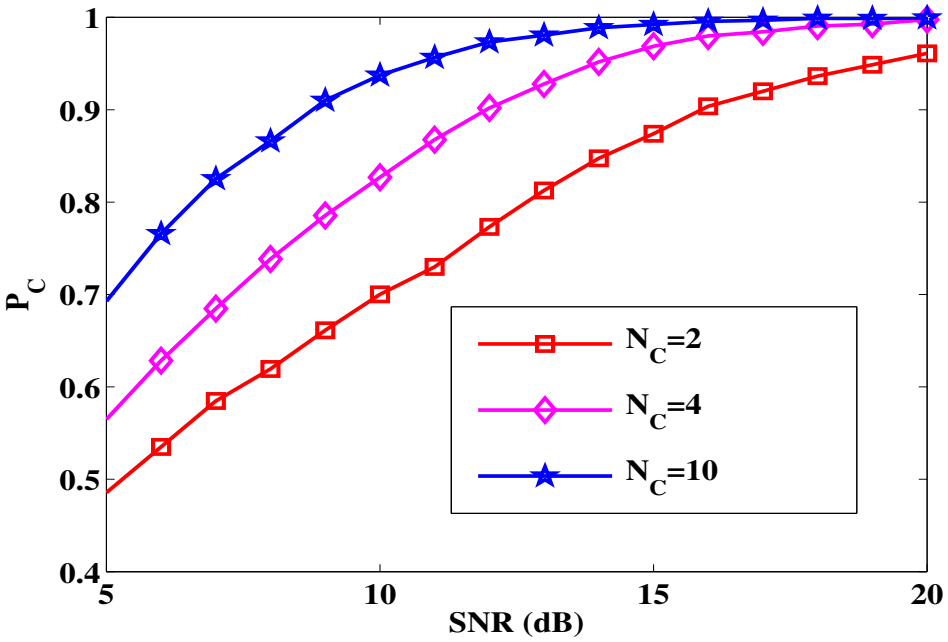

Figure 6.7: P_C versus SNR in the case of classifying QPSK, $\frac{\pi}{4}$-QPSK, 8-PSK and 16-QAM using the feature vector $\mathbf{v}^M$ with $N = 2000$ and $|\rho_R| = |\rho_T| = 0$

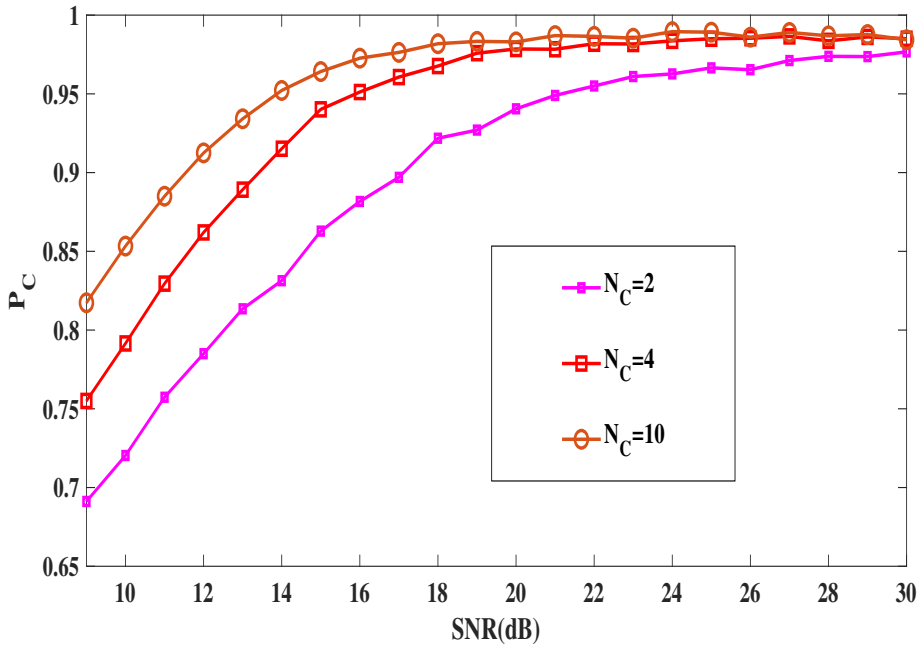

Figure 6.8: P_C versus SNR in the case of classifying BPSK, OQPSK, QPSK, $\frac{\pi}{4}$-QPSK, 8-PSK and 16-QAM using the RA-AMC technique with $N = 2000$ and $|\rho_R| = |\rho_T| = 0$

Table 6.2: P_C with an SNR value of 12 dB, $N = 2000$ and $|\rho_R| = |\rho_T| = 0$ in the case of classifying QPSK, $\frac{\pi}{4}$-QPSK, 8-PSK and 16-QAM using the feature vector $\mathbf{v}^M$ for different values of N_C

N_C	P_C
2	0.7732
4	0.9018
10	0.9732

Table 6.3: P_C with an SNR value of 12 dB, $N = 2000$ and $|\rho_R| = |\rho_T| = 0$ in the case of classifying BPSK, OQPSK, QPSK, $\frac{\pi}{4}$-QPSK, 8-PSK and 16-QAM using the RA-AMC technique for different values of N_C

N_C	P_C
2	0.7850
4	0.8620
10	0.9125

attains $P_C = 0.9702$ for $|\rho_R| = |\rho_T| = 0.5$, while at the same SNR, N and N_C, it attains $P_C = 0.9546$ for $|\rho_R| = |\rho_T| = 0.7$. Table 6.4 shows P_C attained by the classifier with $\mathbf{u}^M$ as feature vector with an SNR value of 12 dB, $N = 2000$ and $N_C = 4$ for different antenna correlation values. The decrease in P_C with an increase in the antenna correlation value is attributed to the reduced diversity gain as a correlated low rank channel model yields only receiver array gain.

Figs. 6.12-6.14 show P_C versus SNR in the case of classifying QPSK, $\frac{\pi}{4}$-QPSK, 8-PSK and 16-QAM using the feature vector $\mathbf{v}^M$ over an AF- relay fading channel for different antenna correlation values. There is a decrease in P_C with an increase in the antenna correlation value. For instance, with an SNR value of 12 dB, $N = 2000$ and $N_C = 10$, the classifier with $\mathbf{v}^M$ as feature vector attains $P_C = 0.9034$ for $|\rho_R| = |\rho_T| = 0.5$, while at the same SNR, N and N_C, it attains $P_C = 0.7881$ for $|\rho_R| = |\rho_T| = 0.7$. Table 6.5 shows P_C attained by the classifier with $\mathbf{v}^M$ as feature vector with an SNR value of 12 dB, $N = 2000$ and $N_C = 10$ for different antenna correlation values. The decrease in P_c with an increase in the antenna correlation value is contributed by the noise amplification at the equalizer output.

Figs. 6.15-6.17 show P_C versus SNR in the case of classifying BPSK, OQPSK, QPSK, $\frac{\pi}{4}$-QPSK, 8-PSK and 16-QAM using the RA-AMC technique (two-step classification) over an AF- relay fading channel for different antenna correlation values. There is a decrease in P_C with an increase in the antenna correlation value. For instance, with an SNR value of 12 dB,

$N = 2000$ and $N_C = 10$, the RA-AMC technique attains $P_C = 0.9125$ for $|\rho_R| = |\rho_T| = 0.5$, while at the same SNR, N and N_C, it attains $P_C = 0.8225$ for $|\rho_R| = |\rho_T| = 0.7$. Table 6.6 shows P_C attained by the RA-AMC technique with an SNR value of 12 dB, $N = 2000$ and $N_C = 10$ in the case of classifying BPSK, OQPSK, QPSK, $\frac{\pi}{4}$-QPSK, 8-PSK and 16-QAM for different antenna correlation values. The decrease in P_C with an increase in the antenna correlation is because of the reduced diversity gain and the noise amplification at the equalizer output.

One can also note from Figs. 6.9-6.17 that P_C improves as SNR increases. For example, one can note from Fig. 6.16 that for $N = 2000$, $N_C = 4$ and $|\rho_R| = |\rho_T| = 0.7$, RA-AMC attains $P_C = 0.7853$ at an SNR value of 12 dB while for the same value of N, N_C and antenna correlation, the RA-AMC technique attains $P_C = 0.9037$ at an SNR value of 16 dB. Table 6.7 shows the P_C attained by the RA-AMC technique at different SNR values for $N = 2000$, $N_C = 4$ and $|\rho_R| = |\rho_T| = 0.7$. It is clear from Table 6.7 that P_C improves as SNR increases.

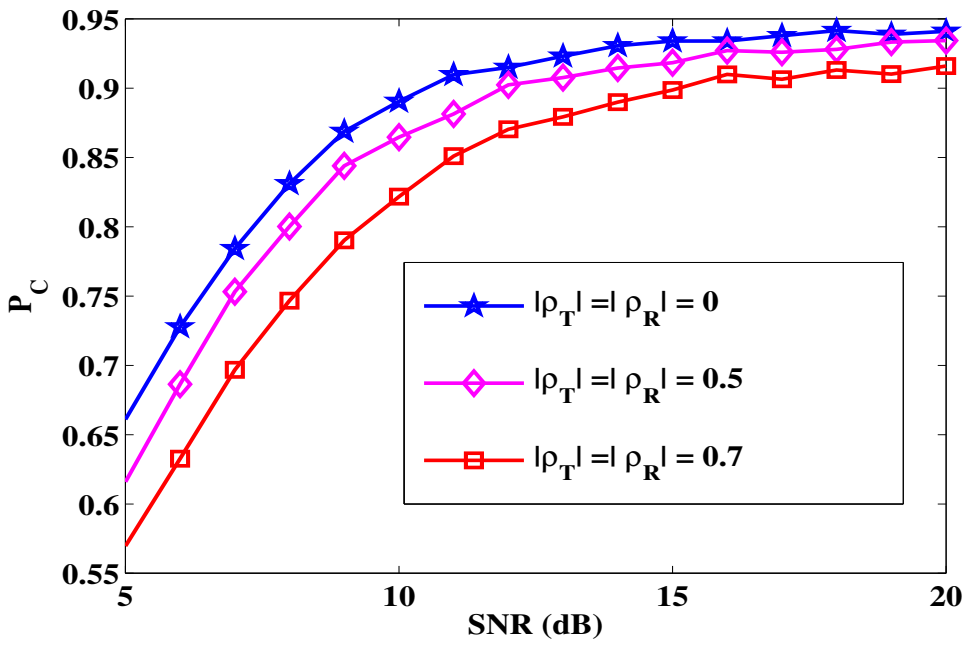

Figure 6.9: P_C versus SNR in the case of classifying BPSK, OQPSK and Q_1 using the feature vector $\mathbf{u}^M$ with $N = 500$ and $N_C = 4$

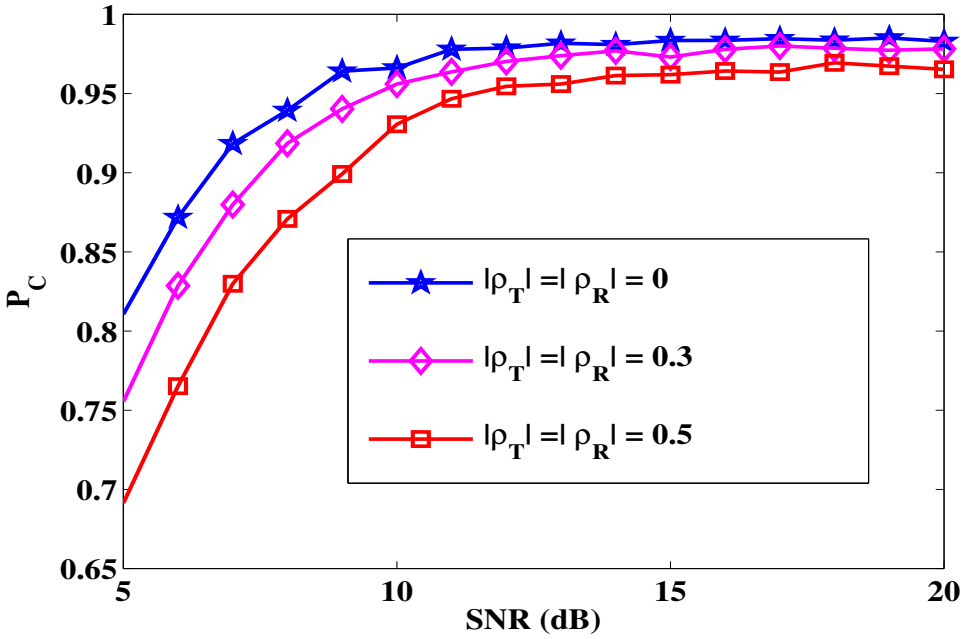

Figure 6.10: P_C versus SNR in the case of classifying BPSK, OQPSK and Q_1 using the feature vector $\mathbf{u}^M$ with $N = 2000$ and $N_C = 4$

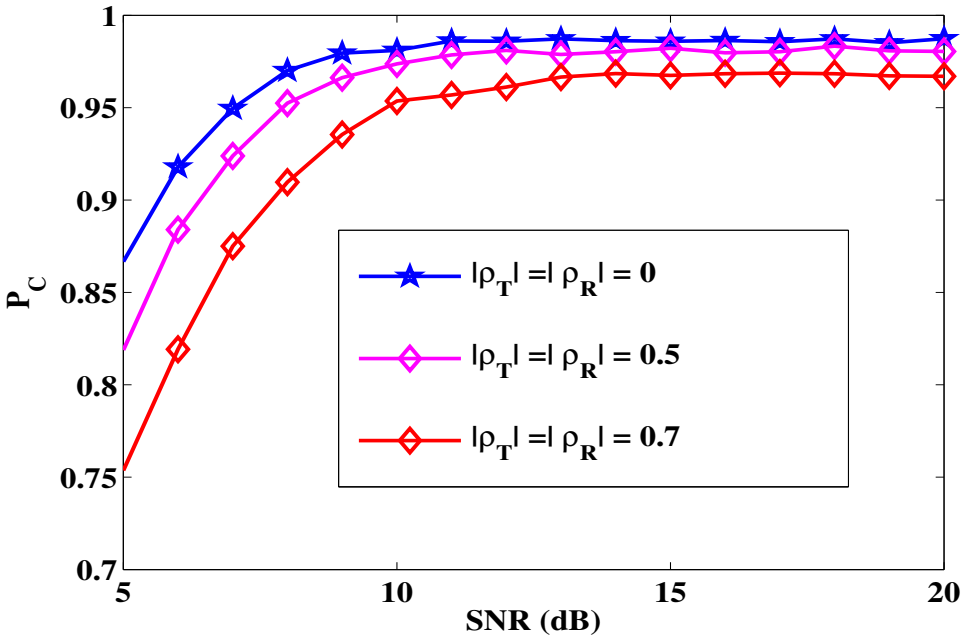

Figure 6.11: P_C versus SNR in the case of classifying BPSK, OQPSK and Q_1 using the feature vector $\mathbf{u}^M$ with $N = 4000$ and $N_C = 4$

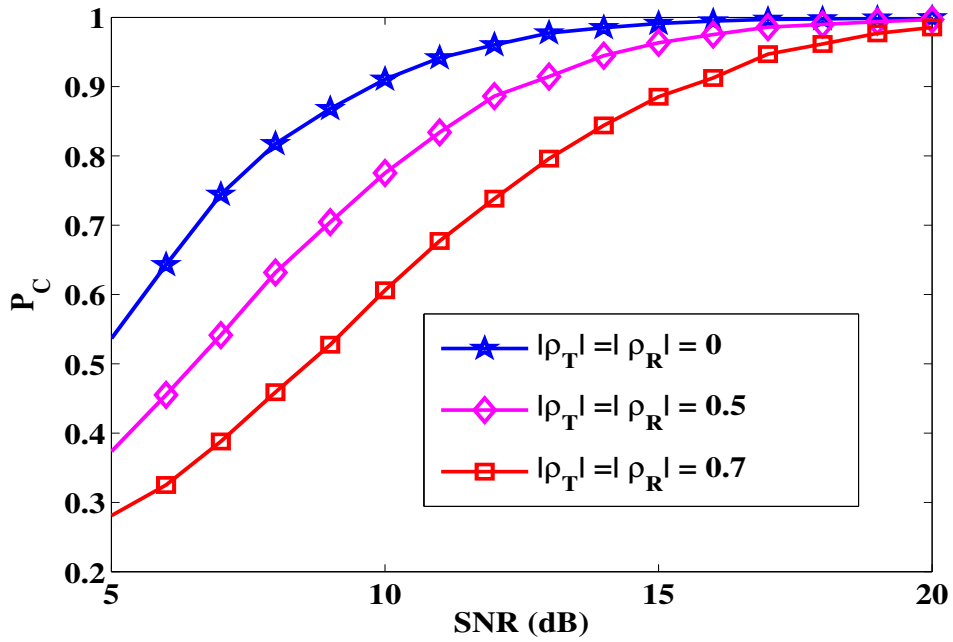

Figure 6.12: P_C versus SNR in the case of classifying QPSK, OQPSK, $\frac{\pi}{4}$-QPSK and 8-PSK using the feature vector $\mathbf{v}^M$ with $N = 500$ and $N_C = 10$

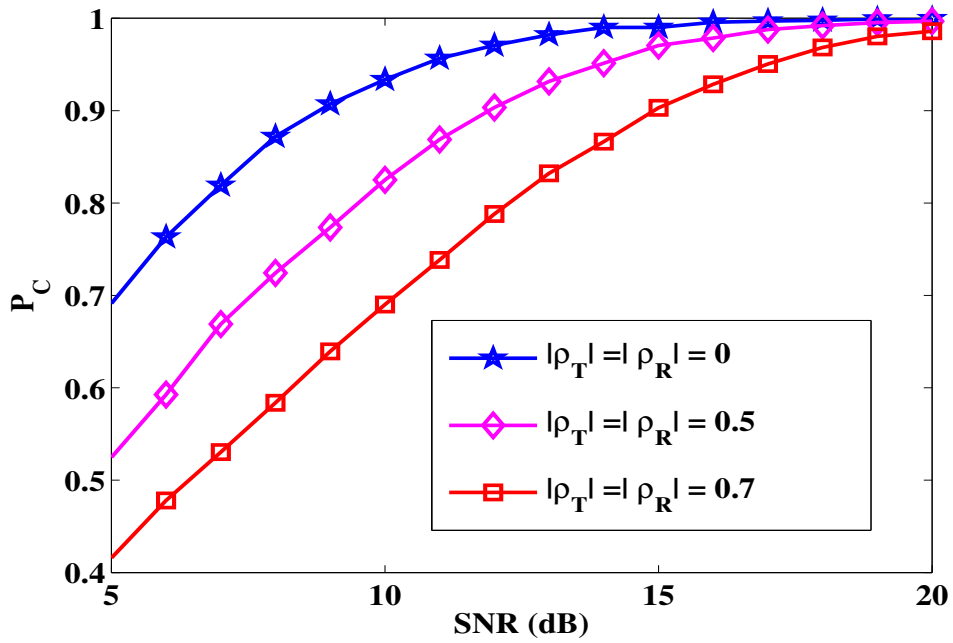

Figure 6.13: P_C versus SNR in the case of classifying QPSK, OQPSK, $\frac{\pi}{4}$-QPSK and 8-PSK using the feature vector $\mathbf{v}^M$ with $N = 2000$ and $N_C = 10$

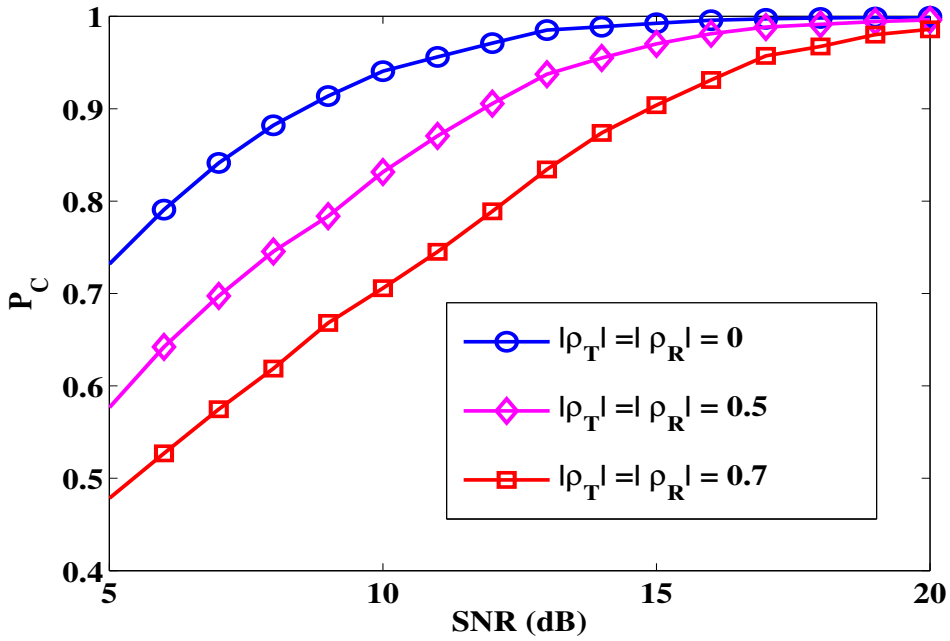

Figure 6.14: P_C versus SNR in the case of classifying QPSK, OQPSK, $\frac{\pi}{4}$-QPSK and 8-PSK using the feature vector $\mathbf{v}^M$ with $N = 4000$ and $N_C = 10$

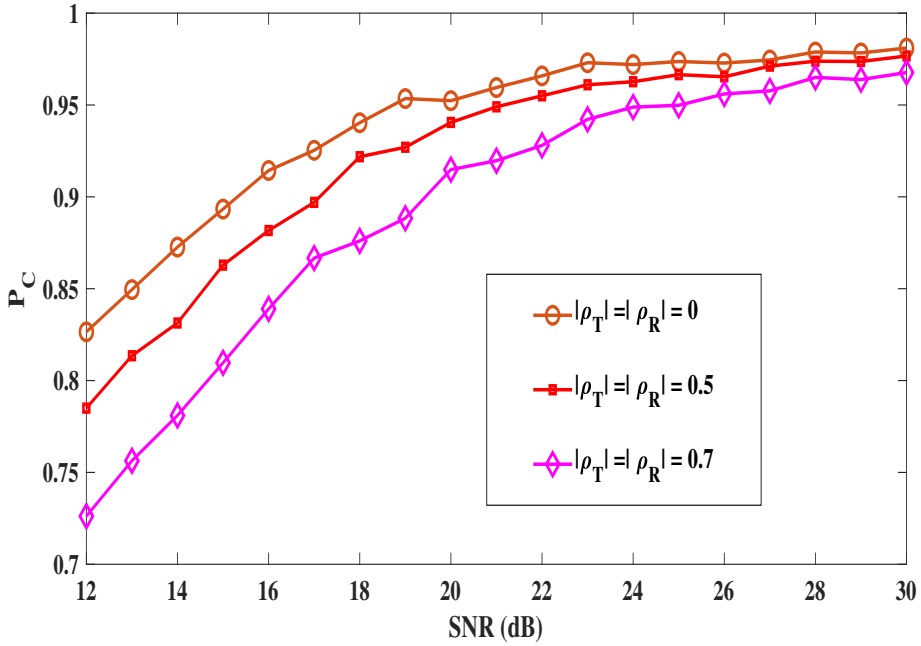

Figure 6.15: P_C versus SNR in the case of classifying BPSK, OQPSK, QPSK, $\frac{\pi}{4}$-QPSK, 8-PSK and 16-QAM using the RA-AMC technique with $N = 2000$ and $N_C = 2$

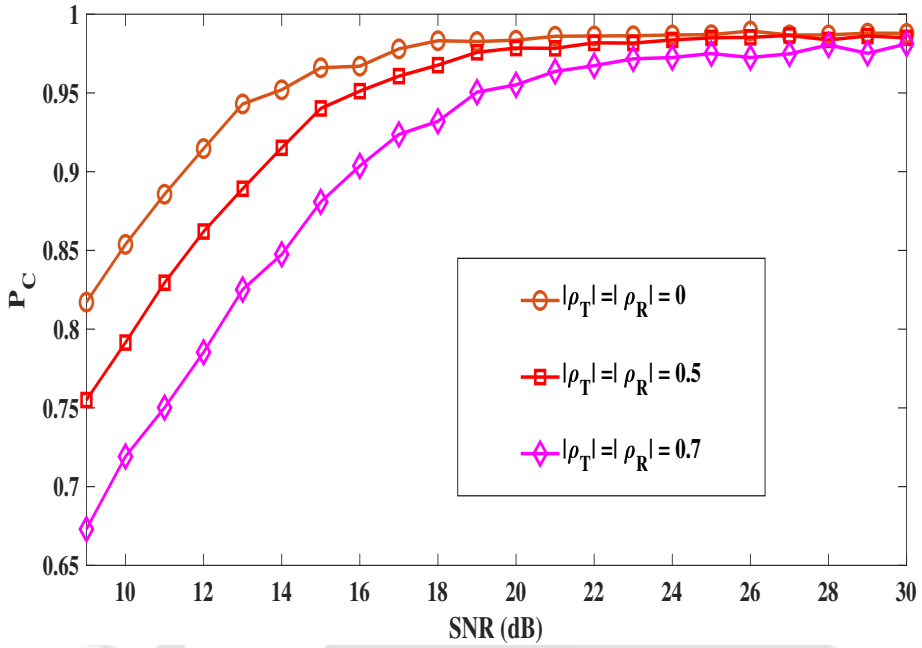

Figure 6.16: P_C versus SNR in the case of classifying BPSK, OQPSK, QPSK, $\frac{\pi}{4}$-QPSK, 8-PSK and 16-QAM using the RA-AMC technique with $N = 2000$ and $N_C = 4$

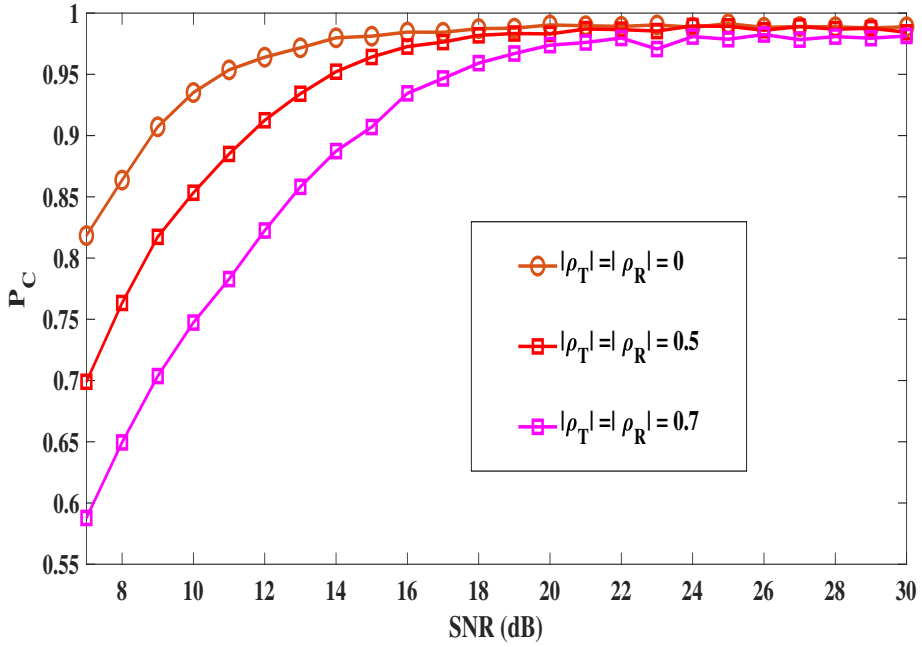

Figure 6.17: P_C versus SNR in the case of classifying BPSK, OQPSK, QPSK, $\frac{\pi}{4}$-QPSK, 8-PSK and 16-QAM using the RA-AMC technique with $N = 2000$ and $N_C = 10$

Table 6.4: P_C with an SNR value of 12 dB, $N = 2000$ and $N_C = 4$ in the case of classifying BPSK, OQPSK and Q_1 using the feature vector $\mathbf{u}^M$ for different antenna correlation values $|\rho| = |\rho_R| = |\rho_T|$

$\|\rho\|$	P_C
0	0.9787
0.5	0.9702
0.7	0.9546

Table 6.5: P_C with an SNR value of 12 dB, $N = 2000$ and $N_C = 10$ in the case of classifying QPSK, $\frac{\pi}{4}$-QPSK, 8-PSK and 16-QAM using the feature vector $\mathbf{v}^M$ for different antenna correlation values $|\rho| = |\rho_R| = |\rho_T|$

$\|\rho\|$	P_C
0	0.9708
0.5	0.9034
0.7	0.7881

Table 6.6: P_C with an SNR value of 12 dB, $N = 2000$ and $N_C = 10$ in the case of classifying BPSK, OQPSK, QPSK, $\frac{\pi}{4}$-QPSK, 8-PSK and 16-QAM using the RA-AMC technique for different antenna correlation values $|\rho| = |\rho_R| = |\rho_T|$

$\|\rho\|$	P_C
0	0.9640
0.5	0.9125
0.7	0.8225

Table 6.7: P_C at $N = 2000$, $N_C = 4$ and $|\rho_R| = |\rho_T| = 0.7$ in the case of classifying BPSK, OQPSK, QPSK, $\frac{\pi}{4}$-QPSK, 8-PSK and 16-QAM using the RA-AMC technique for different SNR values

SNR (dB)	P_C
12	0.7853
14	0.8475
16	0.9037
18	0.9320

6.5 Summary

This chapter addressed the AMC of MIMO signals over correlated AF-relay fading channels. An AMC method, namely RA-AMC, was proposed to classify a pool of modulation types, namely BPSK, OQPSK, QPSK, $\frac{\pi}{4}$-QPSK, 8-PSK and 16-QAM. The proposed method involved two steps. In the first step, the method employed a cumulant feature vector derived directly from the received signal to distinguish BPSK, OQPSK and the sub-pool $Q_1 = \{QPSK, \frac{\pi}{4} - QPSK, 8 - PSK, 16 - QAM\}$ as a whole. This cumulant feature provided resistance against the noise amplification which occurs in a correlated AF-relay system. In the second step, it employed a cumulant feature vector derived from the equalized signal to distinguish the modulation types in Q_1. The simulation results showed that the proposed method performed satisfactorily over a correlated AF-relay fading channel. For instance, with an SNR value of 12 dB, $N = 2000$,$N_T = 2$, $N_R = 4$ and $N_C = 10$, the RA-AMC technique attained $P_C = 0.9125$ for $|\rho_R| = |\rho_T| = 0.5$.

7

Conclusion and Future Work

Contents

7.1 Conclusion

Designing AMC algorithms for MIMO systems is a challenging task, because the mutual interference generated by MIMO spatial channels changes the statistical properties of the modulated signal. Many studies have addressed this challenging problem. However, there remain several research issues. The thesis addressed some of these issues. We adopted an FB framework with the HOCs as AMC features. The research contributions were presented in four contributory chapters and they are summarized below.

Chapter 3 dealt with the AMC of the QPSK-variant (QPSK, OQPSK and $\frac{\pi}{4}$-QPSK) and 8-PSK signals over spatially correlated MIMO channels. The HOCs are popular as AMC features because of their resilience to the Gaussian noise. However, the HOCs estimated directly from the equalized signal fail to distinguish the QPSK variants and 8-PSK. It was shown that the fourth-order cumulants of the QPSK and the OQPSK signals are identical, so also of $\frac{\pi}{4}$-QPSK and 8-PSK signals. To distinguish the above modulation types, we proposed a feature vector $\mathbf{v}^M = [C_{40}(x), C_{42}(\nabla x), C_{40}(x^e)]$, where x,∇x and x^e are RVs associated with data sequence $x(k)$,$\nabla x(k) = x(k) - x(k-1)$ and $x^e = x(2k)$, respectively, $k = 0, 1, ...$ The proposed method performed satisfactorily over spatially correlated MIMO channels. For example, with an SNR value of 5 dB, $N_T = 2$, $N_R = 4$ and $N = 500$, the proposed method with the JADE technique as equalizer attains $P_C = .9720$ for $|\rho_R| = |\rho_T| = 0.3$ over a Rayleigh channel.

The emergence of WSNs and CR networks makes cooperative classification an attractive alternative to improve the AMC performance. **Chapter 4** presented a cooperative AMC method for MIMO systems in a multi-antenna sensor network. The proposed CAMC method employed a centralized cooperative classification framework with feature-level fusion. In such a centralized framework, each sensor node estimates a set of HOC features. These features are then combined at the FC using the MRC technique. The estimated feature vector is then subjected to a minimum distance classifier that uses the Euclidean distance as the measure of feature similarity. The modulation types considered for classification were BPSK, OQPSK, QPSK, $\frac{\pi}{4}$-QPSK, 8-PSK,16-QAM and 64-QAM. The method performed reasonably well over correlated Rayleigh channels. For instance, with an SNR value of 3 dB,$N_T = 2$, $N_R = 4$, $N = 1000$ and

$|\rho_R| = |\rho_T| = 0.5$, the CAMC technique attained $P_C = 0.8173$ for $N_S = 1$, while for the same SNR, sample length and antenna correlation value, it attained $P_C = 0.9325$ for $N_S = 8$ with $N_T = 2$, $N_R = 4$.

The majority of the AMC algorithms for MIMO systems considered the rich scattering environment that offers a full rank channel matrix. However, a rank deficient channel, such as a keyhole channel can severely degrade the AMC performance. **Chapter 5** addressed the AMC of MIMO signals over correlated Keyhole channels. A novel algorithm, namely the DMR algorithm, was proposed to distinguish the lower order PSK constellations, namely BPSK, QPSK and OQPSK. The proposed algorithm employed the ratios of HOCs derived from the received signal and its backward difference as AMC features. These features were chosen so that the contributions of the channel-coefficients are cancelled. Thus, the DMR algorithm does not require the CSI at the receiver. The simulation results showed that the proposed method performed satisfactorily under the keyhole channel. For instance, with an SNR value of 4 dB, $N_T = 2$, $N_R = 4$, $N = 2000$ and $|\rho_R| = |\rho_T| = 0.5$, the proposed method attained $P_C = 0.9476$.

Cooperative relaying is an attractive solution to overcome the rank deficiency of MIMO channels. These cooperative relays act as active scatterers, which eventually turns a keyhole channel into a multi-keyhole channel. **Chapter 6** addressed the AMC of MIMO signals over a correlated AF-relay fading channel. An AMC method, namely the RA-AMC method, was proposed to classify a pool of modulation types, namely BPSK, OQPSK, QPSK, $\frac{\pi}{4}$-QPSK, 8-PSK and 16-QAM, over an AF-relay fading channel. The proposed method involved two steps. In the first step, the method employed a cumulant feature vector derived directly from the received signal to distinguish BPSK, OQPSK and the sub-pool $Q_1 = \{QPSK, \frac{\pi}{4} - QPSK, 8 - PSK, 16 - QAM\}$ as a whole. This cumulant feature provided resistance against noise amplification which occurs in a correlated AF-relay system. In the second step, it employed a cumulant feature vector derived from the equalized signal to distinguish the modulation types in Q_1. The simulation results showed that the proposed method performed satisfactorily over a correlated AF-relay fading channel. For instance, with an SNR value of 12 dB, $N = 2000$, $N_T = 2$, $N_R = 4$ and $N_C = 10$, the RA-AMC technique attained $P_C = 0.9125$ for $|\rho_R| = |\rho_T| = 0.5$.

7.1.1 Scope for Future Work

The works presented in this can be expanded in several directions. We identify the following interesting future works:

1. In this thesis work, the carrier frequency offset (CFO) is not considered. The CFO is contributed by an imperfect receiver. Model mismatch can occur on account of this, thereby degrading the AMC performance. A preprocessing step can be included to estimate the frequency offset.

2.An interesting future work will be to compare the performance of the proposed DMR method with the reduced rank space-time equalizer and the independent low-rank matrix analysis (ILRMA) technique

3. It is reported in [81] that practical wireless channels experience a combination of both the man-made and natural noise. The combined noise is highly non-Gaussian nature. Research can be conducted to investigate the effect of non-Gaussian noise on the performance of the AMC for MIMO systems. Particularly, the HOC-based methods may be adapted for better performance under non-Gaussian noise.

4. It will be an interesting future work to investigate the effect of noise compensation in the context of AMC for MIMO systems.

5. AMC over Space-time coded MIMO channels is an interesting research area. There are two main challenges : classification of the employed space time block code (STBC) and modulation type in the presence of the mutual-interference generated by the spatial channel.

6. Research can be conducted to investigate the effect of different Relaying strategies on the AMC performance. For instance, AMC over a MIMO AF-relay networks with transmit antenna selection and maximal ratio combining (TAS/MRC) can be studied.

7. Deep learning (DL) is an attractive classification tool that has been employed successfully in many arenas such as image classification, machine translation, automatic speech recognition and network optimization. A few works have been devoted to AMC for SISO systems based on DL [82–85]. Three DL architectures employed for AMC are : 1) a convolutional long short-term deep neural network (CLDNN), 2) a long short-term memory neural network (LSTM), and 3) a

deep residual network (Resnet) [86]. However, its usage in the context of the AMC of MIMO signals has not been well investigated. It will be interesting to apply DL based approaches to the AMC of MIMO signals and assess their performances relative to the methods developed in this thesis.

Bibliography

[1] M. S. Mühlhaus, M. Öner, O. A. Dobre, H. U. Jäkel, and F. K. Jondral, "A Novel Algorithm for MIMO Signal Classification Using Higher-Order Cumulants," in *2013 IEEE Radio and Wireless Symposium*. IEEE, 2013, pp. 7–9.

[2] K. Kim and A. Polydoros, "Digital Modulation Classification: the BPSK versus QPSK Case," in *MILCOM 88, 21st Century Military Communications-What's Possible?'. Conference record. Military Communications Conference*. IEEE, 1988, pp. 431–436.

[3] J. Sills, "Maximum-Likelihood Modulation Classification for PSK/QAM," in *MILCOM 1999. IEEE Military Communications. Conference Proceedings (Cat. No. 99CH36341)*, vol. 1. IEEE, 1999, pp. 217–220.

[4] A. Swami and B. M. Sadler, "Hierarchical Digital Modulation Classification Using Cumulants," *IEEE Transactions on communications*, vol. 48, no. 3, pp. 416–429, 2000.

[5] P. Panagiotou, A. Anastasopoulos, and A. Polydoros, "Likelihood Ratio Tests for Modulation Classification," in *MILCOM 2000 Proceedings. 21st Century Military Communications. Architectures and Technologies for Information Superiority (Cat. No. 00CH37155)*, vol. 2. IEEE, 2000, pp. 670–674.

[6] D.-C. Chang and P.-K. Shih, "Cumulants-Based Modulation Classification Technique in Multipath Fading Channels," *IET Communications*, vol. 9, no. 6, pp. 828–835, 2015.

[7] O. A. Dobre, A. Abdi, Y. Bar-Ness, and W. Su, "Survey of Automatic Modulation Classification Techniques: Classical Approaches and New Trends," *IET communications*, vol. 1, no. 2, pp. 137–156, 2007.

[8] H.-C. Wu, M. Saquib, and Z. Yun, "Novel Automatic Modulation Classification Using Cumulant Features for Communications via Multipath Channels," *IEEE Transactions on Wireless Communications*, vol. 7, no. 8, pp. 3098–3105, 2008.

[9] O. A. Dobre, Y. Bar-Ness, and W. Su, "Robust QAM Modulation Classification Algorithm Using Cyclic Cumulants," in *2004 IEEE Wireless Communications and Networking Conference (IEEE Cat. No. 04TH8733)*, vol. 2. IEEE, 2004, pp. 745–748.

[10] B. Ramkumar, "Automatic Modulation Classification for Cognitive Radios Using Cyclic Feature Detection," *IEEE Circuits and Systems Magazine*, vol. 9, no. 2, pp. 27–45, 2009.

[11] P. Liu and P.-L. Shui, "A New Cumulant Estimator in Multipath Fading Channels for Digital Modulation Classification," *IET Communications*, vol. 8, no. 16, pp. 2814–2824, 2014.

[12] V. Orlic and M. Dukic, "Multipath Channel Estimation Algorithm for Automatic Modulation Classification Using Sixth-Order Cumulants," *Electronics letters*, vol. 46, no. 19, pp. 1348–1349, 2010.

[13] V. D. Orlic and M. L. Dukic, "Automatic Modulation Classification Algorithm Using Higher-Order Cumulants Under Real-World Channel Conditions," *IEEE Communications Letters*, vol. 13, no. 12, pp. 917–919, 2009.

[14] J. R. Hampton, *Introduction to MIMO Communications*. Cambridge university press, 2013.

[15] M. S. Mühlhaus, M. Öner, O. A. Dobre, H. U. Jkel, and F. K. Jondral, "Automatic Modulation Classification for MIMO Systems Using Fourth-Order Cumulants," in *2012 IEEE Vehicular Technology Conference (VTC Fall)*. IEEE, 2012, pp. 1–5.

[16] Z. Zhu, "Automatic Classification of Digital Communication Signal Modulations," Ph.D. dissertation, 2014.

[17] V. Choqueuse, S. Azou, K. Yao, L. Collin, and G. Burel, "Blind Modulation Recognition for MIMO systems," *MTA Review*, vol. 19, no. 2, pp. 183–196, 2009.

[18] K. Hassan, I. Dayoub, W. Hamouda, C. N. Nzeza, and M. Berbineau, "Blind Digital Modulation Identification for Spatially-Correlated MIMO systems," *IEEE Transactions on Wireless Communications*, vol. 11, no. 2, pp. 683–693, 2011.

[19] M. S. Muhlhaus, M. Oner, O. A. Dobre, and F. K. Jondral, "A Low Complexity Modulation Classification Algorithm for MIMO Systems," *IEEE Communications Letters*, vol. 17, no. 10, pp. 1881–1884, 2013.

[20] Y. Liu, A. M. Haimovich, W. Su, J. Dabin, and E. Kanterakis, "Modulation Classification of MIMO-OFDM Signals by Independent Component Analysis and Support Vector Machines," *arXiv preprint arXiv:1307.4430*, 2013.

[21] E. Kanterakis and W. Su, "Modulation Classification in MIMO systems," in *MILCOM 2013-2013 IEEE Military Communications Conference*. IEEE, 2013, pp. 35–39.

[22] W. B. Chikha, I. Dayoub, W. Hamouda, and R. Attia, "Modulation Recognition for MIMO Relaying Broadcast Channels with Direct Link," *IEEE Wireless Communications Letters*, vol. 3, no. 1, pp. 50–53, 2013.

[23] W. B. Chikha, I. Dayoub, and R. Attia, "Modulation Detection in Intelligent Transportation Systems Based on Cooperative MIMO Networks over Nakagami-m Fading," in *2014 International Conference on Electrical Sciences and Technologies in Maghreb (CISTEM)*. IEEE, 2014, pp. 1–6.

[24] S. Kharbech, I. Dayoub, M. Zwingelstein-Colin, E. P. Simon, and K. Hassan, "Blind Digital Modulation Identification for Time-Selective Mimo channels," *IEEE wireless communications letters*, vol. 3, no. 4, pp. 373–376, 2014.

[25] Z. Zhu and A. K. Nandi, "Blind Modulation Classification for MIMO systems Using Expectation Maximization," in *2014 IEEE Military Communications Conference*. IEEE, 2014, pp. 754–759.

[26] M. Turan, M. Öner, and H. A. Çırpan, "Joint Modulation Classification and Antenna Number Detection for MIMO systems," *IEEE Communications Letters*, vol. 20, no. 1, pp. 193–196, 2015.

[27] S. Kharbech, I. Dayoub, M. Zwingelstein-Colin, and E. P. Simon, "On Classifiers for Blind Feature-Based Automatic Modulation Classification over Multiple-Input–Multiple-Output Channels," *IET Communications*, vol. 10, no. 7, pp. 790–795, 2016.

[28] M. R. Bahloul, M. Z. Yusoff, A.-H. Abdel-Aty, M. N. M. Saad, and M. Al-Jemeli, "Modulation Classification for MIMO Systems: State of the Art and Research Directions," *Chaos, Solitons & Fractals*, vol. 89, pp. 497–505, 2016.

[29] L. Castedo, C. J. Escudero, and A. Dapena, "A Blind Signal Separation Method for Multiuser Communications," *IEEE Transactions on Signal Processing*, vol. 45, no. 5, pp. 1343–1348, 1997.

[30] C. B. Papadias and A. J. Paulraj, "A Constant Modulus Algorithm for Multiuser Signal Separation in Presence of Delay Spread Using Antenna Arrays," *IEEE signal processing letters*, vol. 4, no. 6, pp. 178–181, 1997.

[31] J.-F. Cardoso and A. Souloumiac, "Blind Beamforming for Non-Gaussian signals," in *IEE proceedings F (radar and signal processing)*, vol. 140, no. 6. IET, 1993, pp. 362–370.

[32] D. N. Rutledge and D. J.-R. Bouveresse, "Independent Components Analysis with the JADE Algorithm," *TrAC Trends in Analytical Chemistry*, vol. 50, pp. 22–32, 2013.

[33] E. Lindskog and C. Tidestav, "Reduced Rank Space-Time Equalization," in *Ninth IEEE International Symposium on Personal, Indoor and Mobile Radio Communications (Cat. No.98TH8361)*, vol. 3, 1998, pp. 1081–1085 vol.3.

[34] Y. Mitsui, D. Kitamura, S. Takamichi, N. Ono, and H. Saruwatari, "Blind Source Separation Based on Independent Low-Rank Matrix Analysis with Sparse Regularization for Time-Series Activity," in *2017 IEEE International Conference on Acoustics, Speech and Signal Processing (ICASSP)*, 2017, pp. 21–25.

[35] G. B. Marković, "Cooperative Modulation Classification by Using Multiple Sensors in Dispersive Fading Channels," in *2014 22nd Telecommunications Forum Telfor (TELFOR)*. IEEE, 2014, pp. 264–271.

[36] M. Abdelbar, B. Tranter, and T. Bose, "Cooperative Cumulants-Based Modulation Classification under Flat Rayleigh fading Channels," in *2015 IEEE International Conference on Communications (ICC)*. IEEE, 2015, pp. 7622–7627.

[37] Y. Zhang, N. Ansari, and W. Su, "Optimal Decision Fusion Based Automatic Modulation Classification by Using Wireless Sensor Networks in Multipath Fading Channel," in *2011 IEEE Global Telecommunications Conference-GLOBECOM 2011*. IEEE, 2011, pp. 1–5.

[38] M. Abdelbar, W. H. Tranter, and T. Bose, "Cooperative Cumulants-Based Modulation Classification in Distributed Networks," *IEEE Transactions on Cognitive Communications and Networking*, vol. 4, no. 3, pp. 446–461, 2018.

[39] G. Markovic and M. Dukic, "Cooperative Modulation Classification with Data Fusion for Multipath Fading Channels," *Electronics Letters*, vol. 49, no. 23, p. 1494, 2013.

[40] J. L. Xu, W. Su, and M. Zhou, "Distributed Automatic Modulation Classification with Multiple Sensors," *IEEE Sensors Journal*, vol. 10, no. 11, pp. 1779–1785, 2010.

[41] ——, "Asynchronous and High-Accuracy Digital Modulated Signal Detection by Sensor Networks," in *2011-MILCOM 2011 Military Communications Conference*. IEEE, 2011, pp. 589–594.

[42] W. Su and J. Kosinski, "Framework of Network Centric Signal Sensing for Automatic Modulation Classification," in *2010 International Conference on Networking, Sensing and Control (ICNSC)*. IEEE, 2010, pp. 534–539.

[43] Y. Zhang, N. Ansari, and W. Su, "Multi-Sensor Signal Fusion-Based Modulation Classification by Using Wireless Sensor Networks," *Wireless Communications and Mobile Computing*, vol. 15, no. 12, pp. 1621–1632, 2015.

[44] O. Ozdemir, R. Li, and P. K. Varshney, "Hybrid Maximum Likelihood Modulation Classification Using Multiple Radios," *IEEE Communications Letters*, vol. 17, no. 10, pp. 1889–1892, 2013.

[45] D. Gesbert, H. Bolcskei, D. Gore, and A. Paulraj, "MIMO Wireless Channels: Capacity and Performance Prediction," in *Globecom'00-IEEE. Global Telecommunications Conference. Conference Record (Cat. No. 00CH37137)*, vol. 2. IEEE, 2000, pp. 1083–1088.

[46] P. Almers, F. Tufvesson, and A. F. Molisch, "Keyhole Effect in MIMO Wireless Channels: Measurements and Theory," *IEEE Transactions on Wireless Communications*, vol. 5, no. 12, pp. 3596–3604, 2006.

[47] A. Maaref and S. Aissa, "Impact of Spatial Fading Correlation and Keyhole on the Capacity of MIMO Systems with Transmitter and Receiver CSI," *IEEE Transactions on Wireless Communications*, vol. 7, no. 8, pp. 3218–3229, 2008.

[48] S. Sanayei and A. Nosratinia, "Antenna selection in keyhole channels," *IEEE transactions on communications*, vol. 55, no. 3, pp. 404–408, 2007.

[49] Y. Gong and K. B. Letaief, "On the Error Probability of Orthogonal Space-Time Block Codes over Keyhole MIMO channels," *IEEE Transactions on Wireless Communications*, vol. 6, no. 9, pp. 3402–3409, 2007.

[50] C. He, X. Chen, and Z. J. Wang, "Performance of General STCs over Spatially Correlated MIMO Single-Keyhole Channels," *IEEE Transactions on Vehicular Technology*, vol. 64, no. 7, pp. 3285–3291, 2014.

[51] H. Zhao, Y. Gong, Y. L. Guan, and Y. Tang, "Performance Analysis of *m*-PSK/*m*-QAM Modulated Orthogonal Space–Time Block Codes in Keyhole Channels," *IEEE Transactions on vehicular technology*, vol. 58, no. 2, pp. 1036–1043, 2008.

[52] G. Levin and S. Loyka, "On the Outage Capacity Distribution of Correlated Keyhole MIMO channels," *IEEE Transactions on Information Theory*, vol. 54, no. 7, pp. 3232–3245, 2008.

[53] Y. Karasawa, M. Tsuruta, and T. Taniguchi, "Multi-keyhole model for mimo radio-relay systems," *IET*, 2007.

[54] S. H. Chae, S.-W. Jeon, and S.-Y. Chung, "Cooperative Relaying for the Rank-Deficient Mimo Relay Interference Channel," *IEEE Communications Letters*, vol. 16, no. 1, pp. 9–11, 2011.

[55] Y. Fan and J. Thompson, "MIMO Configurations for Relay Channels: Theory and Practice," *IEEE Transactions on Wireless Communications*, vol. 6, no. 5, pp. 1774–1786, 2007.

[56] C. Zhong, T. Ratnarajah, Z. Zhang, K.-K. Wong, and M. Sellathurai, "Performance of Rayleigh-Product MIMO Channels with Linear Receivers," *IEEE Transactions on Wireless Communications*, vol. 13, no. 4, pp. 2270–2281, 2014.

[57] B. Wang, J. Zhang, and A. Host-Madsen, "On the Capacity of MIMO Relay Channels," *IEEE Transactions on Information theory*, vol. 51, no. 1, pp. 29–43, 2005.

[58] A. Wittneben and B. Rankov, "Impact of Cooperative Relays on the Capacity of Rank-Deficient Mimo channels," *Proceedings of the 12th IST Summit on Mobile and Wireless Communications*, vol. 2, pp. 421–425, 2003.

[59] I. Hammerstroem, M. Kuhn, B. Rankov, and A. Wittneben, "Space-Time Processing for Cooperative Relay Networks," in *2003 IEEE 58th Vehicular Technology Conference. VTC 2003-Fall (IEEE Cat. No. 03CH37484)*, vol. 1. IEEE, 2003, pp. 404–408.

[60] H. Bolcskei, R. U. Nabar, O. Oyman, and A. J. Paulraj, "Capacity Scaling Laws in MIMO Relay Networks," *IEEE Transactions on Wireless Communications*, vol. 5, no. 6, pp. 1433–1444, 2006.

[61] G. Levin and S. Loyka, "Multi-Keyhole MIMO Channels: Asymptotic Analysis of Outage Capacity," in *2006 IEEE International Symposium on Information Theory*. IEEE, 2006, pp. 1305–1309.

[62] A. P. Harrison and D. Joseph, "Numeric Tensor Framework: Exploiting and Extending Einstein Notation," *Journal of computational science*, vol. 16, pp. 128–139, 2016.

[63] J.-P. Kermoal, L. Schumacher, K. I. Pedersen, P. E. Mogensen, and F. Frederiksen, "A stochastic mimo radio channel modelwith experimental validation," *IEEE Journal on selected areas in Communications*, vol. 20, no. 6, pp. 1211–1226, 2002.

[64] K. Yu, M. Bengtsson, B. Ottersten, D. McNamara, P. Karlsson, and M. Beach, "Modeling of wide-band mimo radio channels based on nlos indoor measurements," *IEEE Transactions on Vehicular Technology*, vol. 53, no. 3, pp. 655–665, 2004.

[65] S. Özyurt and O. Kucur, "Performance analysis of maximal ratio combining with transmit antenna selection and signal space diversity under exponential antenna correlation," *IET Communications*, vol. 12, no. 5, pp. 612–619, 2018.

[66] S. L. Loyka, "Channel Capacity of Mimo Architecture Using the Exponential Correlation Matrix," *IEEE Communications letters*, vol. 5, no. 9, pp. 369–371, 2001.

[67] Z. Xu, S. Sfar, and R. S. Blum, "Analysis of mimo systems with receive antenna selection in spatially correlated rayleigh fading channels," *IEEE Transactions on Vehicular Technology*, vol. 58, no. 1, pp. 251–262, 2008.

[68] P. Lombardo, G. Fedele, and M. M. Rao, "Mrc performance for binary signals in nakagami fading with general branch correlation," *IEEE Transactions on Communications*, vol. 47, no. 1, pp. 44–52, 1999.

[69] B. Holter and G. Oien, "On the Amount of Fading in MIMO Diversity Systems," *IEEE Transactions on Wireless Communications*, vol. 4, no. 5, pp. 2498–2507, 2005.

[70] A. Hyvarinen, J. Karhunen, and E. Oja, *Independent Component Analysis*, 2001.

[71] M. M. Sohul, B. Ramkumar, and T. Bose, "Multiuser Automatic Modulation Classification for Cognitive Radios Using Distributed Sensing in Multipath Fading Channels," in *2012 7th international ICST conference on cognitive radio oriented wireless networks and communications (CROWNCOM)*. IEEE, 2012, pp. 71–76.

[72] P. A. Forero, A. Cano, and G. B. Giannakis, "Distributed Feature-Based Modulation Classification Using Wireless Sensor Networks," in *MILCOM 2008-2008 IEEE Military Communications Conference*. IEEE, 2008, pp. 1–7.

[73] B. R. Tomiuk and N. C. Beaulieu, "A New Look at Maximal Ratio Combining," in *Globecom'00-IEEE. Global Telecommunications Conference. Conference Record (Cat. No. 00CH37137)*, vol. 2. IEEE, 2000, pp. 943–948.

[74] X. Cui and Z. Feng, "Lower Capacity Bound for MIMO Correlated Fading Channels with Keyhole," *IEEE Communications Letters*, vol. 8, no. 8, pp. 500–502, 2004.

[75] J. Salo, H. M. El-Sallabi, and P. Vainikainen, "Impact of Double-Rayleigh Fading on System Performance," in *2006 1st International Symposium on Wireless Pervasive Computing*. IEEE, 2006, pp. 5–pp.

[76] K. T. Truong, P. Sartori, and R. W. Heath, "Cooperative Algorithms for MIMO Amplify-and-Forward Relay Networks," *IEEE Transactions on Signal Processing*, vol. 61, no. 5, pp. 1272–1287, 2013.

[77] Q. Wang, T. Chen, and T. Lan, "Linear Processing Design of Amplify-and-Forward Relays for Maximizing the System Throughput," *Journal of Electrical and Computer Engineering*, vol. 2018, 2018.

[78] C. Zhong, S. Jin, K.-K. Wong, M.-S. Alouini, and T. Ratnarajah, "Low SNR Capacity for MIMO Rician and Rayleigh-Product Fading Channels with Single Co-Channel Interferer and Noise," *IEEE Transactions on Communications*, vol. 58, no. 9, pp. 2549–2560, 2010.

[79] S. Jin, M. R. McKay, K.-K. Wong, and X. Gao, "Transmit Beamforming in Rayleigh Product MIMO Channels: Capacity and Performance Analysis," *IEEE Transactions on Signal Processing*, vol. 56, no. 10, pp. 5204–5221, 2008.

[80] W. Guan and H. Luo, "Joint MMSE Transceiver Design in Non-Regenerative MIMO Relay Systems," *IEEE Communications Letters*, vol. 12, no. 7, pp. 517–519, 2008.

[81] V. G. Chavali and C. R. Da Silva, "Maximum-Likelihood Classification of Digital Amplitude-Phase Modulated Signals in Flat Fading Non-Gaussian Channels," *IEEE Transactions on Communications*, vol. 59, no. 8, pp. 2051–2056, 2011.

[82] T. J. OShea, T. Roy, and T. C. Clancy, "Over-the-Air Deep Learning Based Radio Signal Classification," *IEEE Journal of Selected Topics in Signal Processing*, vol. 12, no. 1, pp. 168–179, 2018.

[83] A. Ali and F. Yangyu, "Automatic Modulation Classification Using Deep Learning Based on Sparse Autoencoders with Nonnegativity Constraints," *IEEE Signal Processing Letters*, vol. 24, no. 11, pp. 1626–1630, 2017.

[84] A. Ali and F. Yangyu, "Unsupervised Feature Learning and Automatic Modulation Classification Using Deep Learning Model," *Physical Communication*, vol. 25, pp. 75–84, 2017.

[85] F. Meng, P. Chen, L. Wu, and X. Wang, "Automatic Modulation Classification: A Deep Learning Enabled Approach," *IEEE Transactions on Vehicular Technology*, vol. 67, no. 11, pp. 10 760–10 772, 2018.

[86] S. Ramjee, S. Ju, D. Yang, X. Liu, A. E. Gamal, and Y. C. Eldar, "Fast Deep Learning for Automatic Modulation Classification," *ArXiv Preprint arXiv:1901.05850*, 2019.

List of Publications

Published Journal

1. **D. Das**, P. Bora and R. Bhattacharjee, "Blind Modulation Recognition of the Lower Order PSK Signals Under the MIMO Keyhole Channel", *IEEE COMMUNICATIONS LETTERS*, vol. 22, no. 9, pp. 1834 - 1837, Sept. 2018. DOI: 10.1109/LCOMM.2018.2853638.

Manuscripts under Submission

1. **D. Das**, P. Bora and R. Bhattacharjee, "Automatic Modulation Classification over Correlated MIMO Amplify and Forward (AF)-Relay Fading Channels"

2. **D. Das**, P. Bora and R. Bhattacharjee, "Cooperative Automatic Modulation Classification for MIMO Systems in a Multi-Antenna Sensor Network"

Conference publications

1. **D. Das**, P. Bora and R. Bhattacharjee," Cumulant Based Automatic Modulation Classification of QPSK, OQPSK, 8-PSK and 16-PSK", International Conference on Communication Systems and Networks (COMSNETS), Bangalore, 2016.

2. **D. Das**, P. Bora and R. Bhattacharjee," Cumulant Based Automatic Modulation classification of QPSK, OQPSK, $\frac{\pi}{4}$-QPSK and 8-PSK in MIMO environment", *International Conference on Signal Processing and Communications (SPCOM)*, Bangalore, 2016.